

MASTER OF SCIENCE THESIS

A Study of the Buckling Behaviour of Stiffened Panels under Compression and Lateral Pressure

Lijian Qi

Faculty of Aerospace Engineering · Delft University of Technology



A Study of the Buckling Behaviour of Stiffened Panels under Compression and Lateral Pressure

MASTER OF SCIENCE THESIS

For obtaining the degree of Master of Science in Aerospace Engineering
at Delft University of Technology

Lijian Qi

January 23, 2018



Copyright © Lijian Qi
All rights reserved.

DELFT UNIVERSITY OF TECHNOLOGY
FACULTY OF AEROSPACE ENGINEERING
DEPARTMENT OF AEROSPACE STRUCTURES AND MATERIALS

GRADUATION COMMITTEE

Dated: January 23, 2018

Chair holder:

Pro. Chiara Bisagni

Committee members:

Dr. ir. Julien van Campen

Dr. Atsushi Nagai

Acknowledgments

I would like to express my sincerest gratitude to my supervisor Pro. Chiara Bisagni for providing me the thesis topic. I could not have finished the thesis without her patient guidance and continuous encouragement throughout the completion of this project.

I would also like to thank the committee members of my thesis defence, Dr.ir.Julien van Campen and Dr. Atsushi Nagai for their time and effort spent on my thesis work.

Special thanks to Kautuk Sinha for reviewing and correcting the thesis; to Davide Jester Gatta for solving the problems in cluster; to Duo Zou and Tijs de Boer for their kind assistance in Abaqus simulation.

Furthermore, I would like to express my appreciation to my classmates and comrades, Peixuan, Yuanyuan and Jiachen. I cherish every time we stay up to the midnight in the library to meet assignment deadlines.

I am grateful to all my friends that provided help during the Master period. To Hongzhi, Javier and Yuqian for sharing the scientific research experiences and resources; To Honglin, Quan, Lin and Li for kindly giving suggestions when I first came TU Delft.

My gratitude also goes to my housemates, Tao, Xing, Yu, Xiaoyan and Yawen. It is so lucky to share the same house with you and the days we spent together playing and cooking will never fade away.

Last but not least, I am greatly in debt to my family for their unconditional love and support during the whole Master period. My utmost gratitude goes to my wife, Dan Wang, it is her sacrifice and encouragement to let me go through the most difficult days. I could not achieve this thesis without her.

Abstract

The main objective of this thesis is to develop a method to investigate stability behaviours of stiffened and unstiffened panels under the influence of in-plane compression and out-of-plane lateral pressure using appropriate simplifications. A test fixture to conduct buckling experiments with lateral pressure is also designed. Due to the deflection caused by the lateral pressure, considerable complexities will be introduced in terms of loading interactions and geometric nonlinearities, which make the analysis both theoretically difficult and computationally intensive. In addition, in aerospace structures, non-cylindrical wing and fuselage panels are potentially exposed to the combined action of in-plane compression and out-of-plane pressure, and the assessment of their stability behaviours becomes an issue of growing concern of structural engineers. To this end, the study of the buckling behaviour of stiffened panels under compression and lateral pressure is of practical importance.

Step by step investigations are performed on typical structures from unstiffened isotropic plates to stiffened composite panels using both analytical and finite element approaches. First, linear based methods using equilibrium and energy equations based on classical plate theories are reviewed, and predictions indicate that these methods only validate within the range of small deformation under small pressure loading. Eigenvalue buckling analysis and explicit dynamic procedures are adopted as numerical methods for verification. Simulated results of explicit dynamic procedures in Abaqus predicted the buckling loads fairly well compared with those in literature, revealing that lateral pressure has a positive impact on the stability behaviour of rectangular isotropic plates by postponing the buckling onset. Composite panels behave similarly as isotropic plates in terms of buckling and postbuckling responses. Given a large pressure, the critical buckling load of a simply supported laminate is able to reach up to four times as that of the uniaxially compressed plate.

A conceptual design of a test fixture for buckling experimental studies involving compression and lateral pressure is proposed in which pressurized airbags are adopted for generating uniform pressure load. The lateral loads are controlled by the internal pressure of airbags through a pressure gauge. Compression sensors are utilized to calibrate the pressure loads

by measuring the reaction forces. A rubber filler pad is laid inside the panel's bays between stringers to eliminate the unevenness on the stiffener side of the panel. Test rigs are designed with the consideration of compatibility with classical buckling experiments to lower the cost. Dynamic explicit simulations of the test reveal that the locations of the first local buckling onsets are shifted from the skin to stiffeners with the increase of lateral pressure. Buckling strengths of the entire stiffened panels exhibit an increase with the increase of lateral pressure. However, this trend is reversed when the pressure load exceeded a certain value at which stiffeners buckle before the skin.

Table of Contents

Acknowledgments	vii
1 Introduction	1
1.1 Background and Motivation	1
1.2 Research Questions and Objectives	3
1.3 Thesis Layout	3
2 Literature Review and Fundamental Theories	5
2.1 Literature Review	5
2.1.1 Buckling Analysis	6
2.1.2 Postbuckling Analysis	7
2.1.3 Experimental Investigation	8
2.2 Theoretical Fundamentals	14
2.2.1 Isotropic Plates	15
2.2.2 Composite Plates	19
2.3 Summary	21
3 Buckling and Postbuckling Behaviour of Isotropic Plates	23
3.1 Introduction	23
3.2 Plates under Uniaxial Compression	24

3.2.1	Buckling Analysis of Uniaxial Compressive Plates	25
3.2.2	Postbuckling Analysis of Uniaxial Compressive Plates	27
3.3	Plates under Lateral Pressure	30
3.3.1	Small Deformation of Plates under Out-of-Plane Loading	30
3.3.2	Large Deformation of Plates under Out-of-Plane Loading	31
3.4	Plates under Uniaxial Compression and Lateral Pressure	34
3.4.1	Buckling Analysis of Plates under Combined Loads	35
3.4.2	Postbuckling Analysis of Plates under Combined Loads	40
3.5	Finite Element Analysis	43
3.5.1	Model Description	43
3.5.2	Eigenvalue Analysis	47
3.5.3	Explicit Dynamic Analysis	49
3.6	Conclusions	54
4	Buckling and Postbuckling Behaviour of Composite Plates	55
4.1	Introduction	55
4.2	Composite Plates under Uniaxial Compression	56
4.3	Composite Plates under Lateral Pressure	58
4.4	Composite Plates under Combined Loads	59
4.4.1	Governing Differential Equation Method	59
4.4.2	Energy Methods	60
4.5	Finite Element Analysis	64
4.5.1	Model Description	64
4.5.2	Eigenvalue Analysis	65
4.5.3	Explicit Dynamic Analysis	66
4.6	Conclusions	71
5	Conceptual Design of the Testing Setups for Buckling Experiments	73
5.1	Evaluation of Existing Experiments	73
5.2	Conceptual Design of Test Setups	74
5.2.1	Stiffened Panels	75

5.2.2	Test Rigs and Supports	76
5.2.3	Application of Lateral Pressure Loading	77
5.2.4	Airbags	79
5.2.5	Boundary Fixtures	81
5.3	Conclusions and Recommendations	82
6	Finite Element Modeling of Stiffened Panels in Testing Setups	85
6.1	Introduction	85
6.2	Model Description	86
6.2.1	Geometry and Mesh	86
6.2.2	Boundary Conditions	87
6.2.3	Loading Cases	87
6.3	Eigenvalue Buckling Analysis	87
6.4	Dynamic Explicit Analysis of Stiffened Panels	88
6.5	Dynamic Explicit Analysis of Stiffened Panels with Rubber	95
6.5.1	Rubber Material Definition	95
6.5.2	Model Description	95
6.5.3	Boundary and Load Conditions	96
6.5.4	Load-Shortening Curves	96
6.6	Conclusion	99
7	Summaries and Recommendations	101
7.1	Thesis Overview and Conclusions	101
7.2	Recommendations	103
	References	105
A	Appendix	111
A.1	Isotropic Plates under Pure Pressure	111
A.2	Isotropic Plates under Uniaxial Compression and Pressure	111
A.3	FEM Verification	113

List of Figures

1.1	HWB pressure cabin crown panel loading	2
1.2	Upper wing panel	2
2.1	COLTS	9
2.2	Mini-COLTS setup	11
2.3	D-box test fixture	11
2.4	Contact area of airbags	13
2.5	Multiple airbags	13
2.6	Pressurized Chamber	14
2.7	Buckling tests using multiple jacks	15
2.8	Coordinate system and external forces at the mid-plane of a rectangular plate . .	15
2.9	Force resultants acted on the plate element	16
3.1	Stiffened panel of structural application	24
3.2	Unit stiffened panel	24
3.3	Combined forces acting on the flat plate	24
3.4	Roadmap of isotropic plate analysis	25
3.5	The buckling parameter versus the plate aspect	27
3.6	Central deflection versus uniform lateral pressure for simply supported square plate	34
3.7	Convergence study	44

3.8	The sketch of the model in Abaqus	45
3.9	External loading applied on the plate	46
3.10	Eigenmodes of a rectangular plate under uniaxial compression	48
3.11	Lateral pressure and edge shortening versus time curves	49
3.12	The postbuckling behaviour of isotropic plates (p_0)	50
3.13	Deflection the out-of-plane deformation (p_0)	50
3.14	Front view of the out-of-plane deformation (p_0)	51
3.15	The postbuckling behaviour of isotropic plates (p_1)	51
3.16	Deflection the out-of-plane deformation (p_1)	51
3.17	Front view of the out-of-plane deformation (p_1)	51
3.18	The postbuckling behaviour of isotropic plates (p_2)	52
3.19	Top view of the out-of-plane deformation (p_2)	52
3.20	Front view of the out-of-plane deformation (p_2)	52
3.21	The postbuckling behaviour of isotropic plates (p_3)	53
3.22	Top view of the out-of-plane deformation (p_3)	53
3.23	Front view of the out-of-plane deformation (p_3)	53
4.1	Compression applied on the composite laminate	56
4.2	Lateral pressure and edge shortening vs time curve	67
4.3	Postbuckling behaviour of composite plates and corresponding displacement fields (p_0)	67
4.4	Postbuckling behaviour of composite plates (p_0)	68
4.5	Postbuckling behaviour of composite plates and corresponding displacement fields (p_1)	68
4.6	Postbuckling behaviour of composite plates (p_1)	69
4.7	Postbuckling behaviour of composite plates and corresponding displacement fields (p_2)	69
4.8	Postbuckling behaviour of composite plates (p_2)	70
4.9	Postbuckling behaviour of composite plates and corresponding displacement fields (p_3)	70
4.10	Postbuckling behaviour of composite plates (p_3)	71

5.1	Buckling tests by London College	75
5.2	Specimen with potting pads at ends	76
5.3	Basic supports of the test	76
5.4	The application of lateral pressure by a pressurized airbag	77
5.5	Cross-section view of the test setups	78
5.6	Loading cases of specimen fixtures	78
5.7	High-pressurized lifting airbags and low-pressurized air balloon	80
5.8	Airbag contact situations	80
5.9	Compression sensors for measurement of lateral loads	81
5.10	The assembly of the testing components	81
5.11	Test fixtures	82
6.1	The configuration of stiffened panels	86
6.2	Boundary conditions of the panel	87
6.3	Application of pressure load to the stiffened panel	88
6.4	Eigenvectors of stiffened panels subjected to combined loading	89
6.5	Load-shortening curve and out-of-plane displacement of stiffened panel ($p_0 = 0$) .	91
6.6	Load-shortening curve and out-of-plane displacement of stiffened panel ($p_1 = 0.013MPa$)	92
6.7	Load-shortening curve and out-of-plane displacement of stiffened panel($p_2 = 0.065MPa$)	93
6.8	Load-shortening curve and out-of-plane displacement of stiffened panel($p_3 = 0.13MPa$)	94
6.9	Cross section of rubber pads	96
6.10	Boundary and loading conditions of stiffened panels with rubber filler	96
6.11	Comparison of load-shortening curve of stiffened panels with and without rubber (p_0)	97
6.12	Comparison of load-shortening curve of stiffened panels with and without rubber (p_1)	97
6.13	Comparison of load-shortening curve of stiffened panels with and without rubber (p_2)	98
6.14	Comparison of load-shortening curve of stiffened panels with and without rubber (p_3)	98
A.1	Central deflection versus uniform lateral pressure for simply supported square plate	112

A.2 Effect of lateral pressure on postbuckling behavior of square plates(Eq. 3.96) . . . 112

A.3 Verification of postbuckling behaviours of simply supported square plates under various lateral pressure 113

List of Tables

2.1	Presented experiments for combine-loaded bucking test	10
3.1	Load-deflection relations under various load cases	42
3.2	Finite element model properties	43
3.3	Critical buckling load for isotropic plates under uniaxial compression	44
3.4	Boundary conditions	45
3.5	Internal pressure (cabin pressure $P = 9.2 \text{ psi}$)	46
3.6	Eigenvalue analysis using a single step	47
3.7	Eigenvalue analysis using multiple steps	47
3.8	The critical buckling load for isotropic plates	48
3.9	Dynamic explicit analysis using multiple steps	49
3.10	The critical buckling load for isotropic plates	54
4.1	Material property of IM7/8552 layers	64
4.2	Stacking sequence of the laminate	65
4.3	Eigenvalue simulation results of laminates	66
5.1	Advantages and disadvantages of former experiments	74
5.2	Reaction forces resulted from airbags ($p_z = 0.13MPa$)	78
5.3	Skin stresses of various dimensions of airbags ($p_z = 0.13MPa$)	79

6.1	The stacking sequence and thickness	86
6.2	Results of eigenvalue analysis	88
6.3	Buckling loads of components in stiffened panels under combined loads	91

Chapter 1

Introduction

1.1 Background and Motivation

In aeronautical application, stiffened panels are widely adopted in primary aircraft structures including wings and fuselages due to their high structural efficiency in terms of load-carrying capacity and stiffness to weight ratio. In most cases, ultimate strengths of stiffened panels are primarily dependent on the stability behaviour, and weight reduction can be achieved by operating the panels into a deep postbuckling field in which considerable strength in excess of the critical buckling load is achieved. In order to exploit the strength and stiffness potentially offered by stiffened panels with higher structural effectiveness, considerable efforts have been devoted to the studies of stability behaviours of the thin-walled structures subjected to various loading environments. However, in these studies, external loads are frequently limited within the range of in-plane forces. In some cases, structures are expected to sustain simultaneously applied transverse loads, e.g. lateral pressure acting on the panel surface.

One specific application of such cases is the upper fuselage panel of an advanced Hybrid Wing Body (HWB) configuration as shown in Fig 1.1 [1] [2]. Unlike the cylindrical fuselage panel of a conventional airplane in which internal pressure load is balanced by the circumferential stress of the skin, the quasi-flat panels in HWB tend to sustain the pressure through stiffeners, which potentially increases the risk of instability and stringer weight resulted from structural reinforcement. Similar examples can also be found in the upper wing structures, in which the panels are subjected to the combined action of lateral pressure aroused by aerodynamic loading and axial compression resulted from wing bending as shown in Fig. 1.2.

The inclusion of sufficiently high lateral pressure can invalidate the small deformation assumption on which linear buckling analysis is based[1]. Nonlinear analysis based on the large deflection theory is, therefore, necessary to be taken into account and further studied. Due to the large deflection caused by the lateral pressure, considerable complexities will be intro-

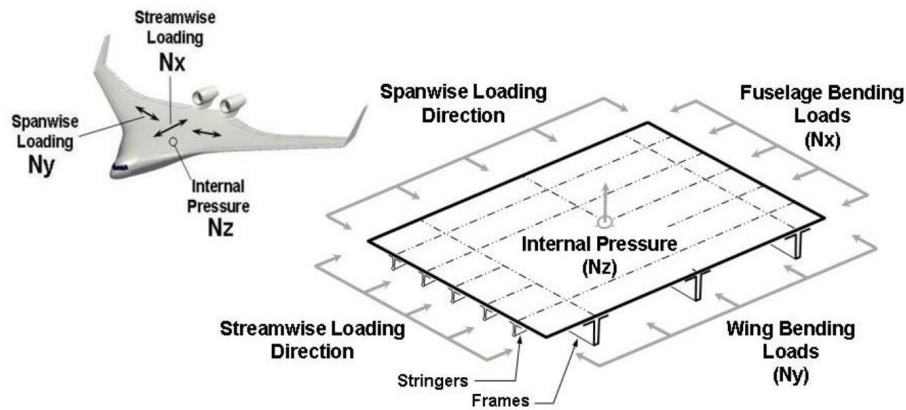


Figure 1.1: HWB pressure cabin crown panel loading [1]

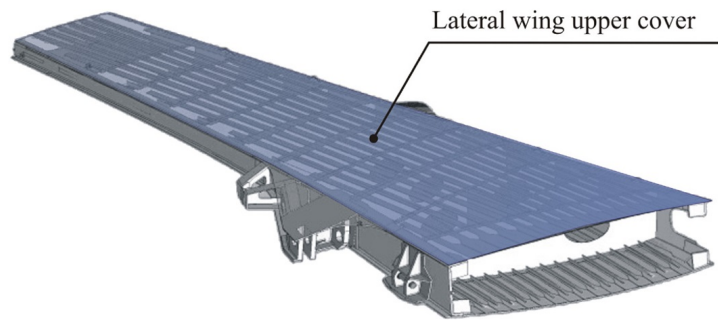


Figure 1.2: Upper wing panel[3]

duced in terms of load interactions and geometric nonlinearities, which makes the analysis both theoretically difficult and computationally intensive. As a result, a combination of finite element (FE) and experimental approach is commonly utilized to analysis the stability behaviour of stiffened panels.

A full scaled experiment has been implemented on a pressurized wing box by NASA using a complex testing facility. Despite the attractive capabilities in achieving sufficient accurate results, the experiment system did not satisfy the requirements of current studies in terms of high efficiency and low cost. In the primary design, optimization and iteration are required due to the larger number of structural variables and constructive configurations of the stiffened panels. As a result, a massive specimens are need to be manufactured and tested. For this reason, it is more suitable to conduct small-scale buckling experiments which are convenient in elementary studies. Current buckling experiments on small-scale stiffened panes with lateral pressure involved are often carried out in relation to the marine structures such as bottom panels of the ship's hulls. Pressure loads were often applied by virtue of airbags (filled with air or water) and exerted on the outer skin of the panels. This is different from those of aircraft fuselage structures in which pressure acts from the stiffener side. Problems will be encountered when airbags are contacting the uneven panel surface which is caused by the stiffeners. Therefore, it is of importance to develop a new buckling experiment to imitate the load case in a stiffened panel with lateral pressure appropriately applied.

1.2 Research Questions and Objectives

The main questions regarding the subject are depicted as follows:

1. What are the most effective methods to assess the buckling and postbuckling behaviour of a rectangular stiffened panel under the combined action of both axial compression and lateral pressure?
2. To what extent would the lateral pressure affect the stability strength of an axially compressed stiffened or unstiffened panel?
3. How to design a feasible experimental setup with a relatively lower cost yet acceptable accuracy to test the load-deformation response of stiffened panels under uniaxial compression and lateral pressure?

The aims of this thesis are supposed to be achieved by following steps:

1. Predict the buckling and postbuckling response of a flat plate to external forces including uniaxial compression and lateral pressure based on the classic plate theory.
2. Verify the prediction of analytical methods by comparing with literature.
3. Conduct FE simulation in commercial software Abaqus using eigenvalue analysis and dynamic explicit analysis.
4. Propose a conceptual design for buckling experiments of stiffened panels under combined loads by considering the cost and feasibility.

1.3 Thesis Layout

The thesis report is organized and presented in two parts. The first part focuses on the fundamental theoretical analysis and finite element simulation, while the second part is relevant to the design of buckling experiments for stiffened panels under combined loads. The literature on predicting the stability behaviour of both unstiffened and stiffened plates subjected to lateral pressure and compression will be reviewed in Chapter 2. Theoretical fundamentals on which the following chapters are based are also briefly presented. In Chapter 3, primary efforts will be devoted to the study of buckling and postbuckling behaviours of axially compressive isotropic plates when lateral pressure is simultaneously applied. Finite element code Abaqus is employed to verify the predicted results. Analogue investigation of plates made of composite materials is carried out in Chapter 4. In Chapter 5, a conceptual design for buckling experiments of stiffened panels subjected to both uniaxial compression and lateral pressure will be discussed with the emphasis on the application of lateral pressure. Predictions using FE methods with respect to critical buckling loads and postbuckling responses of stiffened panels will be discussed in Chapter 6. Conclusions and recommendations of the thesis will be drawn in Chapter 7.

Literature Review and Fundamental Theories

Extensive research has been done on the stability behaviour of stiffened panels under compression and lateral pressure which could be approximately categorized into three groups according to the adopted analysis tools, namely analytical, finite element and experimental methods. In this chapter, the approaches addressed by researchers to solve the proposed problem will be thoroughly reviewed, and the related references concerning buckling and postbuckling behaviour of stiffened panels and unstiffened plates exposed to in-plane compression and lateral pressure are about to thoroughly inspected. In addition, the fundamental theoretical definition and equations based on the plate theories will also be addressed.

2.1 Literature Review

Compared to the studies on stability behaviours of unstiffened plates or stiffened panels under in-plane forces, few studies can be found on the stability analysis of panels under combined loads of out-of-plane pressure and in-plane compression. Most of the textbooks and journals mainly cover the buckling responses of the plates and panels to the in-plane loading such as the axial compression [4], shears [5] or their combination [6]. Investigations on stiffened panels subjected to in-plane combined forces have been conducted by Shama [7] with isotropic materials and by Kassapoglou[8] with composite materials. The buckling and postbuckling responses of stiffened panels under any combined loads are always derived by solving the governing equations based on the plate theories associated with different boundary conditions. They are commonly obtained by providing the solutions of the Navier or Galerkin's method of rectangular plates based on the Von Karman governing equations under Kirchhoff hypothesis [9]. By utilizing the Von Karman equations, easier analytical methods and simpler models are

established and developed to solve the stability problems. The methods presented by other authors will be introduced in the following parts.

2.1.1 Buckling Analysis

From the structural engineers' perspective, stiffened panels are designed in such a way that local panel buckling between stiffeners takes place before stiffener web buckling or global buckling of the entire panel [10]. As a result, the buckling capacity of stiffened panels, in most of the cases, can be represented by plate buckling strength. Supporting stiffeners and frames are equivalently considered as boundary conditions of the surrounded panels.

In the textbook of Murari [11], plate buckling problems were solved based on the classical plate theory (CPT) in which Kirchhoff hypothesis was satisfied. Under this approximation, the mathematical model was significantly simplified with higher order items of strains neglected and governing differential equations of a simply supported rectangular plate under lateral pressure and uniaxial compression was then established. Two analytical methods, namely governing differential equation and energy methods, were adopted to derive the closed form expression of critical buckling load and deflection. Results indicate that lateral pressure will not affect the critical buckling load if small deformation assumption was made.

However, as the pressure load increases, out-of-plane deformations resulted directly from the pressure load becomes sufficiently large that methods described in [11] will not valid as they have ignored the membrane strains and stresses which cannot be neglected in large-deformed plates [4]. To reveal the stability behaviour of compressive plates subjected to relatively large lateral pressure, Levy proposed a method for finding the solutions to Von Karman governing equations of a rectangular plate under edge compression and lateral pressure [12]. Nonlinearity effects are taken into account in terms of in-plane stresses induced by large deflection. On top of this approach, case studies of a rectangular plate under simply supported [13] or clamped [14] boundary conditions were implemented. Buckling load at four different values of lateral pressure were studied and compared, indicating that the normal loading has a beneficial effect on improving the stability capacity. This method together with its fundamental background is further summarized by Chia [15] where the nonlinear theories concerning about both isotropic and composite plates are addressed.

Yosiki et al. [16] studied the buckling behaviour of a simply supported rectangular plate under edge compression and lateral hydraulic pressure. Governing equations were solved using Galerkin's method with lateral pressure introduced as constant parameters. Compression load-deflection curves indicate that the buckled waveform configuration is dramatically influenced by the lateral pressure. Similarly, Brown et al. [17] also addressed a study on large deflections of plates under combined loading. In this study, governing partial differential equations were replaced by corresponding finite difference equivalents in order to be solved numerically.

In 1997, Yao et al. performed a semi-analysis to clarify the buckling behaviour of a rectangular plate under lateral pressure and transverse compression in large deflection state based on elasticity assumption [18]. A curve-fitting formula was obtained to evaluate the influenced

critical stress under combined loading by utilizing the results from FE simulation. The results also showed that lateral pressure had a positive effect on the buckling strength of a rectangular isotropic plate.

Steen et al. pointed out that when a combination of lateral pressure and bi-axial compression are subjected to a stiffened panel, buckling behaviours analysis tend to be complicated because of the mode coupling and potential waveform transferring during the loading process [19]. One of the convenient ways to simplify the situation is to split the analyzing process into two parts, namely compression buckling part and pure lateral pressure. In this approach, the former part was constructed and calculated based on nonlinear von Karman equations while the latter was tackled based on the principle of energy method.

With the introduction of in-plane stresses, governing differential equations based on the large deflection theory are computationally complicated, and thus numerical solutions are necessary. Byklum et al. developed a method of high efficiency for evaluating the stability property of isotropic plates under combined loads including incrementally increased in-plane compression and constant out-of-plane pressure [20]. Plate deflections and membrane stresses are reformulated as double Fourier trigonometric series and substituted into the governing equations. Solutions are obtained by solving the potential energy equations using numerical methods.

Difficulties will be encountered when mathematical models of stiffened panels are established. To prevent complicated calculations, Giles developed an engineering method to study the buckling behaviour of stiffened panels [21]. In this method, the lateral pressure was to some extent considered equivalent to load eccentricity, from which additional bending moments will be resulted. These moments were then superposed to axial forces that applied on the skin or stringers of the panel.

From the reviewed research, systematic analyses for buckling behaviour of stiffened panels under the combined action of lateral and axial compression are still rare in this areas, especially for composite panels, which consequently necessitate the investigation of this thesis.

2.1.2 Postbuckling Analysis

It is acknowledged that additional load-carrying capacity will be gained in thin-walled structures at postbuckling stages, which is of practical importance in structure design. Traditional methods in dealing with the postbuckling problems mainly rely on the nonlinear large-deflection plate theory, from which von Karman governing equations are established.

In the paper of Shen [22] in 1989, the post-buckling behaviour of an isotropic plate under constant lateral pressure and variable edge compression loads was analytically investigated with geometry imperfection analysis in it. Given the simply supported boundary condition of a plate, the lateral pressure was treated as initial imperfection based on the large deflection equations of Von Karman. In this method, the lateral pressure was converted into an initial deflection by using Galerkin method. Governing equations with various parameters including the lateral pressure were then solved by perturbation methods. Later on, Shen et al. [23] extended this method to the analysis of postbuckling of a composite laminate under the

action of both in-plane and out-of-plane loads resting on a two-parameter elastic foundation. On the basis of the classical laminated plate theory (CLPT), estimated buckling loads and postbuckling equilibrium paths were determined and traced using perturbation approach.

As for the plate with a moderate thickness, CLPT was no longer validated and should be replaced by the first-order shear deformation plate theory (FSDT). Shen et al. [24] gave an analysis for buckling response of a composite plate with moderate thickness subjected to lateral pressure and compression, in which the effect of lateral pressure on the strain-loading relations was considered as an initial geometric imperfection. By using the perturbation technique, the load-deflection curve in the postbuckling stage is obtained.

Assuming a composite laminate plate under the combined loading, complexity such as anisotropic mechanical properties and load conditions will make the rigorous estimation of stability behaviours more complicated, and only numerical methods were found to be useful in the investigation of composites. In the paper of Han, an Element-based Lagrangian formulation was adopted due to the single mapping model and fast convergence speed, giving a satisfactory level of accuracy in comparison with the FE results [25].

When the stiffened plates under a combination of axial and lateral loading, stress distribution becomes more complicated especially for analytical calculation. In this case, many studies have been mainly focused on the FEM simulation using the commercial finite element codes. Mohammad et al. [26] addressed a numerical investigation concerning postbuckling behaviour and ultimate strength of aluminium panels under the increase of magnitude of lateral pressure and in-plane loading using finite element code ANSYS. The derived stress-strain curves under different values of loading showed that lateral pressure has a significant effect on the postbuckling response of stiffened panels. As the interaction of stiffeners and the plate, the buckling onset of the entire panel was not explicitly observed.

Currently, most of the research have been mainly focused on metallic plates and thorough investigation on composite stiffened panels are still required.

2.1.3 Experimental Investigation

Apart from the analytical and numerical methods, considerable experiments with respect to the stability properties of stiffened panels under lateral pressure have been developed.

In practice, design work in the aerospace structure is supposed to be a result of the iterative process of calculation and simulation based on the theoretical formulations and finite element packages respectively. In order to investigate and verify such components under various combined load cases that represent real loading environment, experiments are often of great importance and fundamentally necessary for complex structure or crucial components especially when the novel materials were utilized. However, loading environments in reality often differ from preset conditions in the simulating process.

Laboratory experiments regarding the buckling and postbuckling behaviour of stiffened panels under in-plane compression or shear loading combined with lateral pressure have already been

carried out for decades. Application of lateral pressure in the experiment is affected by many factors such as facility cost, boundary conditions and accuracy tolerance. Many researchers devoted their efforts to the exploration of how to give an efficient testing method. According to the manner in which lateral forces are applied, those methods could be classified into following groups, namely Combined Loads Test System(COLTS), pressurized airbags, pressure-box and point loads methods. A brief description of these tests associated with their scaled sketches is illustrated in Table 2.1.

Combined Loads Test System

Recently, Boeing and NASA developed a modern conceptual aircraft which adopted pressurized Hybrid Wing Body structure. The testing equipment accommodating large assemblies was particularly designed to meet the requirement of complex combined loading cases, i.e. internal pressure and in-plane compression. Thus, a specialized facility COLTS, for testing the wing box structure with sufficient accuracy by simulating real loading environment was designed as shown in Figure 2.1. The internal pressure was applied via the air pressure injected into the hermetic wing box. This COLTS facility provided a capacity to conduct combined loading including the internal pressure for wing box section with different geometry in order to verify the structure behaviour experimentally.

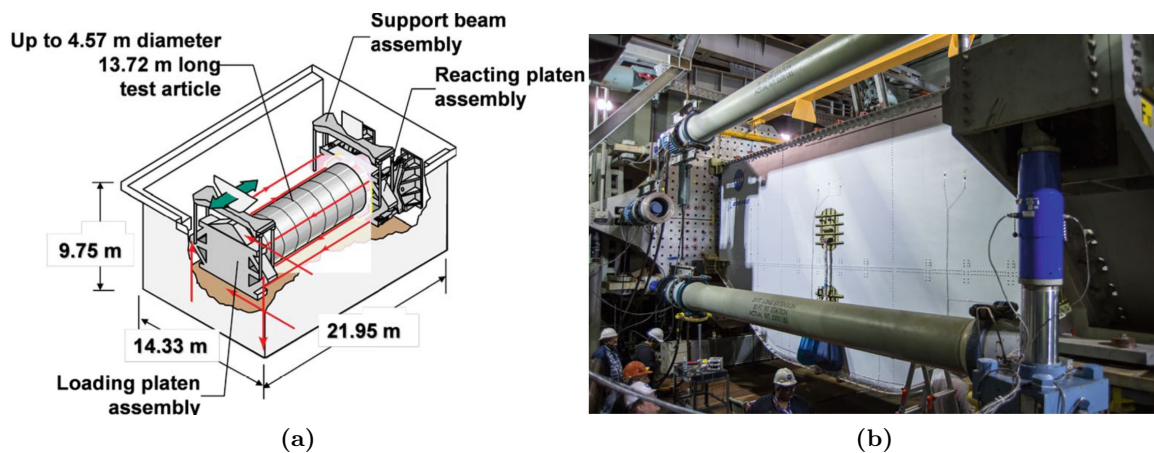


Figure 2.1: COLTS [31]

Besides, two other facilities to test pressurized stiffened panels were also proposed by Rouse [32] consisting of mini-COLTS and D-box test fixture. The former is a sub-scale of COLTS for checking the mechanical loading parameters prior to the actual test as shown in Fig 2.2. The D-box fixture works on a pressurized box made of I-beams assembly with hinges for the attachment of testing panels[33]. In order to eliminate the undesirable deformation, extra cross bar was introduced between the hinge points as shown in Fig 2.3.

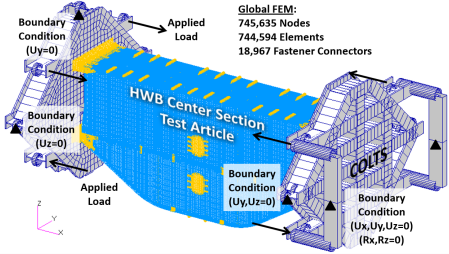
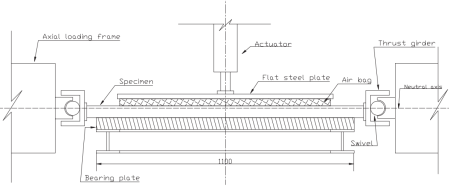
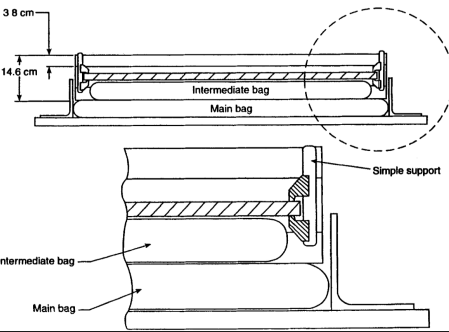
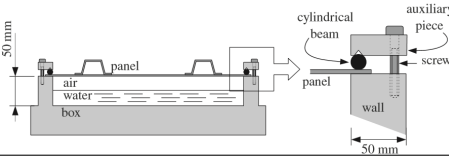
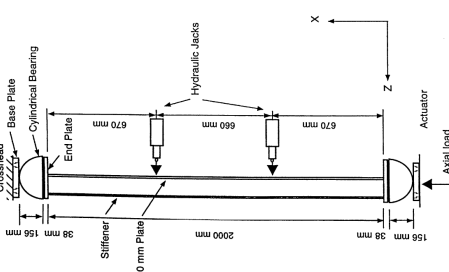
NO.	Test	Properties	Figures	Ref
1	COLTS	Internal pressure and combined loads are included		[1]
2	Pressurized Airbags	Lateral pressure was acted by pressurized bags		[27]
3	Double Airbags	Lateral pressure was conducted by double or multiple airbags		[28]
4	Pressurized Chamber	Lateral pressure was induced by vacuum or pressurized chamber Filled with water and air		[29]
5	Points loads	Lateral pressure was conducted by hydraulic jacks		[30]

Table 2.1: Presented experiments for combine-loaded bucking test

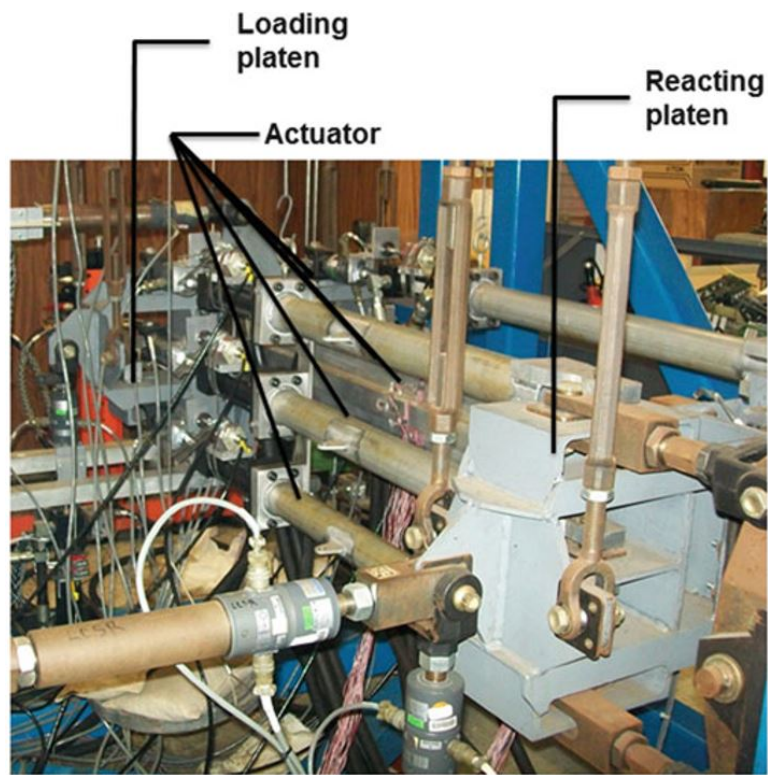


Figure 2.2: Mini-COLTS setup[32]

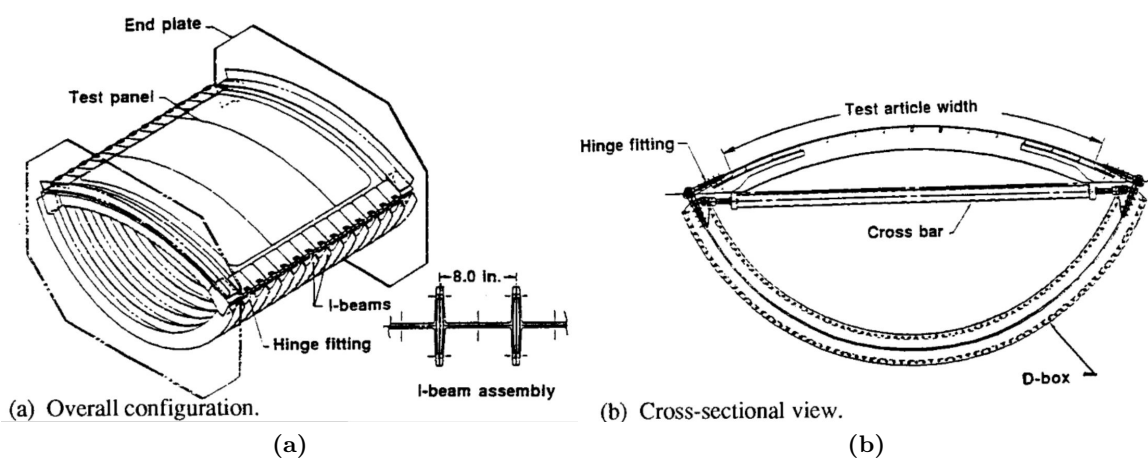


Figure 2.3: D-box test fixture[33]

The COLTS testing equipment has apparent advantages in accuracy due to its "quasi-reality" application of both loading and boundary conditions. However, despite the advantages for COLTS fixture in acquiring accuracy testing results, considerable cost of equipment manufacturing along with maintenance expenses render this method difficult to use for primary research. Therefore, other appropriate testing methods with relatively less cost and meanwhile with sufficient precision are still desirable in the preliminary design of stiffened panels that subjected to combined loading.

Pressurized airbags

As one of the typical components in a marine structure, stiffened panels under combined loads also attracted numerous experimental investigation in ship industry, in which lateral pressure was applied through pressurized air-tight bags. Taylor conducted the investigation on the interaction behaviour between in-plane stress and lateral pressure [34]. In this article, he gave an extremely detailed explanation of the experiment of a flat rectangular unstiffened plate under combined axial and lateral loading. A small-scale model was manufactured and tested in advance to track the effects of uniform pressure on the buckling behaviour. The lateral pressure was applied by pressurized airbags while the axial compression was applied by a pair of roller bearings.

The method using pressurized airbags was also demonstrated by Shanmugm and Donqi[27, 35]. The specimen was located horizontally with stringers facing downwards, and the lateral pressure was applied to the plate from the other side, driven vertically by an actuator. The airbag was laid between the specimen and the actuator, transferring the jack load into uniform pressure. Additional measures were taken to eliminate any possible friction during the text.

A similar experiment using flexible airbags was also carried out by Kumar in 2010 [36]. The orthogonal plate under combined in-plane and out-of-plane loads was tested by a compression test machine. The in-plane axial load was applied by hydraulic jacks while lateral pressure was provided by an inflatable air balloon. The pressurized air balloon was located between the specimen and an auxiliary supporting plate which is assembled in such a way that a self-balanced system would be achieved without adding additional actuators. Air pressure was measured and controlled by a pressure gauge.

Generally, due to the shape of the airbags, the expected pressurized region of the flat panel cannot be fully occupied by the contact area of the pressurized airbags as shown in Fig 2.4, leading to a nonlinear relation between the pressure load and the internal air pressure. Furthermore, the corners may not receive full pressure, and the actual pressurized region could have been overestimated.

In order to eliminate the influence of the nonlinearity caused by the elliptical geometry of the airbag, one of the methods was addressed by Robert [28] using multiple airbags which are stacked in series. The uniaxial compression in this experiment was provided by a hydraulic ram while the uniform out-of-plane pressure was conducted via a series of horizontally assigned pressurized bags filled with water. These pressurized water balloons, named as intermediate bag and main bag, respectively, are illustrated in Fig 2.5. The distribution of the pressure

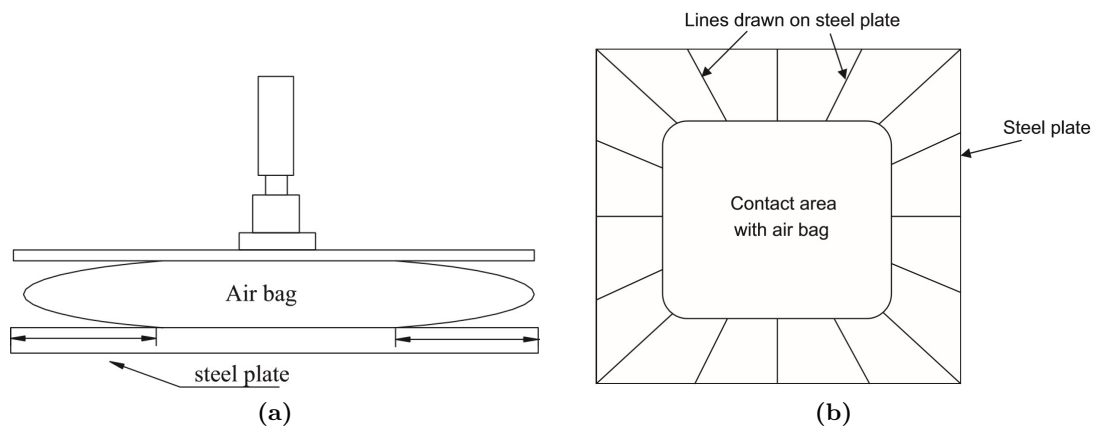


Figure 2.4: Contact area of airbags[27]

that applied on the plates can be improved if the intermediate bag which contacts directly with the specimen was slightly underpressurized. However, despite this measures, possible uneven distribution of the pressure, notable in corners, may still lead to inaccurate results. Besides, there may be some problems if the stringers side of the stiffened panel was subjected to the lateral pressure using the airbags.

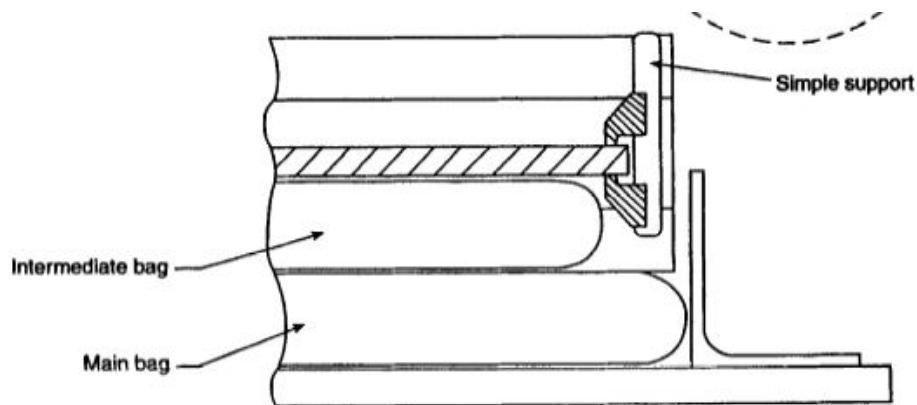


Figure 2.5: Buckling tests using multiple pressurized bags [28]

Pressurized Chamber

In order to completely avoid the potential non-uniform distributed pressure caused by the introduction of airbags, a pressure-box with one face cut off was developed for experimental investigation of the thin-walled structure. This type of pressurized chamber experimental equipment was manufactured for testing the failure load for curved and flat stiffened panels subjected to internal pressure and bi-axial tensile load. The testing specimen was bolted air-tight to the pressurized metal box, and the air pressure was controlled by pressure gauges as described by Rouse [37].

The method of pressure-box was also adopted by Reinoso et al. [29], in which composite

plates under pure pressure were tested to explore the effect of deformation on postbuckling behaviour as shown in Fig.2.6. Similar experiments also conducted via pressurized boxes were recorded by August [38], who designed a simple experimental setup to determine the deformation configuration of orthotropic plates with symmetrical constraints on the edges under uniform out-of-plane pressure. Ambur et al. [39] gave a summary in their paper on these facilities including pressurized chamber and D-box test fixture. Both of these tests have proved that the experimental fixtures can be used to determine the stresses of the specimen in a relatively inexpensive manner yet with reasonable accuracy in comparison with the COLTS facility. By using the pressure-box, stiffened panels made from metal [40] or composite [41] were both tested.

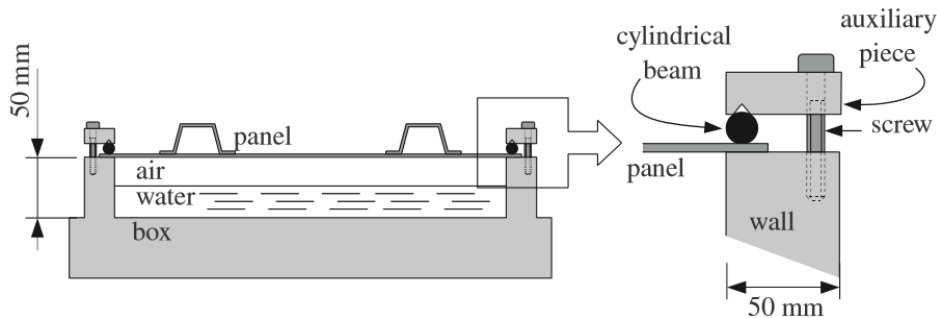


Figure 2.6: Pressurized Chamber[29]

Points loads

Although the experiments with the pressure box could provide an efficient test result, difficulties such as the air-tightness in case of the application of in-plane load still exist and sometimes limit their application in the combined loading environment. An alternative was proposed in literature using the lateral actuator as points loads instead of the airbags or pressure-boxes. A test system for such equipment was built by Shanmugam [42] to evaluate the ultimate strength of stiffened isotropic plates subjected to combined axial compression and lateral load. The axial compression load was applied through a thrust girder actuated by an actuator mounted at one side while extra caution was taken to guarantee that neutral axis of the bearing coincides with the actuator centre-line in order to avoid eccentricity. The lateral pressure was applied vertically as points loads as shown in Fig 2.7.

2.2 Theoretical Fundamentals

Before the implementation of the analysis, theoretical equations and expressions relied on the Kirchhoff assumption will be reviewed in terms of governing equations, stress-strain and force-displacement relations. These assumptions significantly simplify the mathematical expressions by reducing the three-dimensional plate problem to a two-dimensional one [4]. According to the magnitude of out-of-plane deflection in the plate, these expressions can be categorized into linear and nonlinear conditions for thin plates comprised of isotropic and composite materials.

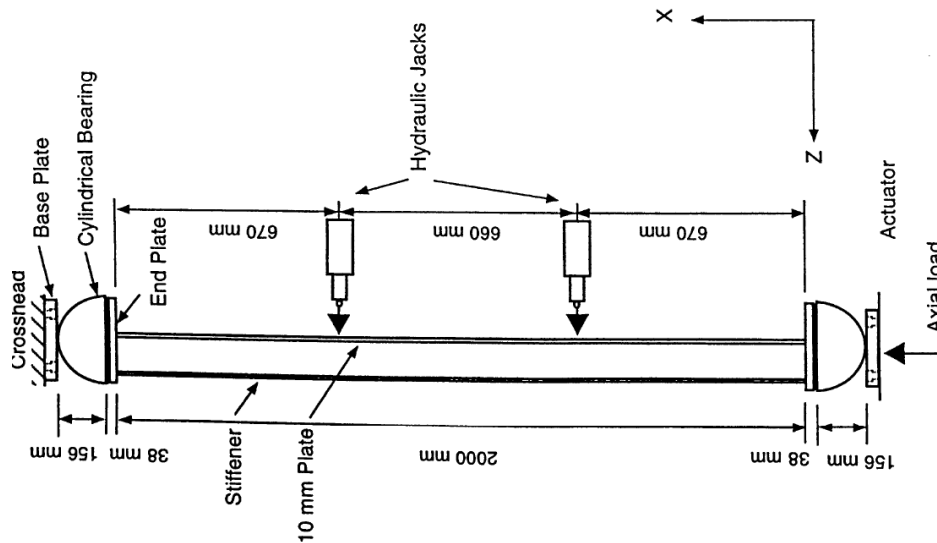


Figure 2.7: Buckling tests using multiple jacks [30]

Consider a rectangular thin plate with edges subjected to uniform edge loading and lateral pressure, the distribution of stresses is generally non-uniform, resulting in the necessity of deriving various static equilibrium equations to describe the relations between external loading and internal stresses and strains.

2.2.1 Isotropic Plates

For plates made of isotropic materials, mechanical properties are the same in all three mutually perpendicular directions. Thus the governing equations could be formed in a relatively simple mathematical manner. Consider a rectangular plate subjected to biaxial compression associated with uniform lateral pressure as shown in Fig 2.8. The starting point of the governing equations is the force equilibrium, the stress-strain equations and the strain-displacement equations. By combining the membrane forces which balances the externally applied loading and transverse shears generated from the lateral pressure and bending of the plate [11], [4] and [15], the static force and moment equilibrium equations are obtained and listed below.

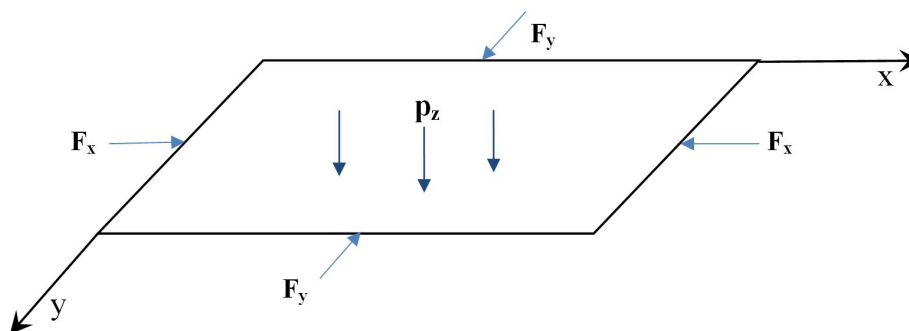


Figure 2.8: Coordinate system and external forces at the mid-plane of a rectangular plate

Equilibrium equations

In the case of a plate with small deflections, linear equations regarding the force equilibrium equations in three principle directions are formed as below by referring to section 8.2 of [11] and section 1.4 of [4].

$$\begin{aligned}\frac{\partial N_x}{\partial x} + \frac{\partial N_{xy}}{\partial y} &= 0 & (x \text{ direction}) \\ \frac{\partial N_{xy}}{\partial x} + \frac{\partial N_y}{\partial y} &= 0 & (y \text{ direction}) \\ \frac{\partial Q_x}{\partial x} + \frac{\partial Q_y}{\partial y} &= 0 & (z \text{ direction})\end{aligned}\quad (2.1)$$

in which N_x , N_y and N_{xy} are the in-plane forces per unit length while p_z stands for the uniform lateral pressure as shown in Fig 2.9. The shear forces of the plate element Q_x and Q_y can be expressed in terms of the moments, which are

$$\begin{aligned}Q_x &= \frac{\partial M_x}{\partial x} + \frac{\partial M_{xy}}{\partial y} \\ Q_y &= \frac{\partial M_{xy}}{\partial x} + \frac{\partial M_y}{\partial y}\end{aligned}\quad (2.2)$$

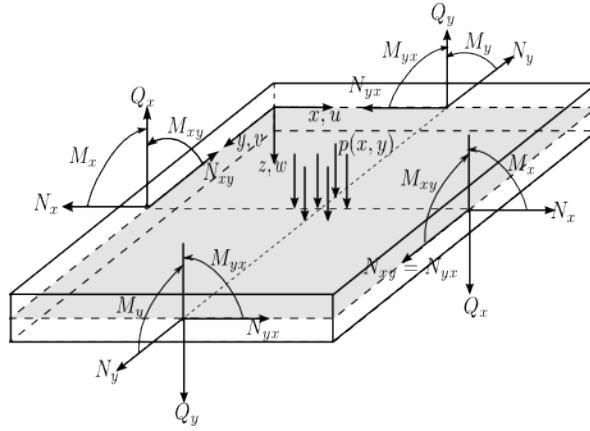


Figure 2.9: Force resultants acted on the plate element

The equations of bending moments resultants of the plate could be formed in terms of the curvatures and out-of-plane deflections w , as following.

$$\begin{aligned}M_x &= -D \left(\frac{\partial^2 w}{\partial x^2} + \nu \frac{\partial^2 w}{\partial y^2} \right) \\ M_y &= -D \left(\frac{\partial^2 w}{\partial y^2} + \nu \frac{\partial^2 w}{\partial x^2} \right) \\ M_{xy} &= D (1 - \nu) \frac{\partial^2 w}{\partial x \partial y}\end{aligned}\quad (2.3)$$

with flexural rigidity of the plate defined as below,

$$D = \frac{Eh^3}{12(1-\nu^2)} \quad (2.4)$$

In case of large deflections in instability problems such as postbuckling or situations when lateral pressure is significantly large, the equilibrium equations are rebuilt by adding nonlinear terms in the z direction (See section 7.4 of [4]).

$$\begin{aligned} \frac{\partial N_x}{\partial x} + \frac{\partial N_{xy}}{\partial y} &= 0 & (x \text{ direction}) \\ \frac{\partial N_{xy}}{\partial x} + \frac{\partial N_y}{\partial y} &= 0 & (y \text{ direction}) \\ \frac{\partial Q_x}{\partial x} + \frac{\partial Q_y}{\partial y} &= N_x \frac{\partial^2 w}{\partial x^2} + N_{xy} \frac{\partial^2 w}{\partial x \partial y} + N_y \frac{\partial^2 w}{\partial y^2} + p_z & (z \text{ direction}) \end{aligned} \quad (2.5)$$

where p_z is the distributed pressure load applied to the plate surface. By replacing the shear forces Q_x and Q_y by Eq.2.2 and Eq.2.3, the force equilibrium equation in z direction can be written as

$$D \nabla^4 w = N_x \frac{\partial^2 w}{\partial x^2} + N_{xy} \frac{\partial^2 w}{\partial x \partial y} + N_y \frac{\partial^2 w}{\partial y^2} + p_z \quad (2.6)$$

The biharmonic operator ∇ has the form of

$$\nabla^4 = \left(\frac{\partial^4}{\partial x^4} + 2 \frac{\partial^4}{\partial x^2 \partial y^2} + \frac{\partial^4}{\partial y^4} \right) \quad (2.7)$$

Compatible Equations

In order to guarantee the physical continuity of the plate, the compatible equation in which strain components are related together is formed by successive differentiation. For small deflection problems, compatible equation is formed as (See section 1.4 of [4]),

$$\frac{\partial^2 \varepsilon_{x0}}{\partial y^2} + \frac{\partial^2 \varepsilon_{y0}}{\partial x^2} - \frac{\partial^2 \gamma_{xy0}}{\partial x \partial y} = 0 \quad (2.8)$$

For large deflection, it becomes (See section 7.4 of [4]),

$$\frac{\partial^2 \varepsilon_{x0}}{\partial y^2} + \frac{\partial^2 \varepsilon_{y0}}{\partial x^2} - \frac{\partial^2 \gamma_{xy0}}{\partial x \partial y} = \left(\frac{\partial^2 w}{\partial x \partial y} \right)^2 - \frac{\partial^2 w}{\partial x^2} \frac{\partial^2 w}{\partial y^2} \quad (2.9)$$

Strain-displacement relations

Under the basis of Kirchhoff's hypotheses, the linear strains ϵ_{x0} , ϵ_{y0} and γ_{xy0} in the mid-plane of the plate can be expressed by the differentials of the in-plane displacements u_0 and v_0 .

$$\begin{aligned}\epsilon_{x0} &= \frac{\partial u_0}{\partial x} \\ \epsilon_{y0} &= \frac{\partial v_0}{\partial y} \\ \gamma_{xy0} &= \frac{\partial u_0}{\partial y} + \frac{\partial v_0}{\partial x}\end{aligned}\quad (2.10)$$

For a large deformation with a transverse displacement w , strain-displacement relations are formed as:

$$\begin{aligned}\epsilon_{x0} &= \frac{\partial u_0}{\partial x} + \frac{1}{2} \left(\frac{\partial w}{\partial x} \right)^2 \\ \epsilon_{y0} &= \frac{\partial v_0}{\partial y} + \frac{1}{2} \left(\frac{\partial w}{\partial y} \right)^2 \\ \gamma_{xy0} &= \frac{\partial u_0}{\partial y} + \frac{\partial v_0}{\partial x} + \left(\frac{\partial w}{\partial x} \right) \left(\frac{\partial w}{\partial y} \right)\end{aligned}\quad (2.11)$$

The stress function ϕ is introduced so that the force equilibrium equations are satisfied. Thus, the expressions of the in-plane loading could be rewritten as:

$$\begin{aligned}N_x &= h \frac{\partial^2 \phi}{\partial y^2} \\ N_y &= h \frac{\partial^2 \phi}{\partial x^2} \\ N_{xy} &= -h \frac{\partial^2 \phi}{\partial x \partial y}\end{aligned}\quad (2.12)$$

Upon the substitution of Eq. 2.12 into the equilibrium equation Eq.2.6, the first von Karman equation can then be derived as

$$\nabla^4 w = \frac{h}{D} \left(\frac{\partial^2 \Phi}{\partial y^2} \frac{\partial^2 w}{\partial x^2} - 2 \frac{\partial^2 \Phi}{\partial x \partial y} \frac{\partial^2 w}{\partial x \partial y} + \frac{\partial^2 \Phi}{\partial x^2} \frac{\partial^2 w}{\partial y^2} + \frac{p_z}{h} \right) \quad (2.13)$$

Noting that, according to Hooke's rule, the strain-loading relations at mid-plane of the plate are

$$\begin{aligned}
\varepsilon_{x0} &= \frac{1}{Eh} (N_x - \nu N_y) \\
\varepsilon_{y0} &= \frac{1}{Eh} (N_y - \nu N_x) \\
\gamma_{xy0} &= \frac{N_{xy}}{Gh} = \frac{2}{Eh} (1 + \nu) N_{xy}
\end{aligned} \tag{2.14}$$

Upon substitution of Eq.2.12 and Eq.2.14, the nonlinear equation of the compatibility of deformations involving the stress function are formed as follows:

$$\nabla^4 \phi = E \left[\left(\frac{\partial^2 w}{\partial x \partial y} \right)^2 - \frac{\partial^2 w}{\partial x^2} \frac{\partial^2 w}{\partial y^2} \right] \tag{2.15}$$

2.2.2 Composite Plates

Stress-strain relations

Unlike the isotropic plate, due to the anisotropic properties, the force and moment resultants for composite laminates which are related to the strains are expressed as [8],

$$\begin{bmatrix} N_x \\ N_y \\ N_{xy} \\ M_x \\ M_y \\ M_{xy} \end{bmatrix} = \begin{bmatrix} A_{11} & A_{12} & A_{16} & B_{11} & B_{12} & B_{16} \\ A_{12} & A_{22} & A_{26} & B_{12} & B_{22} & B_{26} \\ A_{16} & A_{26} & A_{66} & B_{16} & B_{26} & B_{66} \\ B_{11} & B_{12} & B_{16} & D_{11} & D_{12} & D_{16} \\ B_{12} & B_{22} & B_{26} & D_{12} & D_{22} & D_{26} \\ B_{16} & B_{26} & B_{66} & D_{16} & D_{26} & D_{66} \end{bmatrix} \begin{bmatrix} \varepsilon_{x0} \\ \varepsilon_{y0} \\ \gamma_{xy0} \\ \kappa_x \\ \kappa_0 \\ \kappa_{xy} \end{bmatrix} \tag{2.16}$$

in which the A matrix in the upper left corner of the stiffness matrix stands for the membrane stiffness of the laminate, the B matrix represents the membrane-bending coupling matrix while the D matrix is the bending matrix. In case of symmetric laminates, in which membrane-bending matrix vanishes, the stretching and bending responses decouple leading to the separate stress-strain equations rewritten as

$$\begin{bmatrix} N_x \\ N_y \\ N_{xy} \end{bmatrix} = \begin{bmatrix} A_{11} & A_{12} & A_{16} \\ A_{12} & A_{22} & A_{26} \\ A_{16} & A_{26} & A_{66} \end{bmatrix} \begin{bmatrix} \varepsilon_{x0} \\ \varepsilon_{y0} \\ \gamma_{xy0} \end{bmatrix} \tag{2.17}$$

and

$$\begin{bmatrix} M_x \\ M_y \\ M_{xy} \end{bmatrix} = \begin{bmatrix} D_{11} & D_{12} & D_{16} \\ D_{12} & D_{22} & D_{26} \\ D_{16} & D_{26} & D_{66} \end{bmatrix} \begin{bmatrix} \kappa_x \\ \kappa_0 \\ \kappa_{xy} \end{bmatrix} \tag{2.18}$$

Equilibrium equations

Force equilibrium equations for composite plates are same as those made of isotropic materials illustrated in Eq.2.1 and Eq.2.5. For balanced laminates in which D_{16} and D_{66} are assumed to be neglected, the moment resultants become:

$$\begin{aligned} M_x &= -D_{11} \frac{\partial^2 w}{\partial x^2} - D_{12} \frac{\partial^2 w}{\partial y^2} \\ M_x &= -D_{12} \frac{\partial^2 w}{\partial x^2} - D_{22} \frac{\partial^2 w}{\partial y^2} \\ M_{xy} &= -2D_{66} \frac{\partial^2 w}{\partial x \partial y} \end{aligned} \quad (2.19)$$

By replacing the shear loading Q_i items in Eq.2.5 using Eq.2.2 and Eq.2.19, the equilibrium equation of composite laminates experiencing lager deformation can be written as,

$$D_{11} \frac{\partial^4 w}{\partial x^4} + 2(D_{12} + 2D_{66}) \frac{\partial^4 w}{\partial x^2 \partial y^2} + D_{22} \frac{\partial^4 w}{\partial y^4} = N_x \frac{\partial^2 w}{\partial x^2} + N_{xy} \frac{\partial^2 w}{\partial x \partial y} + N_y \frac{\partial^2 w}{\partial y^2} + p_z \quad (2.20)$$

Compatible equations

The compatible equations for composite laminates have the same form with those of isotropic plates with both linear and nonlinear assumptions, that is,

For linear case,

$$\frac{\partial^2 \varepsilon_{x0}}{\partial y^2} + \frac{\partial^2 \varepsilon_{y0}}{\partial x^2} - \frac{\partial^2 \gamma_{xy0}}{\partial x \partial y} = 0 \quad (2.8)$$

For nonlinear case,

$$\frac{\partial^2 \varepsilon_{x0}}{\partial y^2} + \frac{\partial^2 \varepsilon_{y0}}{\partial x^2} - \frac{\partial^2 \gamma_{xy0}}{\partial x \partial y} = \left(\frac{\partial^2 w}{\partial x \partial y} \right)^2 - \frac{\partial^2 w}{\partial x^2} \frac{\partial^2 w}{\partial y^2} \quad (2.9)$$

According to Eq.2.17, the in-plane load-strain relations for a symmetric ($B_i = 0$) and balanced laminate ($A_{16} = A_{26} = 0$) gives:

$$\begin{aligned} N_x &= A_{11} \varepsilon_{x0} + A_{12} \varepsilon_{y0} \\ N_y &= A_{12} \varepsilon_{x0} + A_{22} \varepsilon_{y0} \\ N_{xy} &= A_{66} \gamma_{xy0} \end{aligned} \quad (2.21)$$

Thus, the mid-plane strains could be solved and expressed by the loading as,

$$\begin{aligned}
\varepsilon_{x0} &= \frac{A_{22}}{A_{11}A_{22} - A_{12}^2}N_x - \frac{A_{12}}{A_{11}A_{22} - A_{12}^2}N_y \\
\varepsilon_{y0} &= -\frac{A_{12}}{A_{11}A_{22} - A_{12}^2}N_x + \frac{A_{11}}{A_{11}A_{22} - A_{12}^2}N_y \\
\gamma_{xy0} &= \frac{1}{A_{66}}N_{xy}
\end{aligned} \tag{2.22}$$

Upon the substitution of the strains into the compatible equation combined with the stress function in Eq.2.12, the second von Karman equation that builds the connection between membrane behaviour and out-of-plane curvature of a rectangular laminate are obtained [8]:

$$\begin{aligned}
&\frac{A_{22}}{A_{11}A_{22} - A_{12}^2} \left(A_{22} \frac{\partial^4 \Phi}{\partial^4 y} - 2A_{12} \frac{\partial^4 \Phi}{\partial^2 x \partial^2 y} + A_{11} \frac{\partial^4 \Phi}{\partial^4 x} \right) + \frac{1}{A_{66}} \frac{\partial^4 \Phi}{\partial^2 x \partial^2 y} \\
&= \left(\frac{\partial^2 w}{\partial x \partial y} \right)^2 - \frac{\partial^2 w}{\partial x^2} \frac{\partial^2 w}{\partial y^2}
\end{aligned} \tag{2.23}$$

2.3 Summary

In this chapter, the methodology on how researchers have previously studied the stability problems regarding buckling and postbuckling behaviours for stiffened panels under combined in- and out-of-plane loading has been reviewed. Most of the researchers proposed their methods based on the governing differential equations with the results evaluated by employing the finite element software. It was found that stability behaviours of thin-walled structures can be significantly affected by the lateral pressure with a moderate amplitude. Limited number of experimental studies on buckling experiments of stiffened panels under combined loads can be found, and discussions were focused on the application of lateral pressure. Finally, a set of related fundamental theories and equations that will be utilized in the following analysis are briefly presented.

Buckling and Postbuckling Behaviour of Isotropic Plates

3.1 Introduction

As mentioned in Chapter 2, theoretical studies concerning the buckling behaviour of a stiffened panel subjected to combined loads are relatively rare especially for the cases when out-of-plane pressure is involved. For simplification, it is more convenient to start with an isotropic plate, which has fewer parameters in the governing equations. Primary analyses in this chapter will be devoted to the determination of the stability strength and load-deformation relation of a metal plate under the combination of lateral pressure and in-plane compression. In addition, interactive effects of these two loads on the buckling response will be studied by comparing predicted results with those under uniaxial compression alone.

One of the typical forms of stiffened panels, shown in Fig 3.1, is comprised of longitudinal stringers and transverse frames that are attached to the skin. The duplicated substructures that periodically occur along the longitudinal stiffeners could be considered as a representative unit substructure for analysis (See Fig 3.2). In this case, for further simplification, the substructure could be idealized as a single plate with certain boundary conditions which are dependent on the rotational stiffness of the adjacent stringers and the end frames.

The idealized plate is assumed to have a size of a $a \times b$ and a relatively small thickness h , subjected to uniaxial compression and simultaneous lateral pressure, sketched in Fig 3.3. The origin of the Cartesian coordinate system is assigned at one of the corners.

Analyses in this chapter are performed following the roadmap as shown in Fig 3.4, in which the stability problem of stiffened plates is transferred to a thin plate model. Approximations are presumed, enabling the validation of classical plate theories. Plate responses under uni-

axial compression and lateral pressure are investigated separately and then integrated. First, the linear elastic buckling analysis is carried out based on the linear elastic and small deflection assumption in which nonlinearities are not taken into consideration. Afterwards, plates undergoing large out-of-plane deformation due to the combined loads will be analyzed based on large deflection theories by means of theoretical and numerical methods. Predicted results are obtained in the form of load-shortening and load-deflection curves.



Figure 3.1: Stiffened panel of structural application [43]

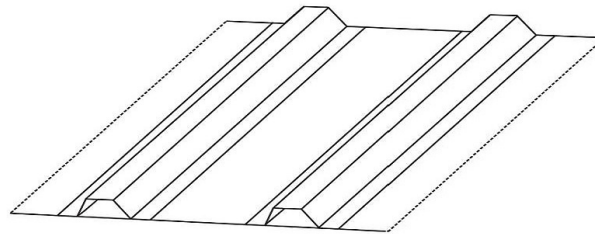


Figure 3.2: Unit stiffened panel [44]

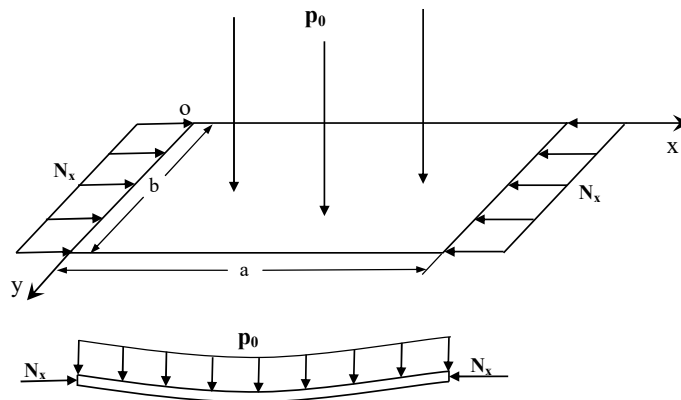


Figure 3.3: Combined forces acting on the flat plate

3.2 Plates under Uniaxial Compression

The main object of this section is to recall and list the buckling and postbuckling governing equations of a rectangular plate subjected to uniaxial compression.

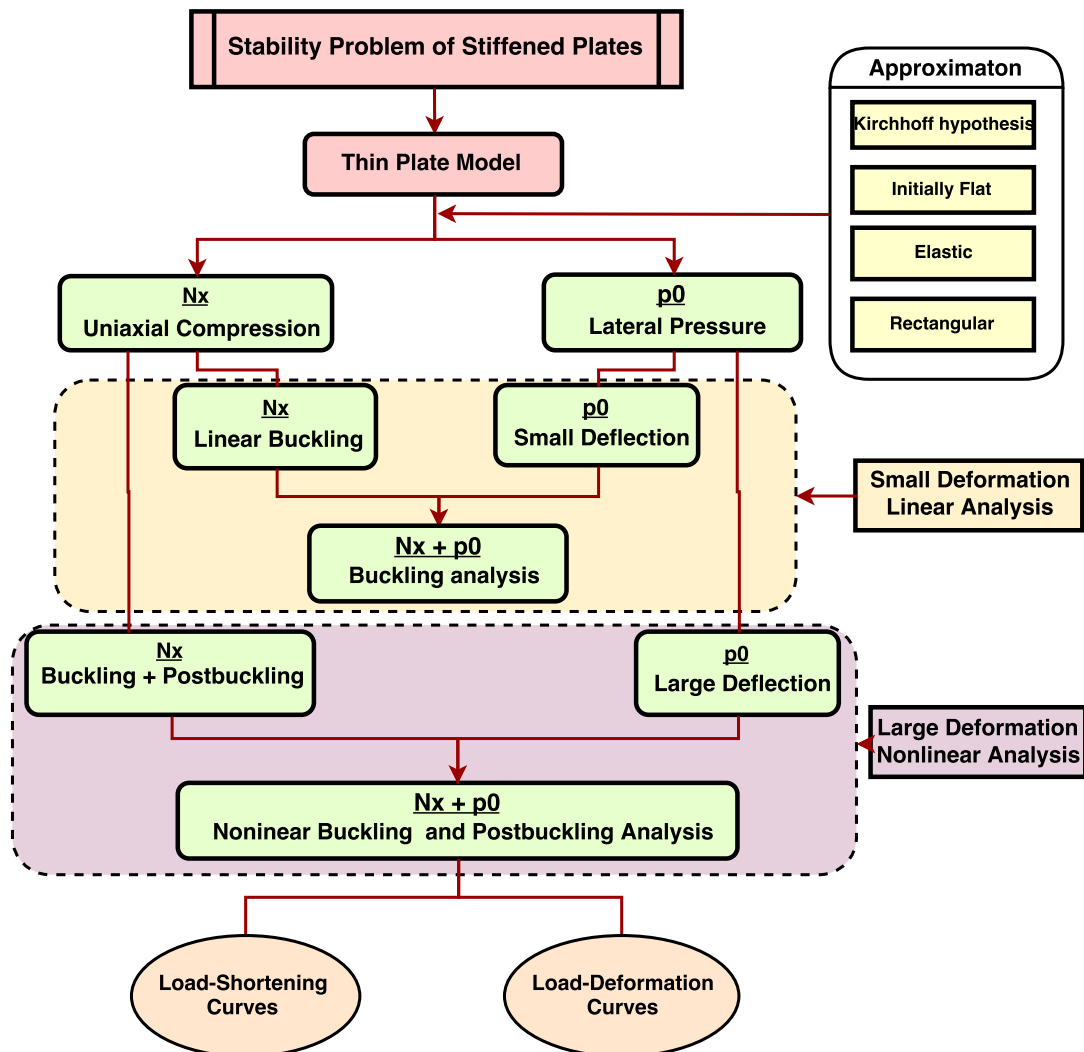


Figure 3.4: Roadmap of isotropic plate analysis

3.2.1 Buckling Analysis of Uniaxial Compressive Plates

Studies on the buckling strength of a rectangular plate under in-plane compression were started decades ago with solutions proposed in numerous references. One of the most commonly used methods for deriving the critical buckling load of thin plates is equilibrium method which is implemented by solving a fourth order partial differential equation, namely von Karman equation. The solving process of a critical buckling loading is presented by referring to the work in [4].

Consider a rectangular plate with simply supported edges subjected to in-plane loading acting in the middle plane of the plate. The first von Karman equation describing the linear buckling equilibrium configuration which has been introduced in Eq2.6 can be reorganized as functions

of in-plane loading and out-of-plane deflection,

$$\frac{\partial^4 w}{\partial x^4} + 2\frac{\partial^4 w}{\partial x \partial y} + \frac{\partial^4 w}{\partial y^4} = \frac{1}{D} \left(N_x \frac{\partial^2 w}{\partial x^2} - 2N_{xy} \frac{\partial^2 w}{\partial x \partial y} + N_y \frac{\partial^2 w}{\partial y^2} \right) \quad (3.1)$$

In the case of a uniaxial loaded plate, a simplified equation will be established in which N_y and N_{xy} vanish and longitudinal in-plane load N_x is the only applied force.

$$\frac{\partial^4 w}{\partial x^4} + 2\frac{\partial^4 w}{\partial x \partial y} + \frac{\partial^4 w}{\partial y^4} = \frac{1}{D} \left(N_x \frac{\partial^2 w}{\partial x^2} \right) \quad (3.2)$$

To satisfy the simply supported boundary conditions of the plate, a sum of linear Fourier function is presumed as deflections of the plate, which gives

$$w(x, y) = \sum_{m=1}^M \sum_{n=1}^N w_{mn} \sin\left(\frac{m\pi x}{a}\right) \sin\left(\frac{n\pi y}{b}\right) \quad (3.3)$$

The undetermined constants w_{mn} denote the magnitude of the displacement. M and N in the Fourier series are selected to meet the convergence requirement.

Upon the substitution of Eq.3.3, the governing equation Eq.3.2 gives

$$\sum_{m=1}^M \sum_{n=1}^N \left\{ D\pi^4 \left(\left(\frac{m}{a}\right)^2 + \left(\frac{n}{b}\right)^2 \right)^2 - N_x \pi^2 \frac{m^2}{a^2} \right\} w_{mn} \sin\frac{m\pi x}{a} \sin\frac{n\pi y}{b} = 0 \quad (3.4)$$

Nontrivial solutions are obtained by setting the quantity in the curly brace to zero, that is,

$$D\pi^4 \left(\left(\frac{m}{a}\right)^2 + \left(\frac{n}{b}\right)^2 \right)^2 - N_x \pi^2 \frac{m^2}{a^2} = 0 \quad (3.5)$$

or:

$$N_x = \frac{D\pi^2}{b^2} \left(\frac{mb}{a} + \frac{a}{mb} n^2 \right)^2 \quad (3.6)$$

Let the buckling parameter be defined as:

$$k_{cr} = \left(\frac{mb}{a} + \frac{a}{mb} n^2 \right)^2 \quad (3.7)$$

It is observed that every choice of m and n corresponds to a unique value of load N_x . Since the buckling load is defined as the minimum value of N_x , it can be obtained by setting $n = 1$ while the value of m is selected according to Fig 3.5.

It could be observed that for arbitrary plate aspect (integers), there always exists a value of "m" at which buckling parameter equals to 4, resulting in the critical buckling load N_{cr} to be:

$$N_{cr} = \frac{4D\pi^2}{b^2} \quad (3.8)$$

where $n = 1$ and $m = \frac{a}{b}$, which represent the number of half-waves in the longitudinal and transverse direction.

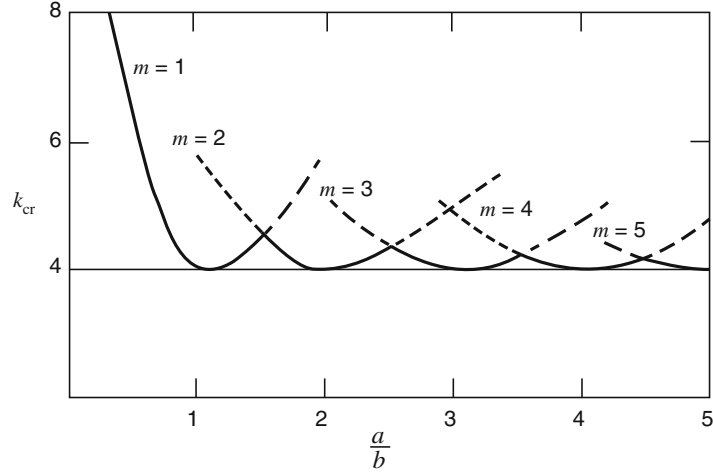


Figure 3.5: The buckling parameter versus the plate aspect ratio [45]

3.2.2 Postbuckling Analysis of Uniaxial Compressive Plates

The buckling analysis in the previous section addressed merely the loads at which buckling occurs. In practice, the additional strength of plates in the postbuckling region is of significant importance. After the occurrence of buckling, the center part of plates bulges out, leading to a redistributed stress field in the plate [4]. As a result, the postbuckling analysis should be paid more attention than that in buckling analysis since the interaction between bending and stretching are triggered by the plate deflection. This may lead to much more complicated mathematical equations. In this section, a simplified study on the postbuckling behaviour will be introduced by referring to the description in Section 8.1 of [4] and Section 7.1 of [8].

Consider a rectangular simply supported plate under uniaxial longitudinally compressive load, recall and rewrite the force equilibrium from Eq.2.13 and compatible equations from Eq.2.15 without accounting for the lateral pressure, that is:

$$\frac{D}{h} \nabla^4 w = \left(\frac{\partial^2 \phi}{\partial y^2} \frac{\partial^2 w}{\partial x^2} - 2 \frac{\partial^2 \phi}{\partial x \partial y} \frac{\partial^2 w}{\partial x \partial y} + \frac{\partial^2 \phi}{\partial x^2} \frac{\partial^2 w}{\partial y^2} \right) \quad (3.9)$$

and

$$\frac{1}{E} \nabla^4 \phi = \left(\frac{\partial^2 w}{\partial x \partial y} \right)^2 - \frac{\partial^2 w}{\partial x^2} \frac{\partial^2 w}{\partial y^2} \quad (3.10)$$

where $\phi = \frac{\Phi}{h}$ is the stress function.

For simplification, only the first term of the predicted deflection expression Eq.3.3 is utilized and substituted into compatible equation Eq.3.10, which is formed as:

$$\frac{1}{E} \nabla^4 \phi = w_{11}^2 \left(\frac{\pi^2}{ab} \right)^2 \left[\cos^2 \left(\frac{\pi x}{a} \right) \cos^2 \left(\frac{\pi y}{b} \right) - \sin^2 \left(\frac{\pi x}{a} \right) \sin^2 \left(\frac{\pi y}{b} \right) \right] \quad (3.11)$$

By carrying out the trigonometric calculation on the right hand of the above equation, a fourth differential equation of stress is formulated,

$$\frac{1}{E} \nabla^4 \phi = \frac{1}{2} w_{11}^2 \left(\frac{\pi^2}{ab} \right)^2 \left[\cos \left(\frac{2\pi x}{a} \right) + \cos \left(\frac{2\pi y}{b} \right) \right] \quad (3.12)$$

From the observation of Eq.3.12, it is convenient to assume the particular solution to the stress function in the form of:

$$\phi_p = C_1 \cos \frac{2\pi x}{a} + C_2 \cos \frac{2\pi y}{b} \quad (3.13)$$

The undetermined coefficients C_1 and C_2 could be easily derived through the substitution for the particular solution ϕ_p into Eq.3.12, that is,

$$\begin{aligned} C_1 &= \frac{E}{32} w_{11}^2 \left(\frac{a}{b} \right)^2 \\ C_2 &= \frac{E}{32} w_{11}^2 \left(\frac{b}{a} \right)^2 \end{aligned} \quad (3.14)$$

Knowing that an average compressive action N_x is subjected to the edges ($x = 0$ and $x = a$),

$$N_x = h \frac{\partial^2 \phi}{\partial y^2} \quad (3.15)$$

, the solution of the homogeneous Eq.3.12 becomes

$$\phi_a = -\frac{N_x y^2}{2h} \quad (3.16)$$

Therefore, the general equation of stress function in Eq.3.11 becomes,

$$\phi = \phi_p + \phi_a = -\frac{N_x y^2}{2h} + \frac{E}{32} w_{11}^2 \left(\frac{a}{b} \right)^2 \cos \frac{2\pi x}{a} + \frac{E}{32} w_{11}^2 \left(\frac{b}{a} \right)^2 \cos \frac{2\pi y}{b} \quad (3.17)$$

and the in-plane stress distribution in the plate will be expressed as:

$$\sigma_x = \frac{\partial^2 \phi}{\partial y^2} = -E \frac{\pi^2}{8} \left(\frac{w_{11}}{a} \right)^2 \cos \frac{2\pi x}{a} - \frac{q_x}{h} \quad (3.18)$$

$$\sigma_y = \frac{\partial^2 \phi}{\partial x^2} = -E \frac{\pi^2}{8} \left(\frac{w_{11}}{b} \right)^2 \cos \frac{2\pi y}{b} \quad (3.19)$$

$$\tau_{xy} = \frac{\partial^2 \phi}{\partial x \partial y} = 0 \quad (3.20)$$

The first item of the deflection coefficient w_{11} is derived by employing the Galerkin's method of which general procedural is referred to the textbook [4]. Here only the final Galerkin's equation will be listed.

$$\int_0^a \int_0^b E_{residual} \varphi dy dx = 0 \quad (3.21)$$

where

$$\varphi = \sin \frac{\pi x}{a} \sin \frac{\pi y}{b} \quad (3.22)$$

The residual error function $E_{residual}$ of Galerkin's method of the postbuckled plate can be formulated by using Eq.3.9, which gives:

$$E_{residual} = \frac{D}{h} \nabla^4 w - \left(\frac{\partial^2 \phi}{\partial y^2} \frac{\partial^2 w}{\partial x^2} - 2 \frac{\partial^2 \phi}{\partial x \partial y} \frac{\partial^2 w}{\partial x \partial y} + \frac{\partial^2 \phi}{\partial x^2} \frac{\partial^2 w}{\partial y^2} \right) \quad (3.23)$$

By substituting Eq.3.22 and Eq.3.23 into Eq.3.21, performing the double integral with respect to the field region and using the Dirac delta function yields the following equation,

$$D \frac{\pi^4 ab}{4} w_{11} \left(\frac{1}{a^2} + \frac{1}{b^2} \right)^2 - N_x w_{11} \frac{\pi^2 ab}{a^2} + E \frac{\pi^4 w_{11}^3}{64} h \left(\frac{1}{a^4} + \frac{1}{b^4} \right) ab = 0 \quad (3.24)$$

where the integral of trigonometric series have the values shown before:

$$\begin{aligned} \int_0^a \int_0^b \sin^2 \frac{\pi x}{a} \sin^2 \frac{\pi y}{b} dy dx &= \frac{ab}{4} \\ \int_0^a \int_0^b \sin^2 \frac{\pi x}{a} \sin^2 \frac{\pi y}{b} \cos \frac{2\pi x}{a} dy dx &= -\frac{ab}{8} \\ \int_0^a \int_0^b \sin \frac{\pi x}{a} \sin \frac{\pi y}{b} dy dx &= \frac{4ab}{\pi^2} \end{aligned} \quad (3.25)$$

Rearranging the equation by eliminating the nonzero parameters in the left side, one derives:

$$D \frac{\pi^4}{4} w_{11} \left(\frac{1}{a^2} + \frac{1}{b^2} \right)^2 - N_x w_{11} \frac{\pi^2}{4a^2} + E \frac{\pi^4 w_{11}^3}{64} h \left(\frac{1}{a^4} + \frac{1}{b^4} \right) = 0 \quad (3.26)$$

or

$$\frac{w_{11}}{h} \left(1 - \frac{N_x a^2}{4\pi^2 D} \right) + \left(\frac{w_{11}}{h} \right)^3 \frac{3(1-\nu^2)}{8} = 0 \quad (3.27)$$

The compression critical load can be exactly solved by assuming $w_{11} \neq 0$, that is,

$$N_{cr} = D \frac{\pi^2}{b^2} \left(\frac{b}{a} + \frac{a}{b} \right)^2 + E \frac{\pi^2 h}{16b^2} w_{11}^2 \left(\frac{b^2}{a^2} + \frac{a^2}{b^2} \right) \quad (3.28)$$

It is apparently observed from this parabolic function, within the range of postbuckling, the plate can sustain a compressive load more significant than that in buckling stage.

The intersection point when $w_{11} = 0$ indicates the critical load which has the form of:

$$N_{cr} = D \frac{\pi^2}{b^2} \left(\frac{b}{a} + \frac{a}{b} \right)^2 \quad (3.29)$$

By comparing with the buckling expression in Eq.3.6, it is observed that this equation is the particular case when the plate buckles with only one half wave in either direction. In case of a square plate, the buckling load formula tends to become Eq.3.6, which is,

$$N_{cr,squ} = \frac{4D\pi^2}{b^2} \quad (3.8)$$

3.3 Plates under Lateral Pressure

As described in [4], thin plates subjected to lateral loading sustain transverse forces via internal bending moments and stretches, depending on their flexural rigidity and deformed configuration. In the case of small deflection, the middle plane deforms slightly and thus membrane forces will vanish in the force equilibrium equations. In other words, the plate with small out-of-plane deformation could be considered as a stiff structure in which only internal bending moments are used to balance the external pressure load.

Under this presumption, the classical plate theory could provide accurate solutions by using the Navier method [11]. However, with the increase of deflection, e.g. ($w > 0.2h$), plates will deflect in such a way that the membrane forces start to play a role in balancing the transverse loads. Stretches in the midplane of the plate cannot be ignored and will become dominant as the deflection reaches a level of $w \approx h$. The inclusion of membrane stretches, coupled with the bending moments, make the mathematical analysis difficult and more attention should be paid to large deflection cases.

3.3.1 Small Deformation of Plates under Out-of-Plane Loading

Solutions to the small deflection function of a plate under pure lateral pressure have already been developed by Navier in 1820. The detailed demonstration could be found in a considerable number of studies such as [4]. Based on the classical plate theory, differential von Karman equations with merely the out-of-plane pressure item on the right-hand side is utilized to generate the relationship between deflection and normal loads.

Recall the governing equation where in-plane forces are approximated to be absent in the pressurized flat plate due to the small deformation.

$$D \nabla^4 w = p_z \quad (3.30)$$

For simply supported boundaries of the rectangular plate, approximate deflection and pressure expression are predicted as follows,

$$w = \sum_{m=1}^{\infty} \sum_{n=1}^{\infty} w_{mn} \sin\left(\frac{m\pi x}{a}\right) \sin\left(\frac{n\pi y}{b}\right) \quad (3.3)$$

and

$$p_z = \sum_{m=1}^{\infty} \sum_{n=1}^{\infty} q_{mn} \sin\left(\frac{m\pi x}{a}\right) \sin\left(\frac{n\pi y}{b}\right) \quad (3.31)$$

where the unknown coefficients q_{mn} of the double Fourier expansion are determined by multiplying the Fourier series a half-range sine series in x and y directions, which leads to a form as follows:

$$q_{mn} = \frac{4p_z}{ab} \int_0^a \int_0^b \sin\frac{m\pi x}{a} \sin\frac{n\pi y}{b} dy dx = \frac{16p_z}{\pi^2 mn} \quad (3.32)$$

in which m and n are taken as positive odd integers (See page 48 of [4]).

Upon substitution for w and p_z into the reduced governing equation 3.30, one obtains,

$$\sum_{m=1}^{\infty} \sum_{n=1}^{\infty} \left\{ w_{mn} \left(\pi^4 \left[\left(\frac{m}{a}\right)^2 + \left(\frac{n}{b}\right)^2 \right]^2 - \frac{q_{mn}}{D} \right) \sin\frac{m\pi x}{a} \sin\frac{n\pi y}{b} \right\} = 0 \quad (3.33)$$

The nontrivial solutions are derived by setting the constants in the bracket to be zero, leading to the deflection coefficients as:

$$w_{mn} = \frac{1}{\pi^4 D} \frac{q_{mn}}{\left(\frac{m^2}{a^2} + \frac{n^2}{b^2}\right)^2} = \frac{16p_z}{\pi^6 D} \left(\frac{m^2}{a^2} + \frac{n^2}{b^2}\right)^2 (mn) \quad (3.34)$$

Thus, upon substitution, the displacement field of the simply supported plate under small lateral pressure is obtained and shows linear relations with respect to the magnitude of pressure p_z .

$$w = \frac{16p_z}{\pi^6 D} \sum_{m=1,3,5,\dots}^{\infty} \sum_{n=1,3,5,\dots}^{\infty} \frac{1}{\left(\frac{m^2}{a^2} + \frac{n^2}{b^2}\right)^2} \sin\left(\frac{m\pi x}{a}\right) \sin\left(\frac{n\pi y}{b}\right) \quad (3.35)$$

It is easily observed that the center point of the plate ($x = \frac{a}{2}, y = \frac{b}{2}$) has the maximum deflection.

3.3.2 Large Deformation of Plates under Out-of-Plane Loading

Consider a rectangular plate subjected to a uniformly distributed pressure p_z . From the study in [4] (Section 7.4), an approximate method for predicting the load-deflection curve is presented as follows.

Recall the nonlinear governing equations of rectangular thin plates in Chapter 2,

$$D \nabla^4 w = N_x \frac{\partial^2 w}{\partial x^2} - 2N_{xy} \frac{\partial^2 w}{\partial x \partial y} + N_y \frac{\partial^2 w}{\partial y^2} + p_z \quad (3.36)$$

and

$$D \nabla^4 \phi = E \left[\left(\frac{\partial^2 w}{\partial x \partial y}\right)^2 - \frac{\partial^2 w}{\partial x^2} \frac{\partial^2 w}{\partial y^2} \right] \quad (3.37)$$

in which in-plane loads are expressed in terms of stresses ϕ :

$$\begin{aligned} N_x &= h \frac{\partial^2 \phi}{\partial y^2} \\ N_y &= h \frac{\partial^2 \phi}{\partial x^2} \\ N_{xy} &= -h \frac{\partial^2 \phi}{\partial x \partial y} \end{aligned} \quad (3.38)$$

To meet the simply supported boundary condition, the approximate function of displacement of the plate under lateral pressure is:

$$w = \sum_{m=1}^{\infty} \sum_{n=1}^{\infty} w_{mn} \sin\left(\frac{m\pi x}{a}\right) \sin\left(\frac{n\pi y}{b}\right) \quad (3.3)$$

For the sake of simplification, only the first term $w_{11} \sin \frac{\pi x}{a} \sin \frac{\pi y}{b}$ on the right-hand side is adopted.

By replacing the displacement w in Eq.3.36 and Eq.3.37, one obtains:

$$w_{11} D \pi^4 \left(\frac{1}{a^2} + \frac{1}{b^2} \right)^2 \varphi = h w_{11} \pi^2 \left(-\frac{\partial^2 \phi}{\partial y^2} \frac{\varphi}{a^2} - 2 \frac{\partial^2 \phi}{\partial x \partial y} \frac{\psi}{ab} - \frac{\partial^2 \phi}{\partial x^2} \frac{\varphi}{b^2} \right) + p_z \quad (3.39)$$

and

$$\nabla^4 \phi = w_{11}^2 \frac{E \pi^4}{a^2 b^2} (\psi^2 - \varphi^2) \quad (3.40)$$

in which

$$\varphi = \sin \frac{\pi x}{a} \sin \frac{\pi y}{b}, \quad \psi = \cos \frac{\pi x}{a} \cos \frac{\pi y}{b} \quad (3.41)$$

By carrying out the trigonometric operation, Eq.3.40 is rewritten as:

$$\nabla^4 \phi = \frac{1}{2} w_{11}^2 \frac{E \pi^4}{a^2 b^2} \left(\cos \frac{2\pi x}{a} + \cos \frac{2\pi y}{b} \right) \quad (3.42)$$

By using the same method in Section 3.2.2, solutions to Eq.3.42 are approximated as:

$$\phi = C_1 \cos \frac{2\pi x}{a} + C_2 \cos \frac{2\pi y}{b} \quad (3.43)$$

where C_1 and C_2 are referred to Eq.3.14. The constant parameters C_1 and C_2 are observed to have the relation of:

$$\begin{aligned} C_1 &= \frac{E}{32} w_{11}^2 \left(\frac{a}{b} \right)^2 \\ C_2 &= \frac{E}{32} w_{11}^2 \left(\frac{b}{a} \right)^2 \end{aligned} \quad (3.44)$$

Substitute the displacement expression w (Eq.3.3) and the approximate stress function ϕ (Eq.3.43) into the governing equations Eq.3.39, one obtains:

$$w_{11}D\pi^4\left(\frac{1}{a^2} + \frac{1}{b^2}\right)^2\varphi - hw_{11}\frac{4\pi^4}{a^2b^2}\varphi\left(C_1\cos\frac{2\pi x}{a} + C_2\cos\frac{2\pi y}{b}\right) - p_z = 0 \quad (3.45)$$

Consider the left-hand side of Eq.3.45 as the first term approximation of the residual error based on the Galerkin's method, which means that the residual errors E_{res1} is expressed in form of:

$$E_{res1} = w_{11}D\pi^4\left(\frac{1}{a^2} + \frac{1}{b^2}\right)^2\varphi - hw_{11}\frac{4\pi^4}{a^2b^2}\varphi\left(C_1\cos\frac{2\pi x}{a} + C_2\cos\frac{2\pi y}{b}\right) - p_z \quad (3.46)$$

Multiply the shape function $\sin\frac{\pi x}{a}\sin\frac{\pi y}{b}$ on both side of the Eq.3.46 and integrate them with respect to the plate region, that is:

$$\int_0^a \int_0^b E_{res1}\sin\frac{\pi x}{a}\sin\frac{\pi y}{b}dydx = 0 \quad (3.47)$$

Combination of Eq.3.46 and Eq.3.47 leads to

$$w_{11}D\left(\frac{\pi^2}{a^2} + \frac{\pi^2}{b^2}\right)^2 + w_{11}h\frac{2\pi^4}{a^2b^2}(C_1 + C_2) = \frac{16p_z}{\pi^2} \quad (3.48)$$

Eliminate the coefficients C_1 and C_2 by the replacement of Eq.3.44, the relation between maximum deflection of the plate and lateral pressure in terms of w_{11} and p_z gives

$$\pi^4w_{11}D\left(\frac{1}{a^2} + \frac{1}{b^2}\right)^2 + Ehw_{11}^3\frac{\pi^4}{16}\left(\frac{1}{a^4} + \frac{1}{b^4}\right) = \frac{16p_z}{\pi^2} \quad (3.49)$$

It is noted that the current maximum displacement denoted by w_{11} is an approximate value since only the first term of the Fourier series in Eq.3.3 was accounted.

For a square plate when $a = b$, the load-displacement relation becomes

$$\frac{w_{11}}{h} + \frac{3(1-\nu^2)}{8}\left(\frac{w_{11}}{h}\right)^3 = \frac{4p_z a^4}{\pi^6 D h} \quad (3.50)$$

or in another form as:

$$\frac{\pi^6}{16}\left(\frac{1}{3(1-\nu^2)}\frac{w_{11}}{h} + \frac{1}{8}\left(\frac{w_{11}}{h}\right)^3\right) = \frac{p_z a^4}{Eh^4} \quad (3.51)$$

Comparisons can be carried out by referring to the results of Ventsel et.al. [4] (for Eq.3.50) and Chia [15] (for Eq.3.51), as shown in Fig 3.6.

$$\frac{w_{11}}{h} + \frac{128(1-\nu^2)}{3\pi^4} \left(\frac{w_{11}}{h}\right)^3 = \frac{4p_z a^4}{\pi^6 D h} \quad (\text{Equation 7.91 [4]})$$

$$\frac{\pi^6}{16} \left(\frac{1}{3(1-\nu^2)} \frac{w_{11}}{h} + 0.06429 \left(\frac{w_{11}}{h}\right)^3 \right) = \frac{p_z a^4}{E h^4} \quad (\text{Equation 2.50 [15]})$$

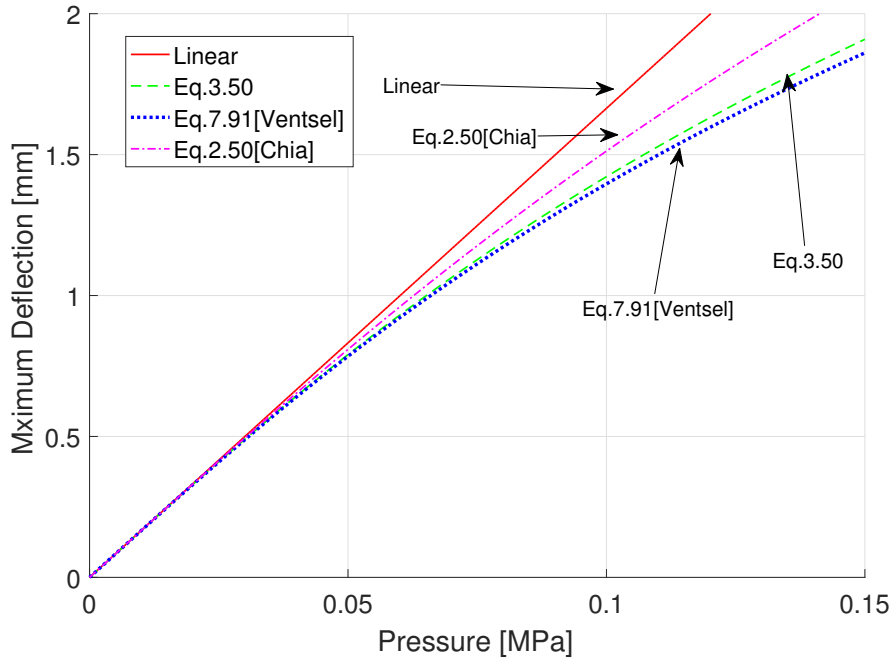


Figure 3.6: Central deflection versus uniform lateral pressure for simply supported square plate

In Fig 3.6, the linear curve is derived from Eq.3.34 by setting $m = 1$, $n = 1$ and $a = b$, that is $w_{11} = \frac{4p_z}{\pi^6 D}$. All curves agree well within the range of small pressure while significant discrepancies are observed as the pressure loading exceeds 0.05MPa . The prediction curve using Eq.3.50 compares fairly well with those in literature under relatively larger pressure loads.

3.4 Plates under Uniaxial Compression and Lateral Pressure

In this part, buckling and postbuckling analysis of a plate subjected to edge compression and lateral pressure will be performed. In view of the fact that the introduction of lateral loading will bring considerable mathematical difficulties into the solving process of governing equations, certain approximations would be required. For small deformations of the plate under the combined action of lateral pressure and longitudinal edge compression, classical plate theory remains valid and is capable of generating sufficiently accurate results. With the increase of lateral pressure, the initially flat plate deflects to a certain extent that can

be considered as a geometry imperfection, affecting the buckling and postbuckling responses of the plate. In most of the cases, the critical buckling loading of plates with geometric imperfections could not be identified explicitly, and load-shortening or load-deflection curves are adopted to describe their stability behaviours.

In this section, the method of seeking buckling load of plates under small lateral pressure is introduced based on the classical plate theory by referring to the literature in [11]. Afterward, the postbuckling behaviour of plates with large deformation will be investigated analytically under certain approximations.

3.4.1 Buckling Analysis of Plates under Combined Loads

Based on the description in [9, 11], two approaches, namely governing differential equation method and energy method, are employed to cope with the linear buckling behaviour of a rectangular plate under combined in-plane and out-of-plane loads. The governing differential equation method is based on the equilibrium equations while the energy method is solved using the Ritz method.

Equilibrium Method

The differential equation, in a simply supported rectangular plate subjected to constant uniaxial compression and lateral uniform distributed pressure, can be written as

$$\nabla^4 w + \left(\frac{N_x}{D}\right) \frac{\partial^2 w}{\partial x^2} = \frac{p_z}{D} \quad (3.52)$$

Solutions to Eq.3.52 must satisfy the boundary conditions for all edges, giving rise to the out-of-plane displacement in the form of the same configuration as in Eq.3.3.

$$w(x, y) = \sum_{m=1}^{\infty} \sum_{n=1}^{\infty} w_{mn} \sin\left(\frac{m\pi x}{a}\right) \sin\left(\frac{n\pi y}{b}\right) \quad (3.3)$$

Similarly, the lateral pressure is assumed in the form of:

$$p_z = \sum_{m=1}^{\infty} \sum_{n=1}^{\infty} q_{mn} \sin\left(\frac{m\pi x}{a}\right) \sin\left(\frac{n\pi y}{b}\right) \quad (3.53)$$

q_{mn} are the coefficients of pressure, which are determined by the technique of multiplying both sides of the equation by the trial function $\sin(m\pi x/a) \sin(n\pi y/b)$ [45]. By using orthogonality properties of the trigonometric functions and integrating 3.53 over the domain of the plate, q_{ij} is solved as

$$q_{mn} = \frac{4}{ab} \int_0^a \int_0^b p_z \sin\frac{m\pi x}{a} \sin\frac{n\pi y}{b} dy dx \quad (3.54)$$

In case of uniformly distributed pressure when p_z is a constant,

$$q_{mn} = \frac{4p_z}{ab} \int_0^a \int_0^b \sin \frac{m\pi x}{a} \sin \frac{n\pi y}{b} dy dx = \frac{16p_z}{\pi^2 mn} \quad (3.55)$$

in which m and n are odd integers for nonzero q_{mn} .

Upon the substitution for Eq.3.3 and Eq.3.53 into the left-hand side of Eq.3.52, the governing equation Eq.3.52 is reorganized into the form of:

$$\sum_{m=1}^{\infty} \sum_{n=1}^{\infty} \left\{ w_{mn} \left[\pi^4 \left(\left(\frac{m}{a} \right)^2 + \left(\frac{n}{b} \right)^2 \right)^2 - \pi^2 \frac{N_x}{D} \left(\frac{m}{a} \right)^2 \right] - \frac{q_{mn}}{D} \right\} \sin \frac{m\pi x}{a} \sin \frac{n\pi y}{b} = 0 \quad (3.56)$$

Thus, the nontrivial solutions for all the x and y are obtained by setting the items in the curly brace into zero, which gives:

$$w_{mn} = \frac{1}{\pi^4 D} \frac{q_{mn}}{\left[\left(\frac{m^2}{a^2} + \frac{n^2}{b^2} \right)^2 - \frac{N_x}{\pi^2 D} \left(\frac{m}{a} \right)^2 \right]} \quad (3.57)$$

Replace the coefficients q_{mn} by Eq.3.55, the function of displacement $w(x, y)$ of the plate becomes:

$$w(x, y) = \frac{16p_z}{\pi^6 D} \sum_{m=1,3,5,\dots}^{\infty} \sum_{n=1,3,5,\dots}^{\infty} \frac{\sin \left(\frac{m\pi x}{a} \right) \sin \left(\frac{n\pi y}{b} \right)}{\left[\left(\frac{m^2}{a^2} + \frac{n^2}{b^2} \right)^2 - \frac{N_x}{\pi^2 D} \left(\frac{m}{a} \right)^2 \right] (mn)} \quad (3.58)$$

In this equation, the sign of N_x is taken positive when it is compression. It could be observed when the denominator vanishes the displacement approaches infinity, which triggers the buckling phenomenon. The critical load N_{cr} will be determined by:

$$\left(\frac{m^2}{a^2} + \frac{n^2}{b^2} \right)^2 - \frac{N_{cr}}{\pi^2 D} \left(\frac{m}{a} \right)^2 = 0 \quad (3.59)$$

Rearrangement makes it become identical to the critical load of uniaxially loaded plate as illustrated in Eq.3.6 in Section 3.2.1,

$$N_{cr} = \frac{\pi^2 D}{b^2} \left[m \left(\frac{b}{a} \right) + \frac{n^2}{m} \left(\frac{a}{b} \right) \right]^2 = k_{cr} \frac{\pi^2 D}{b^2} \quad (3.60)$$

The identical expression of buckling load in both uniaxially compressive plates and those under combined loads suggests that the lateral pressure does not affect the buckling strength. The reason may attribute to the assumption of classical theory and small out-of-plane deformation. Flat plates with moderate or large deformation will be discussed in the next section.

Energy methods

Strain energy in isotropic plate

In a two dimensional elastic plate, the strain energy is expressed as the product of stresses and strains, integrated within the plate region.

$$U = \frac{1}{2} \iiint_V \{ \sigma_x \varepsilon_x + \sigma_y \varepsilon_y + \tau_{xy} \varepsilon_{xy} \} dV \quad (3.61)$$

in which σ_x , σ_y and τ_{xy} stand for the average normal and shear stresses.

Stress-strain relations are given as:

$$\sigma_x = \frac{E}{1 - \nu^2} (\varepsilon_x + \nu \varepsilon_y), \quad \sigma_y = \frac{E}{1 - \nu^2} (\varepsilon_y + \nu \varepsilon_x), \quad \tau_{xy} = \frac{E}{2(1 + \nu)} \gamma_{xy}, \quad (3.62)$$

where ν is the Poisson's ratio.

Since stretches in the plate mid-plane have been assumed to be neglected due to the small deflection, the strains as a result become zero, that is,

$$\varepsilon_{x0} = \varepsilon_{y0} = \gamma_{xy0} = 0 \quad (3.63)$$

where ε_{x0} , ε_{y0} and γ_{xy0} stand for the strains in the midplane of the plate.

On top of this, the strains through the thickness of the plate therefore become:

$$\varepsilon_x = -z \frac{\partial^2 w}{\partial x^2}, \quad \varepsilon_y = -z \frac{\partial^2 w}{\partial y^2}, \quad \gamma_{xy} = -2z \frac{\partial^2 w}{\partial x \partial y} \quad (3.64)$$

Substitute the combination of Eq.3.62, Eq.3.63 and Eq.3.64 into Eq.3.61 and carry out the integration with respect to z through the total thickness of the plate, the strain energy for an isotropic plate is then formulated as:

$$U = \frac{1}{2} \int_0^a \int_0^b D \left\{ \left(\frac{\partial^2 w}{\partial x^2} + \frac{\partial^2 w}{\partial y^2} \right)^2 - 2(1 - \nu) \left[\left(\frac{\partial^2 w}{\partial x^2} \right) \left(\frac{\partial^2 w}{\partial y^2} \right) - \left(\frac{\partial^2 w}{\partial x \partial y} \right)^2 \right] \right\} dx dy \quad (3.65)$$

It is noteworthy that the second item on the right-hand side of Eq.3.65 is defined as Gaussian curvature which would be zero if the edges of the plate are simply supported.

$$\left(\frac{\partial^2 w}{\partial x^2} \right) \left(\frac{\partial^2 w}{\partial y^2} \right) - \left(\frac{\partial^2 w}{\partial x \partial y} \right)^2 = 0 \quad (3.66)$$

As a result, the strain energy stored in the plate under small deformation gives:

$$U = \frac{1}{2} D \int_0^a \int_0^b (\nabla^2 w)^2 dx dy \quad (3.67)$$

with Laplace operator expressed as

$$\nabla^2 w = \Delta w = \left(\frac{\partial^2 w}{\partial x^2} + \frac{\partial^2 w}{\partial y^2} \right) \quad (3.68)$$

Potential energy due to external forces in isotropic plate

The work done by external loads, equal to the change in potential energy of external forces, is calculated by integrating the incremental energy,

$$\delta W_{ex} = \iiint_V \{p_x \delta u + p_y \delta v + p_z \delta w\} dV \quad (3.69)$$

where p_x and p_y stands for the external force acting on the plate edges along the coordinate axes. δu , δv and δw represent the increment displacement in x , y and z axis.

The potential energy function due to external forces is given by referring to the equations in Section 8.3 of [11],

$$V = - \iint_A \left[p_z w + \frac{p_x}{2} \left(\frac{\partial w}{\partial x} \right)^2 \right] dx dy \quad (3.70)$$

where V denotes the potential energy of the plate under uniaxial load p_x and lateral pressure p_z .

Minimal potential energy principle

The total potential energy is constituted by

$$\Pi = U + V \quad (3.71)$$

For isotropic plate, by substituting Eq.3.67 and Eq.3.70 into Eq.3.71, the potential energy becomes

$$\Pi = \iint_A \left[\frac{D}{2} \left(\frac{\partial^2 w}{\partial x^2} + \frac{\partial^2 w}{\partial y^2} \right)^2 - p_z w(x, y) - \frac{N_x}{2} \left(\frac{\partial w}{\partial x} \right)^2 \right] dx dy \quad (3.72)$$

Replace w by the double Fourier series function of displacement 3.3 and rewrite the total potential energy equation, one obtains

$$\Pi = \iint_A \left\{ \begin{aligned} & \frac{D}{2} \left[\left(\frac{m\pi}{a} \right)^2 \sum w_{mn} \sin\left(\frac{m\pi x}{a}\right) \sin\left(\frac{n\pi y}{b}\right) \right. \\ & \left. + \left(\frac{n\pi}{b} \right)^2 \sum w_{mn} \sin\left(\frac{m\pi x}{a}\right) \sin\left(\frac{n\pi y}{b}\right) \right]^2 \\ & - p_z \sum w_{mn} \sin\left(\frac{m\pi x}{a}\right) \sin\left(\frac{n\pi y}{b}\right) \\ & \left. - \frac{N_x}{2} \left(\frac{m\pi}{a} \right)^2 \left[\sum w_{mn} \sin\left(\frac{m\pi x}{a}\right) \sin\left(\frac{n\pi y}{b}\right) \right]^2 \right\} dx dy \quad (3.73) \end{aligned} \right.$$

By virtue of orthogonality properties of trigonometric functions, further simplification leads to

$$\Pi = \frac{D}{2} \left[\frac{ab}{4} w_{mn}^2 \left(\left(\frac{m\pi}{a} \right)^2 + \left(\frac{n\pi}{b} \right)^2 \right)^2 \right] - p_z \frac{4ab}{mn\pi^2} w_{mn} - \frac{N_x}{2} \frac{ab}{4} \left(\frac{m\pi}{a} \right)^2 w_{mn}^2 \quad (3.74)$$

where the following integration of trigonometric function is used

$$\int_0^b \int_0^a \sum \sum \sin^2\left(\frac{m\pi x}{a}\right) \sin^2\left(\frac{n\pi y}{b}\right) dx dy = \frac{ab}{4} \quad (3.75)$$

$$\int_0^b \int_0^a \sum \sum \sin\left(\frac{m\pi x}{a}\right) \sin\left(\frac{n\pi y}{b}\right) dx dy = \begin{cases} \frac{4ab}{\pi^2 mn} & (m \text{ and } n \text{ are odd}) \\ 0 & (m \text{ and } n \text{ are even}) \end{cases} \quad (3.76)$$

In the equilibrium configuration state of the plate, potential energy Π arrives at stationary points and the extreme values are obtained by setting the first variation with respect to the undetermined coefficients to zero, that is

$$\frac{\partial \Pi}{\partial w_{mn}} = 0 \quad (3.77)$$

By substituting Eq.3.74 into Eq.3.77, the non-trial deflection coefficients w_{mn} can be obtained as:

$$w_{mn} = \frac{\frac{16p_z}{mn\pi^2}}{D \left(\left(\frac{m\pi}{a} \right)^2 + \left(\frac{n\pi}{b} \right)^2 \right)^2 - N_x \left(\frac{m\pi}{a} \right)^2} \quad (3.78)$$

Note that N_x is compressed load with a positive sign. In this equations, it could be observed that the buckling takes place when the denominator of the deflection parameters tend to be zero, that is

$$D \left(\left(\frac{m\pi}{a} \right)^2 + \left(\frac{n\pi}{b} \right)^2 \right)^2 - N_x \left(\frac{m\pi}{a} \right)^2 = 0 \quad (3.79)$$

Comparison between Eq.3.79 and Eq.3.59 shows that the critical load obtained from the energy method is identical to that with governing equations, which is expressed as:

$$N_{cr} = \frac{\pi^2 D}{b^2} \left[m \left(\frac{b}{a} \right) + \frac{n^2}{m} \left(\frac{a}{b} \right) \right]^2 = k_{cr} \frac{\pi^2 D}{b^2} \quad (3.80)$$

where k_{cr} is the buckling coefficient.

3.4.2 Postbuckling Analysis of Plates under Combined Loads

Compared with the postbuckling phenomenon of plates subjected to uniaxial compression, additional lateral force will be involved in the governing equations of plates under combined loads. Recall and rewrite the force equilibrium from Eq.2.13 and compatible equations from Eq.2.15,

$$\frac{D}{h} \nabla^4 w = \left(\frac{\partial^2 \phi}{\partial y^2} \frac{\partial^2 w}{\partial x^2} - 2 \frac{\partial^2 \phi}{\partial x \partial y} \frac{\partial^2 w}{\partial x \partial y} + \frac{\partial^2 \phi}{\partial x^2} \frac{\partial^2 w}{\partial y^2} \right) + \frac{p_z}{h} \quad (3.81)$$

and

$$\frac{1}{E} \nabla^4 \phi = \left(\frac{\partial^2 w}{\partial x \partial y} \right)^2 - \frac{\partial^2 w}{\partial x^2} \frac{\partial^2 w}{\partial y^2} \quad (3.82)$$

Analogous to the aforementioned method, only the first term of the predicted deflection in Eq.3.3 is adopted and substituted into compatible equation Eq.3.82, which gives:

$$\frac{1}{E} \nabla^4 \phi = w_{11}^2 \left(\frac{\pi^2}{ab} \right)^2 \left[\cos^2 \left(\frac{\pi x}{a} \right) \cos^2 \left(\frac{\pi y}{b} \right) - \sin^2 \left(\frac{\pi x}{a} \right) \sin^2 \left(\frac{\pi y}{b} \right) \right] \quad (3.83)$$

Reorganizing the trigonometric function on the right hand,

$$\frac{1}{E} \nabla^4 \phi = \frac{1}{2} w_{11}^2 \left(\frac{\pi^2}{ab} \right)^2 \left[\cos \left(\frac{2\pi x}{a} \right) + \cos \left(\frac{2\pi y}{b} \right) \right] \quad (3.84)$$

Assume the solutions to the stress function in Eq.3.82 has the form of:

$$\phi_p = C_1 \cos \frac{2\pi x}{a} + C_2 \cos \frac{2\pi y}{b} \quad (3.85)$$

The undetermined coefficients C_1 and C_2 could be easily derived through the substitution for the particular solution ϕ_p back into Eq.3.84, which gives

$$\begin{aligned} C_1 &= \frac{E}{32} w_{11}^2 \left(\frac{a}{b}\right)^2 \\ C_2 &= \frac{E}{32} w_{11}^2 \left(\frac{b}{a}\right)^2 \end{aligned} \quad (3.86)$$

Recall the average compression N_x subjected on the edges ($x = 0$ and $x = a$),

$$N_x = h \frac{\partial^2 \phi}{\partial y^2} \quad (3.87)$$

And the homogeneous solution of Eq.3.84 becomes

$$\phi_a = -\frac{N_x y^2}{2h} \quad (3.88)$$

which constitutes the general equation of stress function in Eq.3.83, that is

$$\phi = \phi_p + \phi_a = -\frac{N_x y^2}{2h} + \frac{E}{32} w_{11}^2 \left(\frac{a}{b}\right)^2 \cos \frac{2\pi x}{a} + \frac{E}{32} w_{11}^2 \left(\frac{b}{a}\right)^2 \cos \frac{2\pi y}{b} \quad (3.89)$$

By using the same method of Section.3.2.2 and employing the Galerkin's method (referred to the textbook [4]), one obtains

$$\int_0^a \int_0^b E_{residual} \sin \frac{\pi x}{a} \sin \frac{\pi y}{b} dy dx = 0 \quad (3.90)$$

The residual error function $E_{residual}$ of Galerkin method of the postbuckled plate can be formulated by using Eq.3.11, which gives:

$$E_{residual} = \frac{D}{h} \nabla^4 w - \left(\frac{\partial^2 \phi}{\partial y^2} \frac{\partial^2 w}{\partial x^2} - 2 \frac{\partial^2 \phi}{\partial x \partial y} \frac{\partial^2 w}{\partial x \partial y} + \frac{\partial^2 \phi}{\partial x^2} \frac{\partial^2 w}{\partial y^2} \right) - \frac{p_z}{h} \quad (3.91)$$

After the replacement of w and ϕ by $w_{11} \sin \frac{\pi x}{a} \sin \frac{\pi y}{b}$ and Eq.3.89, the residual expression become:

$$\begin{aligned} E_{residual} &= D \frac{\pi^4}{h} w_{11} \left(\frac{1}{a^2} + \frac{1}{b^2} \right)^2 \varphi - \frac{N_x}{h} w_{11} \frac{\pi^2}{a^2} \varphi \\ &\quad - E \frac{\pi^4 w_{11}^3}{8} \left[\frac{1}{a^4} \cos \left(\frac{2\pi y}{b} \right) + \frac{1}{b^4} \cos \left(\frac{2\pi x}{a} \right) \right] \varphi - \frac{p_z}{h} = 0 \end{aligned} \quad (3.92)$$

By combining Eq.3.92 with Eq.3.90, one obtains:

$$D \frac{ab\pi^4}{4h} w_{11} \left(\frac{1}{a^2} + \frac{1}{b^2} \right)^2 - N_x w_{11} \frac{ab\pi^2}{4ha^2} + E w_{11}^3 \frac{ab\pi^4}{64} \left(\frac{1}{a^4} + \frac{1}{b^4} \right) = \frac{4p_z ab}{h\pi^2} \quad (3.93)$$

where the integral of trigonometric series have the values shown in Eq.3.94

$$\begin{aligned} \int_0^a \int_0^b \sin^2 \frac{\pi x}{a} \sin^2 \frac{\pi y}{b} dy dx &= \frac{ab}{4} \\ \int_0^a \int_0^b \sin^2 \frac{\pi x}{a} \sin^2 \frac{\pi y}{b} \cos \frac{2\pi x}{a} dy dx &= -\frac{ab}{8} \\ \int_0^a \int_0^b \sin^2 \frac{\pi x}{a} \sin^2 \frac{\pi y}{b} \cos \frac{2\pi y}{b} dy dx &= -\frac{ab}{8} \\ \int_0^a \int_0^b \sin \frac{\pi x}{a} \sin \frac{\pi y}{b} dy dx &= \frac{4ab}{\pi^2} \end{aligned} \quad (3.94)$$

After rearrangement, Eq.3.93 becomes

$$D \frac{\pi^4}{4} w_{11} \left(\frac{1}{a^2} + \frac{1}{b^2} \right)^2 - N_x w_{11} \frac{\pi^2}{4a^2} + E \frac{\pi^4 w_{11}^3}{64} h \left(\frac{1}{a^4} + \frac{1}{b^4} \right) = \frac{4p_z}{\pi^2} \quad (3.95)$$

In the case of a square plate when $a = b$, the load-deflection function is given by:

$$\frac{w_{11}}{h} \left(1 - \frac{N_x a^2}{4\pi^2 D} \right) + \left(\frac{w_{11}}{h} \right)^3 \frac{3(1-\nu^2)}{8} = \frac{4a^4 p_z}{\pi^6 D h} \quad (3.96)$$

The load-deflection formulae of simply supported plates derived from the simplified analysis with nonlinearity taken into consideration are listed in Table 3.1.

External Forces	Plate Configurations	Load-Deflection Relations	Equations
N_x	$a = b$	$\frac{w_{11}}{h} \left(1 - \frac{N_x a^2}{4\pi^2 D} \right) + \left(\frac{w_{11}}{h} \right)^3 \frac{3(1-\nu^2)}{8} = 0$	Eq.3.27
p_z	$a = b$	$\frac{w_{11}}{h} + \left(\frac{w_{11}}{h} \right)^3 \frac{3(1-\nu^2)}{8} = \frac{4a^4 p_z}{\pi^6 D h}$	Eq.3.50
$N_x + p_z$	$a = b$	$\frac{w_{11}}{h} \left(1 - \frac{N_x a^2}{4\pi^2 D} \right) + \left(\frac{w_{11}}{h} \right)^3 \frac{3(1-\nu^2)}{8} = \frac{4a^4 p_z}{\pi^6 D h}$	Eq.3.96

Table 3.1: Load-deflection relations under various load cases

In the case of square plates ($a = b$), the maximum deflections of the plate are represented by the coefficient w_{11} . It is observed that the components of these expressions in Table 3.1 could be categorized into three items according to the power of w_{11} , namely linear, cubic and constant parts. The linear part ($\frac{w_{11}}{h}$) dominates the magnitude of the deflection behaviour while the cubic item only acts as a nonlinear correlation coefficient which can approximately vanish in case of small deformation. The constant part, containing the lateral pressure, provides an initial offset of the out-of-plane deflection.

3.5 Finite Element Analysis

Finite element method (FEM) has been commonly used to assess the stability behaviour of thin plates under various load cases. In this section, validation of the analytical buckling and postbuckling analysis based on plate theories will be implemented by comparing the solutions with simulated results from finite element commercial code Abaqus [46]. Both Abaqus standard and Abaqus explicit modules are utilized. The former module is applied to dealing with the linear buckling problems while the latter one has advanced benefits to nonlinear postbuckling simulation.

Two plates with aspect ratios of 1 ($a = b$) and 4 ($a = 4b$) are modeled in Abaqus in order to conduct the comparison of the FE simulation results to analytical expressions obtained in previous section and literature of [13]. Excepted for the geometry size, these two models share the identical parameter setting and loading cases. Therefore, for simplification, the description of the square model is omitted, and only the modeling of a rectangular plate will be addressed.

The analysis of this part is organized in the following order. In Section 3.5.1, the finite element model regarding the geometry size, material property and mesh type & size is depicted, followed by the definition of boundary conditions (BCs). Based on the same models, simulation will be conducted under various load cases and results are displayed in the form of load-deformation curves.

3.5.1 Model Description

Consider a rectangular thin plate undergoing uniaxial compression and uniform distributed lateral pressure. Conventional shell model was selected as it can provide sufficient accurate solutions to the thin-walled structures without considering the stresses through the thickness of the plate. The material is adopted by referring to the paper of Levy [13], which has an elastic modulus of E , Poisson's ratio ν and density ρ as shown in Table 3.2. Geometry information is also determined according to the same paper, that is $480mm \times 120mm$ for length and width and $2mm$ for thickness as reported in Table 3.2. (For square plate modeling, only the length of the plate has changed to $120mm$.)

E , [MPa]	ν	ρ , [kg/m^3]	a , [mm]	b , [mm]	h , [mm]
70000	0.316	2810	480	120	2

(a) Material property
(b) Geometry size

Table 3.2: Finite element model properties

Mesh

Reduced shell elements *S4R* including four nodes are adopted based on the thin plate assumption. There are six degree of freedoms (DOFs) at each node. Since the resolution of meshes has a significant effect on the prediction accuracy by using eigenvalue analysis, a mesh sensitivity study of finite element model has been assessed in advance with results reported in Table 3.3 and curves of convergence study shown in Fig 3.7.

Mesh density	Mesh Size,mm	Eigenvalue	P_{cr}	$P_{cr}(Analytical)$	Difference
-	-	-	kN	kN	-
6×24	20	0.50918	17.82	17.06	4.49%
12×48	10	0.49051	17.17	17.06	0.66%
24×96	5	0.48507	16.98	17.06	-0.46%
48×192	2.5	0.48	16.91	17.06	-0.87%

Table 3.3: Critical buckling load for isotropic plates under uniaxial compression

For comparison purpose, the buckling load N_{cr} (force per unit length) for simply supported plates under uniaxial compression is obtained analytically via Eq.3.5. The corresponding buckling force P_{cr} that applied to the plate edge consequently is derived by substituting the material properties and geometry data, that is,

$$P_{cr} = N_{cr} * b = \frac{D\pi^2}{b} \pi^4 \left(\frac{mb}{a} + \frac{a}{mb} \right)^2 = 17.15kN \quad (3.97)$$

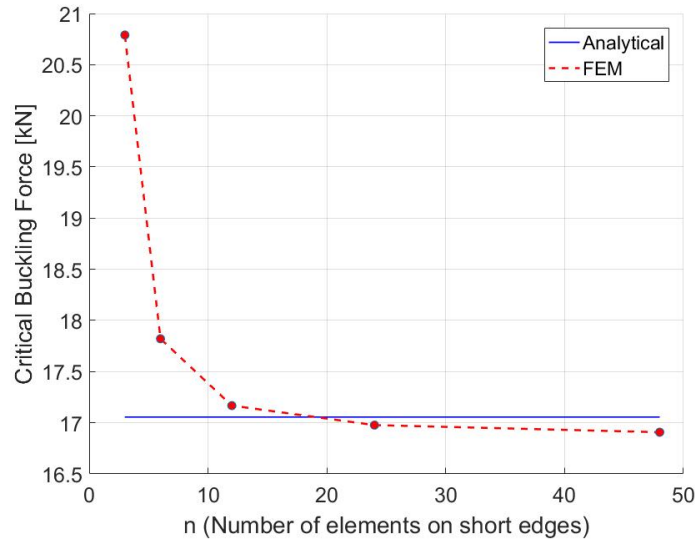


Figure 3.7: Convergence study

From the convergence study conducted by refining the nodes at the loaded edges from 6 to 48 as shown in Fig 3.7, it is observed that the mesh resolution has a huge effect on the buckling

load of plates especially for those with coarse meshes. The predicted critical load starts to converge when 12 elements is modeled in the short edges. Therefore, in order to achieve the sufficient accurate simulation, the nodes should be seeded ensuring at least 12×48 elements with a mesh size of $10mm$. The mesh strategy with a size of $10mm$ will be adopted in this study otherwise additional notices.

Boundary conditions

Since the thin plate model is assumed to be a part of a stiffened panel, neighboring plates and stringers will be expected to restrain the connected region by keeping the plate edges straight. The presence of stringers with rotational stiffness somehow also affect the boundary conditions of the unloaded edges in the form of elastic restraints which are between simply supported or clamped cases. For simplification, all the model in this section are assumed to be simply supported with edges are restricting in out-of-plane motion. Constraints against the in-plane motion are applied by fixing the left edge in the x direction in order to avoid the free body movement and the center node of in y direction to limit the transverse motion (See Fig 3.8 and Table 3.4).

To imitate the straight edges in Abaqus, Multi-Point Constraints (MPCs) is adopted. Slave nodes are bonded together to have the same displacement with the master node. By doing this, the movement of the entire edge will be controlled by merely the master node. In this model, the master node of each edge is selected in the middle of the edge while the rest are classified as slave nodes.

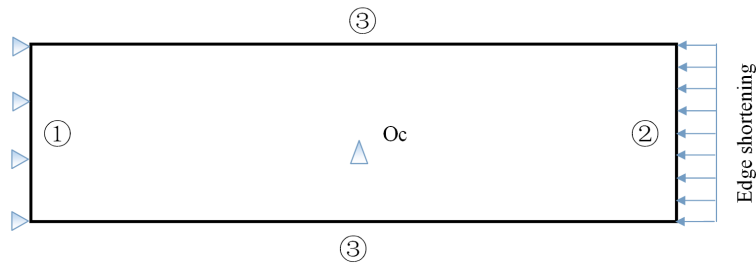


Figure 3.8: The sketch of the model in Abaqus

Boundary Code	Suppressed DOF 's	Other Constraints
①	U_1, U_3	-
②	U_3	-
③	U_3	Stay Straight
O_c	U_2	-

Table 3.4: Boundary conditions

Loads

Longitudinal compression acting on the short edge is simulated as uniform displacements of the nodes on the right edge (See Fig 3.9). By doing this, the loading pattern of FEM is close to that in real experiments. The lateral pressure could be simulated as either uniform distributed pressure acting on the elements of the plate or concentrated loads acting on the distributed nodes of the plate. The option "Following nodal rotation" in the loading editor should be switched on if the latter one is selected, allowing the direction of pressure constantly keep normal to the upper surface of the plate.

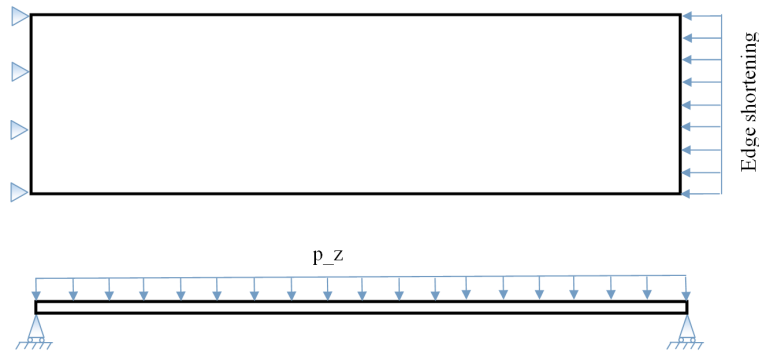


Figure 3.9: External loading applied on the plate

According to the description in the references [1, 47], cabin pressurization loading is determined based on the intended cruise altitude for current commercial airplanes (or HWB as shown in Fig 1.1). The internal pressure inside the airplane is applied on the plate with the magnitude shown in Table 3.5. The symbol P represents the cabin pressure at cruise altitude which equals to 9.2 psi ; DLL stands for design limit loads, which should only be used in center-body of the plane (refer to page 6 of [48]) while DUL represents the design ultimate load, which is generally adopted as the ultimate strength of the structures in FE analysis.

Symbols	Abbreviation	Values in [psi]	Values in [MPa]	
p_0	–	0	0	0
p_1	–	1.84	0.013	$0.2 P$
p_2	P	9.2	0.065	$1 P$
–	DLL	12.24	0.083	$1.33 P$
p_3	DUL	18.36	0.13	$2 P$

Table 3.5: Internal pressure (cabin pressure $P = 9.2 \text{ psi}$)

Among the load cases shown in Table 3.5, four levels of lateral pressure are employed to perform the case study, including p_0 , p_1 , p_2 and p_3 . The corresponding magnitude of lateral pressure will be applied in FE analysis as the input data, which is: $p_0 = 0 \text{ MPa}$, $p_1 = 0.013 \text{ MPa}$, $p_2 = 0.065 \text{ MPa}$ and $p_3 = 0.13 \text{ MPa}$. These values are also correlate to the examples given in the references of [12, 13].

3.5.2 Eigenvalue Analysis

The eigenvalue module in Abaqus which is a linear perturbation procedure has a capability for predicting the elastic buckling load for any "stiff" structures [49], behaving linearly within the prebuckling range. The eigenvalues are derived as a multiplier of the input perturbation loading. The edge compression loading is considered as "live load" during the eigenvalue buckling analysis [49]. The corresponding "dead loads" stand for any loading added on the base state prior to the buckling analysis. The base state of the structure may be undergoing any history response, containing either linear or nonlinear effects [49].

In this section, the base state and the buckling perturbation procedure are assumed to be linear responses, and the estimates of critical buckling loads for thin plates are derived by using the linear buckle module in Abaqus. Nonlinearities in terms of initial geometry imperfections and material plasticity are not taken into account.

According to section 6.2.3 of User's Manuel of Abaqus in [49], the lateral pressure and perturbation edge shortening are applied either in single (See Table 3.6) or multiple steps(See Table 3.7).

	Module	Loading Type	Amplitude	Unit
Step-1	Linear	Pressure and	$\frac{p_z}{Eigenvalue}$ (Pressure)	MPa (Pressure)
	Buckle	Edge shortening	1 (Edge shortening)	mm (Edge shortening)

Table 3.6: Eigenvalue analysis using a single step

	Module	Loading Type	Amplitude	Unit
Step-1	Static(Nlgeom:off)	Pressure	p_z	MPa
Step-2	Linear Buckle	Edge shortening	1	mm

Table 3.7: Eigenvalue analysis using multiple steps

In the single-step pattern as shown in Table 3.6, lateral pressure and edge compression are applied simultaneously in one linear buckle step. By doing this, both loads should be scaled by the load multipliers (eigenvalues) in order to reproduce the actual pressure load and critical buckling load, providing the reason why the input amplitude of lateral pressure is defined as $\frac{p_z}{Eigenvalue}$ (values of p_z could be any levels of the internal pressure load listed in Table 3.5). The initial eigenvalue could be derived with the absence of lateral pressure ($p_z = p_0 = 0$) while the others may need additional iteration.

In the two-step pattern as shown in Table 3.7, lateral pressure and edge compression are added separately in two steps which are "General static" and "Linear buckle". By doing this, pressure loads are input by their actual values and do not need to be divided by eigenvalues.

Simulated results of eigenvalues for plates under various lateral pressure are listed in Table 3.8. The predicted critical loading in FE analysis, denoted by $P_{cr,FEM}$, have been converted to forces to compare with the analytical solution, $P_{cr,a}$, in Eq.3.97.

p_z	Values [MPa]	-	$P_{cr,FEM}$ [kN]	$P_{cr,a}$ [kN]	Diff
p_0	0	0	17.15	17.06	0.5%
p_1	0.013	$0.2P$	17.15	17.06	0.5%
p_2	0.065	P	17.15	17.06	0.5%
p_3	0.13	$2P$	17.15	17.06	0.5%

Table 3.8: The critical buckling load for isotropic plates

From Table 3.8, it is interesting to see that the critical buckling load stay constant with the increase of the lateral load, which is consistent with the elastic analytical results in [11] (page 389). Thus, a conclusion could be drawn that the critical buckling load will be unaffected by the presence of normal pressure under the assumption of small deflection. Additionally, reasonably good consistency is observed between linear eigenvalue predictions and analytical solutions, indicating the correctness of the finite element model.

Eigenmode configurations corresponding to different equilibrium states are obtained as shown in Fig 3.10. It is noteworthy that only the first buckled form with four waves corresponds to the critical load of the plate. These eigenmode results could be introduced as geometry imperfection in the postbuckling analysis.

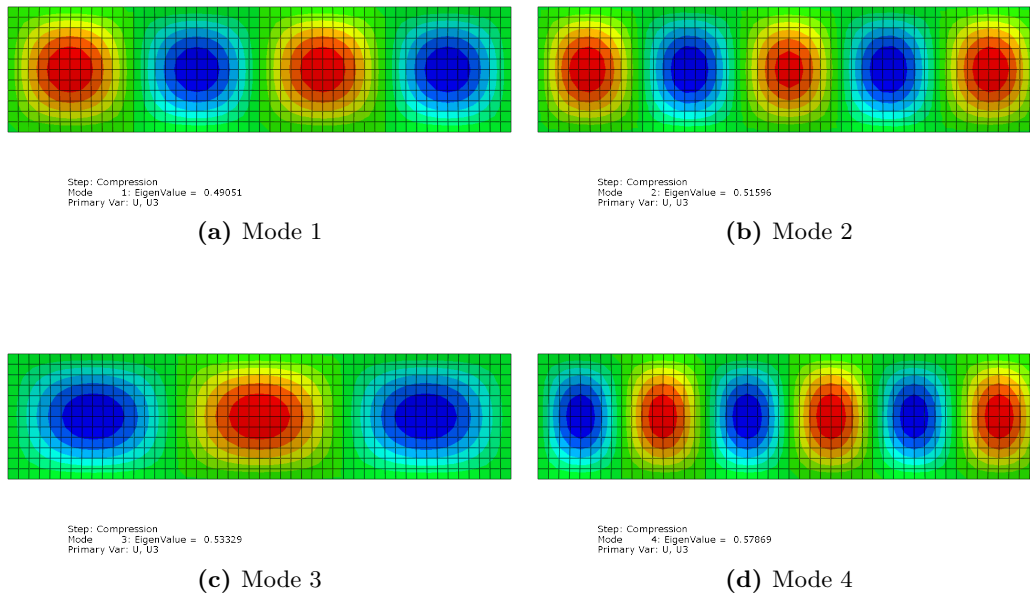


Figure 3.10: Eigenmodes of a rectangular plate under uniaxial compression

3.5.3 Explicit Dynamic Analysis

Finite element code Abaqus/Explicit dynamic analysis has computational advantages in dealing with complex models undergoing large rotations and deformations [50]. It performs a large number of small time increments instead of load-displacement increments in comparison with Lagrangian methods, i.e. Newton-Raphson method.

By employing the same conventional shell model explained in the previous section, the pattern of load application and steps is illustrated in Table 3.9.

	Module	Loading Type	Time	Amplitude	Unit
Step-1	Dynamic Explicit	Pressure	1 s	Fig 3.11(a)	<i>MPa</i>
Step-2	Dynamic Explicit	Pressure Edge shortening	3 s	Fig 3.11(a)(b)	<i>MPa</i>

Table 3.9: Dynamic explicit analysis using multiple steps

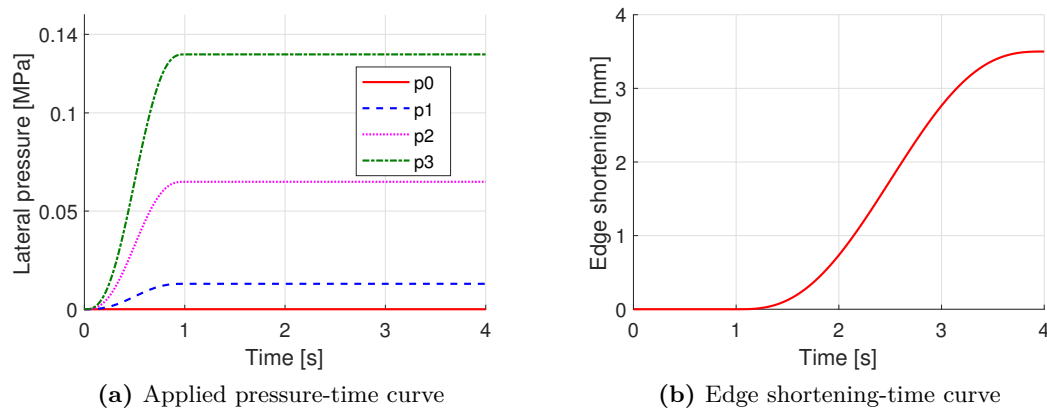


Figure 3.11: Lateral pressure and edge shortening versus time curves

Two-step simulation using dynamic explicit analysis is performed to reveal the postbuckling behaviour of plates under combined loads subjected to uniform distributed compression on the opposite edges and lateral pressure on the surface. As demonstrated in Table 3.9 and Fig 3.11, the lateral pressure are applying to the plate during the entire loading process, rising gradually from zero to p_z in the first step and level off till the end of the second step. The edge shortening, however, is added to the plate from the beginning of the second step with a smoothly increasing amplitude.

Four models have been established for plates under identical uniaxial edge compression and diverse lateral pressure of p_0 , p_1 , p_2 and p_3 . Simulation results are analyzed and illustrated graphically in the form of load-shortening and load-deflection curves shown in Fig 3.12 to Fig 3.23. Value of deflection of plates that recorded in load-deflection curves are measured at a node in which out-of-plane deformation is sensitive to the compressive load. In other words,

the pressure-induced motion at the special point reversals its direction as buckling occurs, which could be considered as a flag to determine the buckling onset. According to deformed configurations in the post-processing analysis of Abaqus, it is convenient to choose the node at one-third of the longitudinal symmetric line as the representative node for measuring the plate deflection. The node is displayed by a red dot in Fig 3.14.

With the absence of lateral pressure ($p_z = p_0 = 0$), postbuckling responses of the uniaxially compressive rectangular plate ($\mu = 4$) are shown in Fig 3.12 associated with the buckling mode configurations during the loading process shown in Fig 3.13 and Fig 3.14. The reacted compression as a function of edge shortening is also plotted with a marked point "A" indicating the buckling onset moment. The red part of solid lines in the load-shortening and load-deflection curves stands for the buckling region of the plate while the blue part represents the postbuckling region.

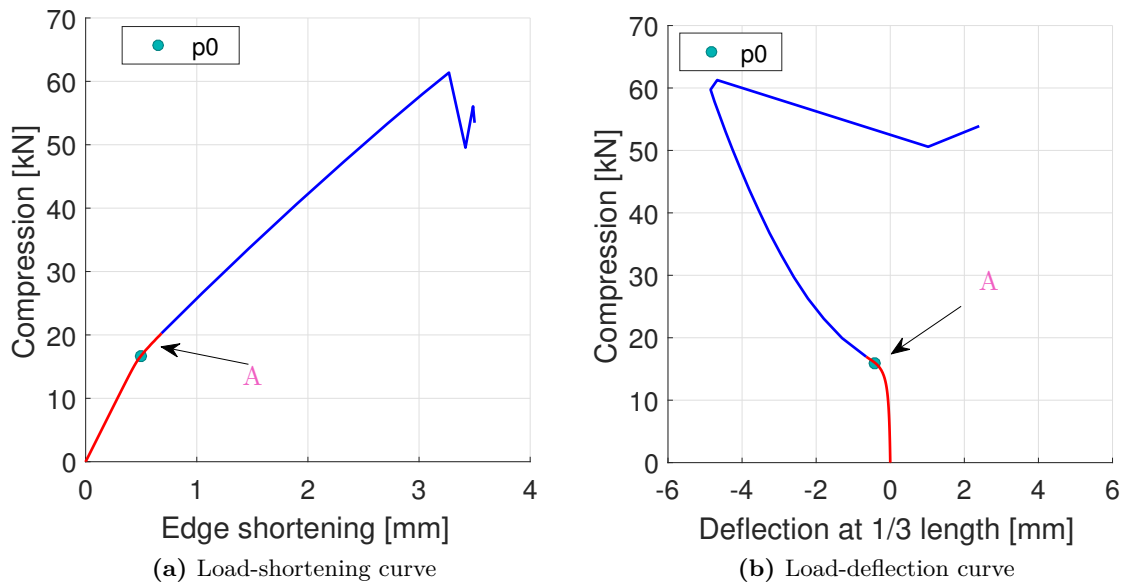


Figure 3.12: The postbuckling behaviour of isotropic plates (p_0)

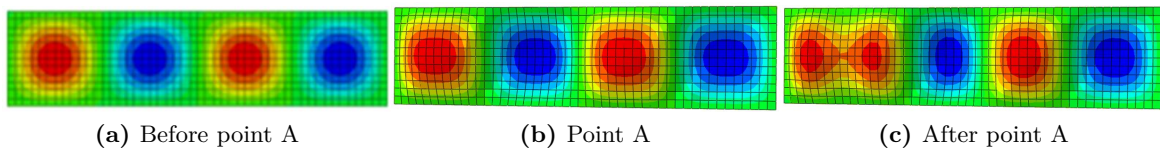


Figure 3.13: Deflection the out-of-plane deformation (p_0)

As pointed out in literature, a simply supported plate will lose parts of its stiffness after buckling yet still having the load-carrying capacity to sustain more loads without collapse. It could be observed in the load-shortening that the slope experiences an apparent change due to the sudden drop of the overall stiffness of the plate and the inflection point "A" should be the occurrence of buckling which reads approximately $17kN$. The bifurcation of the postbuckling path in Fig 3.12 also indicates a similar buckling load.

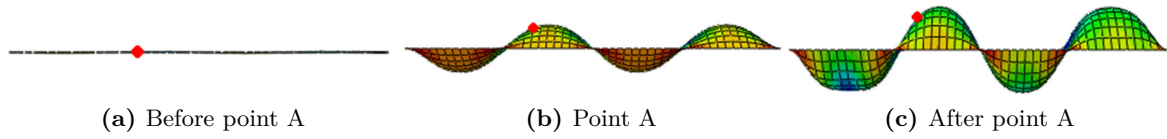


Figure 3.14: Front view of the out-of-plane deformation (p_0)

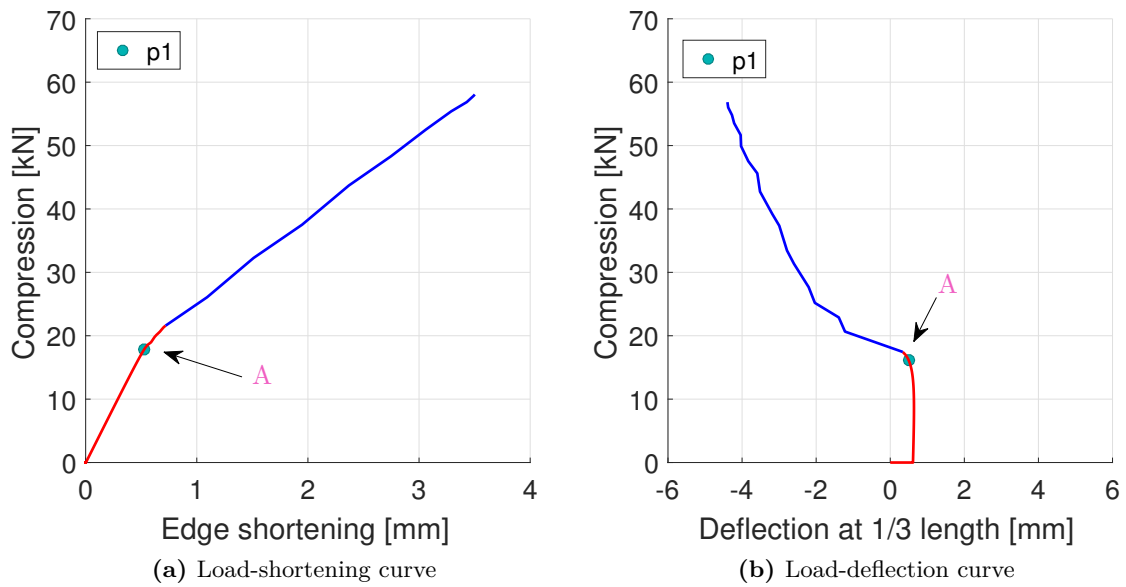


Figure 3.15: The postbuckling behaviour of isotropic plates (p_1)

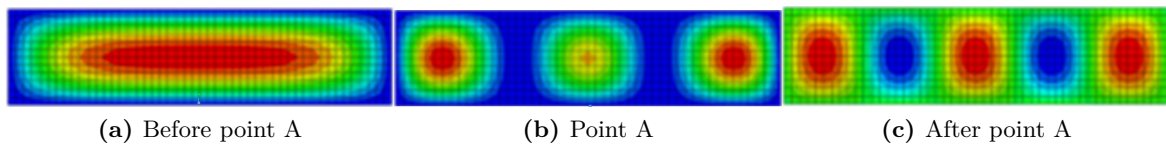


Figure 3.16: Deflection the out-of-plane deformation (p_1)

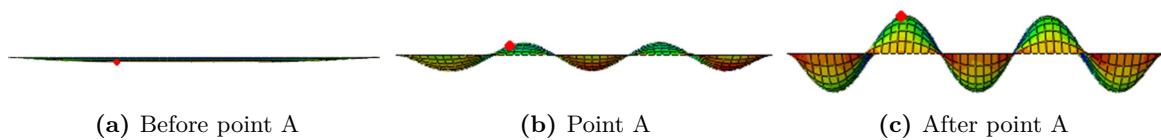


Figure 3.17: Front view of the out-of-plane deformation (p_1)

As for the compressive plate imposing the lateral pressure of $p_1 = 0.013MPa$, shown in Fig 3.15, 3.16 and 3.17, buckling and postbuckling responses exhibit a similar trend with those under pure in-plane compression. The results perform in good accordance with the conclusion that small out-of-plane loading has minor effects on the critical buckling loads of dominantly compressed plates. From these curves, the buckling load marked in point "A" is roughly $17.5 kN$.

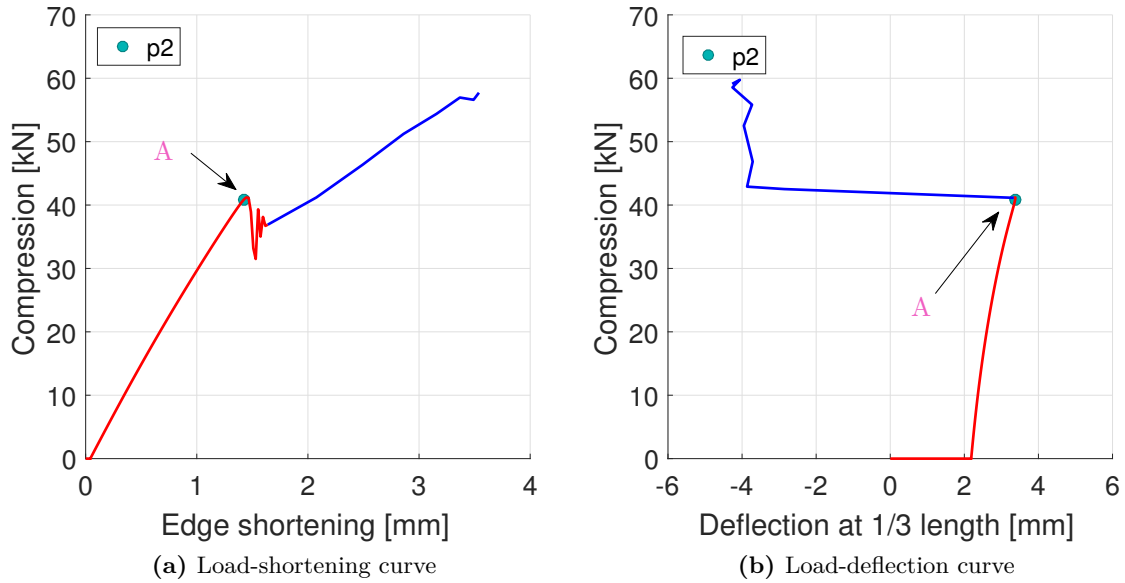


Figure 3.18: The postbuckling behaviour of isotropic plates (p_2)

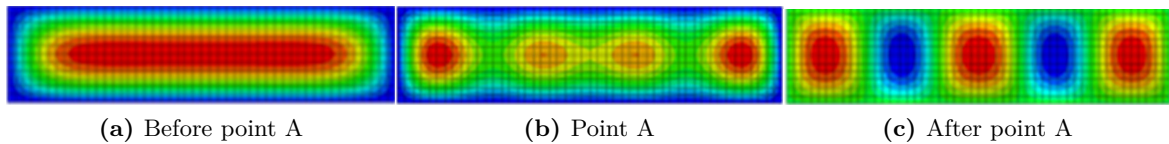


Figure 3.19: Top view of the out-of-plane deformation (p_2)

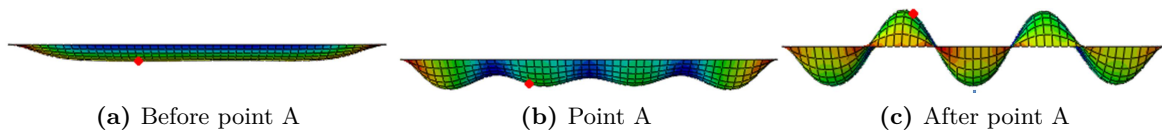


Figure 3.20: Front view of the out-of-plane deformation (p_2)

With the increase of lateral pressure, the load-shortening relation, graphically illustrated in Fig 3.18, experiences a sudden drop, accompanied by a set of oscillation as well. This may be attributed to the inherent feature of a dynamic explicit module of FE analysis, in which the mass inertia of the plate is taken into consideration. This phenomenon is expected to correlate to the buckle mode jump of the deformed plate. The predicted buckling load is taken as the peak of the load-shortening curve at the point prior to the unsteady regime, which is more than two times as the value in uniaxial compression buckling.

When the pressure load reaches as large as twice the cabin pressure ($p_3 = 0.13MPa$), as shown in Fig 3.21, the inflection point continues moving rightward reaching at about $60kN$ in compression load which is approximately four times as that with the absence of lateral pressure. Compare to the plots with lower pressure, an initial offset of edge shortening is observed under p_3 . This may be caused by the considerate membrane stretching induced by the large pressure since the loaded edge is free of in-plane motion as the pressure loading is acting.

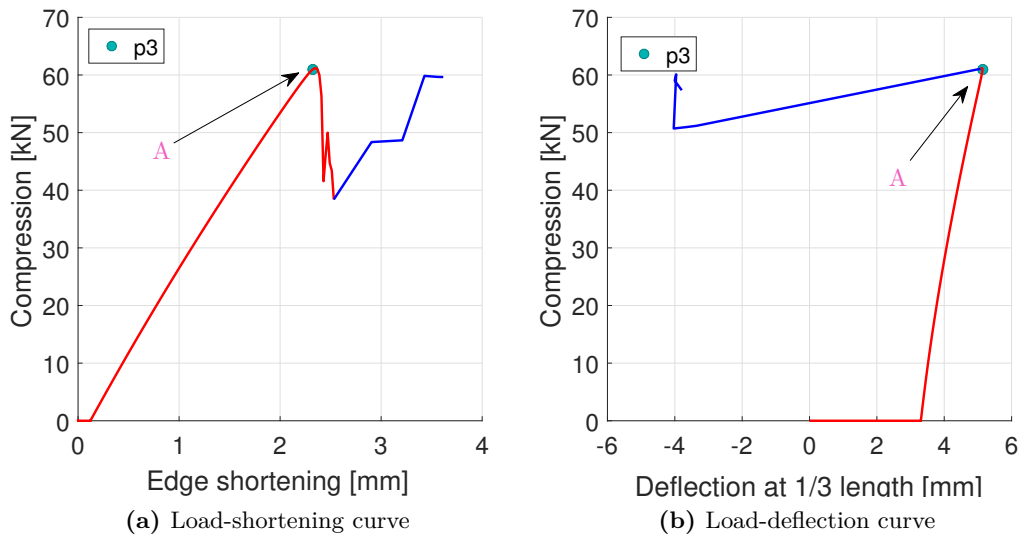


Figure 3.21: The postbuckling behaviour of isotropic plates (p_3)

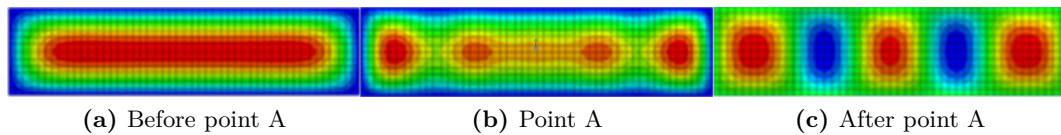


Figure 3.22: Top view of the out-of-plane deformation (p_3)

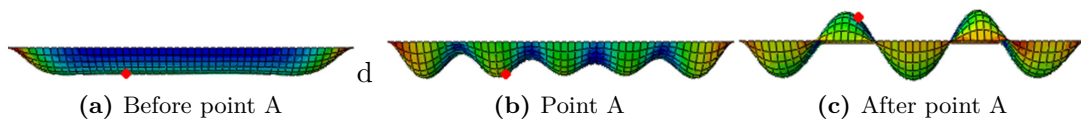


Figure 3.23: Front view of the out-of-plane deformation (p_3)

The anticipated buckling strength of the four plates using FEM is reported in Table 3.10 and evaluated by comparing with the semi-analytical results proposed by Levy [13]. The applied lateral pressure and predicted buckling loads are normalized with respect to the Young's modulus and plate geometry as shown in Eq.3.98.

$p_z, [MPa]$	ζ_z	$P_{cr,FEM}, [kN]$	$\xi_{cr,FEM}$	$\xi_{cr,Levy} [13]$	Diff
$p0= 0$	0	16.3	3.5	3.84	-8.87%
$p1= 0.013$	2.40	18.5	3.9	4.05	-1.80%
$p2= 0.065$	12.02	41.2	8.8	8.56	3.16%
$p3= 0.13$	24.03	60.6	13.0	11.8	10.18%

Table 3.10: The critical buckling load for isotropic plates

$$\zeta_z = \frac{p_z b^4}{Eh^4} \quad \xi_{cr} = \frac{P_{cr} b}{Eh^3} \quad (3.98)$$

In Table 3.10, $\xi_{cr,FEM}$ and $\xi_{cr,Levy}$ represent the normalized predicted buckling loads using FEM and that from the Levy's solutions. ζ_z is the normalized pressure load. The differences between the FE models and Levy's prediction are observed to approximately vary from -10% to 10% , which indicate an acceptable prediction of buckling strength of plate under combine loads using FE method. The FE analysis seems to have underestimated the stability property of plates with medium pressure while overestimated those with large pressure.

From the analysis above, conclusions could be drawn as follows:

- The lateral pressure will postpone the buckling onset leading to a larger critical buckling load of compressive plates.
- Buckling modes of plates are likely to change with the introduction of lateral pressure.
- The change of the stiffness of the deformed plate is smooth for small pressure during the compressive loading process yet abrupt for large pressure.

3.6 Conclusions

The stability problem of a rectangular flat plate subjected to longitudinal in-plane compression, out-of-plane pressure, and their combination was investigated by using analytical equations and finite element method. Classical plate theory was adopted to establish the differential governing equation by which load-deflection relations could be obtained. Under the assumption of small deflection, critical buckling loads for plates under edge compression and the lateral pressure were found to have few effects on the critical buckling loads of plates subjected to uniaxial compression. However, when plates under large deflection, results suggest that the lateral pressure have an advanced benefit to the stability capability by postponing buckling onset.

Buckling and Postbuckling Behaviour of Composite Plates

4.1 Introduction

In the previous chapter, investigations on the stability behaviours of unstiffened isotropic plates have been conducted analytically and numerically. In comparison with plates made of homogeneous materials which have identical values of property in all directions, composite plates are usually composed of multiple layers characterized by distinct mechanical property in each direction. For the sake of simplification, symmetric and balanced stacking pattern are assumed for the composite laminates currently discussed, in which bending-stretching and shearing-stretching coupling are eliminated. In addition, the stack sequence in the composite plate is selected that bending-twisting interaction is small enough to be neglected. Analogous to the isotropic plate, the approaches that adopted in solving the composite problem are still based on the classic laminate plate theory and the through-thickness property are not taken into account.

In this chapter, unstiffened composite laminates with same load cases and boundary conditions to those in the isotropic analysis will be studied, aiming to reveal the potential stability capacity of plates under combined loads. First, critical loading is derived based on the von Karman governing differential equations, followed by the deflection analysis under pure pressure by virtue of Navier's method. Under the small-deformation assumption, buckling strength of laminates under combined loads is discussed using the governing equation and energy methods. Finally, FE predictions are given by means of finite element software Abaqus.

4.2 Composite Plates under Uniaxial Compression

In this section, solutions to the governing differential equations of rectangular composite laminates subjected to uniaxial compression are reviewed based on the classical laminate plate theory [9].

Consider a ideal flat rectangular composite laminate with symmetric and balanced layups, subjected to uniform in-plane forces and shears in the middle plane of the plate and out-of-plane normal pressure on the surface, the force equilibrium equation is recalled in the form of:

$$D_{11} \frac{\partial^4 w}{\partial x^4} + 2(D_{12} + 2D_{66}) \frac{\partial^4 w}{\partial x^2 \partial y^2} + D_{22} \frac{\partial^4 w}{\partial y^4} = N_x \frac{\partial^2 w}{\partial x^2} + N_{xy} \frac{\partial^2 w}{\partial x \partial y} + N_y \frac{\partial^2 w}{\partial y^2} + p_z \quad (2.20)$$

in which w is the deflection function; N_x , N_y and N_{xy} are the uniform distributed force applied to the mid-plane of the plate. The parameters D_{ij} are correlated to the bending-tension (D_{11} , D_{12} or D_{22}) or bending-twisting (D_{16} and D_{26}) coupling terms and the latter are negligible in balanced stacking laminates.

Assume that the only applied load is the axial compression along the x axis (See Fig 4.1), the governing equation of the composite laminate becomes:

$$D_{11} \frac{\partial^4 w}{\partial x^4} + 2(D_{12} + 2D_{66}) \frac{\partial^4 w}{\partial x^2 \partial y^2} + D_{22} \frac{\partial^4 w}{\partial y^4} = N_x \frac{\partial^2 w}{\partial x^2} \quad (4.1)$$

Double Fourier series which satisfy the simply supported boundary conditions are assumed

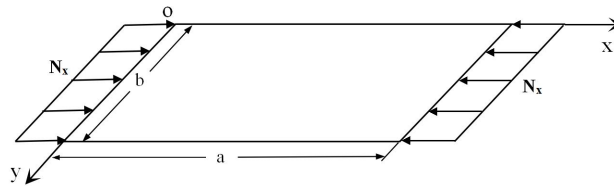


Figure 4.1: Compression applied on the composite laminate

to represent the out-of-plane displacement in the form of Eq.3.3.

$$w = \sum_{m=1}^{\infty} \sum_{n=1}^{\infty} w_{mn} \sin\left(\frac{m\pi x}{a}\right) \sin\left(\frac{n\pi y}{b}\right) \quad (3.3)$$

By Substituting into Eq.4.1 and rearranging, one derives:

$$\sum_{m=1}^{\infty} \sum_{n=1}^{\infty} w_{mn} \left[D_{11} \left(\frac{m\pi}{a} \right)^4 + 2(D_{12} + 2D_{66}) \left(\frac{m\pi}{a} \right)^2 \left(\frac{n\pi}{b} \right)^2 + D_{22} \left(\frac{n\pi}{b} \right)^4 + N_x \left(\frac{m\pi}{a} \right)^2 \right] \sin \left(\frac{m\pi x}{a} \right) \sin \left(\frac{n\pi y}{b} \right) = 0 \quad (4.2)$$

For nontrivial solutions that satisfy arbitrary x and y of the Eq.4.2, one obtains:

$$D_{11} \left(\frac{m\pi}{a} \right)^4 + 2(D_{12} + 2D_{66}) \left(\frac{m\pi}{a} \right)^2 \left(\frac{n\pi}{b} \right)^2 + D_{22} \left(\frac{n\pi}{b} \right)^4 + N_x \left(\frac{m\pi}{a} \right)^2 = 0 \quad (4.3)$$

The expression of critical bulking load N_{cr} for laminates under uniaxial compression are obtained by solving the above equation, which has the form of

$$N_{cr} = \frac{\pi^2 [D_{11}m^4 + 2(D_{12} + 2D_{66})\mu^2 m^2 n^2 + D_{22}n^4 \mu^4]}{a^2 m^2} \quad (4.4)$$

where $\mu = a/b$ is the aspect ratio of the plate.

The buckling load N_{cr} is observed to reach its minimum when $n = 1$. Rearranging the buckling load expression by setting $n = 1$, one obtain:

$$N_{cr} = \frac{\pi^2}{a^4} \left[D_{11}m^2 + 2(D_{12} + 2D_{66})\mu^2 + D_{22} \frac{\mu^4}{m^2} \right] \quad (4.5)$$

Typically, there exists a m that minimizes the buckling load N_{cr} for a given rectangular plate. For the sake of finding the minimum value of N_{cr} , the right-hand side of the Eq.4.5 is differentiated with respect to m ,

$$\frac{\partial N_{cr}}{\partial m} = 2D_{11} \frac{\pi^2}{a^2} m - 2D_{22} \frac{a^2 \pi^2}{b^4 m^3} \quad (4.6)$$

By setting the first derivative (stationary point) equals to zero,

$$\frac{\partial N_{cr}}{\partial m} = 0 \quad (4.7)$$

The correspond m to the minima of N_{cr} is obtained as: (since second derivative $\frac{\partial^2 N_{cr}}{\partial m^2} \geq 0$)

$$m = \frac{a}{b} \sqrt[4]{\frac{D_{22}}{D_{11}}} \quad (4.8)$$

It should be highlighted that m should be rounded up or down in order to become an integer. The detailed demonstration could be found in Section 8.5.2 of textbook [8].

4.3 Composite Plates under Lateral Pressure

In this part, out-of-plane deflection of laminates under pure normal pressure is studied and equations are presented by referring to the textbook of [8].

Consider a simply supported composite laminate subjected to a uniform distributed loading perpendicular to the surface of the plate, the induced out-of-plane displacement can be derived using Navier's method [9] in which small deflection is assumed.

The displacement field w and the pressure loading q_z are expanded in trigonometric series which satisfy the boundary conditions, that is,

$$w = \sum_{m=1}^{\infty} \sum_{n=1}^{\infty} w_{mn} \sin\left(\frac{m\pi x}{a}\right) \sin\left(\frac{n\pi y}{b}\right) \quad (3.3)$$

and

$$p_z = \sum_{m=1}^{\infty} \sum_{n=1}^{\infty} q_{mn} \sin\left(\frac{m\pi x}{a}\right) \sin\left(\frac{n\pi y}{b}\right) \quad (3.31)$$

where the coefficients q_{mn} are calculated by multiplying the shape function on both sides of the equation. Similar method could be referred to Chapter 3.

The unknown coefficients are represented in form of:

$$q_{mn} = \frac{4p_z}{ab} \int_0^a \int_0^b \sin\frac{m\pi x}{a} \sin\frac{n\pi y}{b} dy dx = \frac{16p_z}{\pi^2 mn} \quad (4.9)$$

After the substitution of w and q_z into the governing equation recalled from Eq.2.20:

$$D_{11} \frac{\partial^4 w}{\partial x^4} + 2(D_{12} + 2D_{66}) \frac{\partial^4 w}{\partial x \partial y} + D_{22} \frac{\partial^4 w}{\partial y^4} = p_z \quad (4.10)$$

one obtains:

$$\begin{aligned} & \sum_{m=1}^{\infty} \sum_{n=1}^{\infty} w_{mn} \left[D_{11} \left(\frac{m\pi}{a}\right)^4 + 2(D_{12} + 2D_{66}) \left(\frac{m\pi}{a}\right)^2 \left(\frac{n\pi}{b}\right)^2 \right. \\ & \quad \left. + D_{22} \left(\frac{n\pi}{b}\right)^4 \right] \sin\left(\frac{m\pi x}{a}\right) \sin\left(\frac{n\pi y}{b}\right) \\ & = \sum_{m=1}^{\infty} \sum_{n=1}^{\infty} \frac{16p_z}{\pi^2 mn} \sin\left(\frac{m\pi x}{a}\right) \sin\left(\frac{n\pi y}{b}\right) \end{aligned} \quad (4.11)$$

Rewrite the above function by bring p_z into the bracket,

$$\sum_{m=1}^{\infty} \sum_{n=1}^{\infty} w_{mn} \left[D_{11} \left(\frac{m\pi}{a} \right)^4 + 2(D_{12} + 2D_{66}) \left(\frac{m\pi}{a} \right)^2 \left(\frac{n\pi}{b} \right)^2 + D_{22} \left(\frac{n\pi}{b} \right)^4 - \frac{16p_z}{w_{mn}\pi^2 mn} \right] \sin \left(\frac{m\pi x}{a} \right) \sin \left(\frac{n\pi y}{b} \right) = 0 \quad (4.12)$$

In order to satisfy the equation in the domain of the plate, items in the bracket should be zero, which gives the form of displacement ($w_{mn} \neq 0$) as

$$w_{mn} = \frac{16p_z}{\pi^2 mn \left[D_{11} \left(\frac{m\pi}{a} \right)^4 + 2(D_{12} + 2D_{66}) \left(\frac{m\pi}{a} \right)^2 \left(\frac{n\pi}{b} \right)^2 + D_{22} \left(\frac{n\pi}{b} \right)^4 \right]} \quad (4.13)$$

or

$$w_{mn} = \frac{16p_z a^4}{\pi^6 mn} \left[\frac{1}{m^4 D_{11} + 2(D_{12} + 2D_{66}) \mu^2 m^2 n^2 + D_{22} n^4 \mu^4} \right] \quad (4.14)$$

A linear relation is observed that the pressure-induced deflection is increased proportionally with the pressure loading under the assumption of small deflection.

4.4 Composite Plates under Combined Loads

4.4.1 Governing Differential Equation Method

Similar methods as illustrated in Section 3.4.1 are utilized to deal with the buckling-related equations of composite plates under both in-plane and out-of-plane loads. These methods, originally presented in the textbook [11], have been successfully applied to isotropic plates. In this section, the approaches will be employed to assess the instability characteristics of plates made from non-isotropic composite materials.

Equilibrium equations characterizing the deformation of composite plates are formed by referring to [8], which is,

$$D_{11} \frac{\partial^4 w}{\partial x^4} + 2(D_{12} + 2D_{66}) \frac{\partial^4 w}{\partial x^2 \partial y^2} + D_{22} \frac{\partial^4 w}{\partial y^4} = N_x \frac{\partial^2 w}{\partial x^2} + 2N_{xy} \frac{\partial^2 w}{\partial x \partial y} + N_y \frac{\partial^2 w}{\partial y^2} + p_z \quad (4.15)$$

where D_{ij} are the items from bending stiffness matrix of composite plates, and N_{ij} are the in-plane uniform distributed loads subjected to the mid-plane of the plate.

In the case only uniaxial compression and lateral pressure are applied on the plate, the governing equation can be rewritten as:

$$D_{11} \frac{\partial^4 w}{\partial x^4} + 2(D_{12} + 2D_{66}) \frac{\partial^4 w}{\partial x^2 \partial y^2} + D_{22} \frac{\partial^4 w}{\partial y^4} - N_x \frac{\partial^2 w}{\partial x^2} - p_z = 0 \quad (4.16)$$

By Substituting the predicted displacement function Eq.3.3 and lateral pressure function Eq.3.53 into the governing equation Eq.4.16, the Ritz coefficients (w_{mn} in the displacement function) become:

$$w_{mn} = \frac{a^4 q_{mn}}{\pi^2 ((m^4 D_{11} + 2(D_{12} + 2D_{66}) \mu^2 m^2 n^2 + n^4 \mu^4 D_{22}) \pi^2 - N_x a^2 m^2)} \quad (4.17)$$

By substituting the pressure coefficients 4.9 into 4.17, one has

$$w_{mn} = \frac{16p_z}{\pi^4 m n} \frac{a^4}{((m^4 D_{11} + 2(D_{12} + 2D_{66}) \mu^2 m^2 n^2 + n^4 \mu^4 D_{22}) \pi^2 - N_x a^2 m^2)} \quad (4.18)$$

with m and n odd integers.

The critical load is obtained as the denominator of Eq.4.18 vanishes,

$$N_{cr} = \frac{\pi^2 [D_{11} m^4 + 2(D_{12} + 2D_{66}) \mu^2 m^2 n^2 + D_{22} n^4 \mu^4]}{a^2 m^2} \quad (4.19)$$

or

$$N_{cr} = D_{11} \left(\frac{m\pi}{a} \right)^2 + 2(D_{12} + 2D_{66}) \left(\frac{n\pi}{b} \right)^2 + D_{22} \left(\frac{a\pi}{m} \right)^2 \left(\frac{n}{b} \right)^4 \quad (4.20)$$

From Eq.4.20, it could be concluded that based on the small deflection assumption the lateral load has no effect on the buckling strength of a composite plate with simply supported edges. In the next section, an energy method is applied to solve the same problem.

4.4.2 Energy Methods

In most of the cases finding the critical buckling load could be achieved by considering the principle of stationary points of the total potential energy, which is an effective approach to solving stability problems.

Strain energy in composite plate

Given a deformed plate under external forces, the internal strain energy U can be formed as:

$$U = \frac{1}{2} \iiint_V \{ \sigma_x \varepsilon_x + \sigma_y \varepsilon_y + \tau_{xy} \gamma_{xy} \} dV \quad (4.21)$$

in which σ_x , σ_y and τ_{xy} stand for the average normal and shear stresses while ϵ_{x0} , ϵ_{y0} and γ_{xy0} stand for the strains in the mid-plane of the plate.

Replacing the strains in terms of curvatures and mid-plane strains which are derived based on the Kirckhoff's assumption:

$$\epsilon_x = \epsilon_{x0} + z\kappa_x, \quad \epsilon_y = \epsilon_{y0} + z\kappa_y, \quad \gamma_{xy} = \gamma_{xy0} + z\kappa_{xy} \quad (4.22)$$

where κ_x , κ_y and κ_{xy} are the plate curvatures while z is the distance away from the neutral plane.

After substitution, the strain energy equation becomes,

$$U = \frac{1}{2} \iiint_V \{ \sigma_x (\epsilon_{x0} + z\kappa_x) + \sigma_y (\epsilon_{y0} + z\kappa_y) + \sigma_{xy} (\epsilon_{xy0} + z\kappa_{xy}) \} dV \quad (4.23)$$

Given the relations of stress versus in-plane forces and moments,

$$\int_{-\frac{h}{2}}^{\frac{h}{2}} \begin{bmatrix} \sigma_x \\ \sigma_y \\ \tau_{xy} \end{bmatrix} dz = \begin{bmatrix} N_x \\ N_y \\ N_{xy} \end{bmatrix} \quad \text{and} \quad \int_{-\frac{h}{2}}^{\frac{h}{2}} \begin{bmatrix} z\sigma_x \\ z\sigma_y \\ z\tau_{xy} \end{bmatrix} dz = \begin{bmatrix} M_x \\ M_y \\ M_{xy} \end{bmatrix} \quad (4.24)$$

Strain energy is rebuilt by integrating Eq.4.23 with respect to z through the thickness of the plate.

$$U = \frac{1}{2} \iint_A \{ N_x \epsilon_{x0} + N_y \epsilon_{y0} + N_{xy} \gamma_{xy0} + M_x \kappa_x + M_y \kappa_y + M_{xy} \kappa_{xy} \} dx dy \quad (4.25)$$

Expanding Eq.4.25 by introducing load-stress expression in Eq.2.16,

$$\begin{bmatrix} N_x \\ N_y \\ N_{xy} \\ M_x \\ M_y \\ M_{xy} \end{bmatrix} = \begin{bmatrix} A_{11} & A_{12} & A_{16} & B_{11} & B_{12} & B_{16} \\ A_{12} & A_{22} & A_{26} & B_{12} & B_{22} & B_{26} \\ A_{16} & A_{26} & A_{66} & B_{16} & B_{26} & B_{66} \\ B_{11} & B_{12} & B_{16} & D_{11} & D_{12} & D_{16} \\ B_{12} & B_{22} & B_{26} & D_{12} & D_{22} & D_{26} \\ B_{16} & B_{26} & B_{66} & D_{16} & D_{26} & D_{66} \end{bmatrix} \begin{bmatrix} \epsilon_{x0} \\ \epsilon_{y0} \\ \gamma_{xy0} \\ \kappa_x \\ \kappa_y \\ \kappa_{xy} \end{bmatrix} \quad (2.16)$$

one obtains

$$U = \frac{1}{2} \iint_A \left\{ \begin{aligned} & (A_{11}\epsilon_{x0} + A_{12}\epsilon_{y0} + A_{16}\gamma_{xy0} + B_{11}\kappa_x + B_{12}\kappa_y + B_{16}\kappa_{xy})\epsilon_{x0} + \\ & (A_{21}\epsilon_{x0} + A_{22}\epsilon_{y0} + A_{26}\gamma_{xy0} + B_{12}\kappa_x + B_{22}\kappa_y + B_{26}\kappa_{xy})\epsilon_{y0} + \\ & (A_{61}\epsilon_{x0} + A_{62}\epsilon_{y0} + A_{66}\gamma_{xy0} + B_{16}\kappa_x + B_{26}\kappa_y + B_{66}\kappa_{xy})\gamma_{xy0} + \\ & (B_{11}\epsilon_{x0} + B_{12}\epsilon_{y0} + B_{16}\gamma_{xy0} + D_{11}\kappa_x + D_{12}\kappa_y + D_{16}\kappa_{xy})\kappa_x + \\ & (B_{21}\epsilon_{x0} + B_{22}\epsilon_{y0} + B_{26}\gamma_{xy0} + D_{12}\kappa_x + D_{22}\kappa_y + D_{26}\kappa_{xy})\kappa_y + \\ & (B_{61}\epsilon_{x0} + B_{62}\epsilon_{y0} + B_{66}\gamma_{xy0} + D_{16}\kappa_x + D_{26}\kappa_y + D_{66}\kappa_{xy})\kappa_{xy0} \end{aligned} \right\} dx dy \quad (4.26)$$

Thus, after carrying out the integrals with respect to corresponding increments and regrouping, the following equation of strain energy can be written as (detailed calculation is referred to section 5.4 in [8]):

$$\begin{aligned}
U = & \frac{1}{2} \iint_A \left\{ A_{11} \varepsilon_{x0}^2 + 2A_{12} \varepsilon_{x0} \varepsilon_{y0} + 2A_{16} \varepsilon_{x0} \gamma_{xy0} + \right. \\
& \left. A_{22} \varepsilon_{y0}^2 + 2A_{26} \varepsilon_{y0} \gamma_{xy0} + A_{66} \gamma_{xy0}^2 \right\} dx dy \\
& + \iint_A \left\{ B_{11} \varepsilon_{x0} \kappa_x + B_{12} (\varepsilon_{y0} \kappa_x + \varepsilon_{x0} \kappa_y) + B_{16} (\gamma_{xy0} \kappa_x + \varepsilon_{x0} \kappa_{xy}) + \right. \\
& \left. B_{22} \varepsilon_{y0} \kappa_y + B_{26} (\gamma_{xy0} \kappa_y + \varepsilon_{y0} \kappa_{xy}) + B_{66} \gamma_{xy0} \kappa_{xy} \right\} dx dy \\
& + \frac{1}{2} \iint_A \left\{ D_{11} \kappa_x^2 + 2D_{12} \kappa_x \kappa_y + 2D_{16} \kappa_x \kappa_{xy} + \right. \\
& \left. D_{22} \kappa_y^2 + 2D_{26} \kappa_y \kappa_{xy} + D_{66} \kappa_{xy}^2 \right\} dx dy
\end{aligned} \quad (4.27)$$

Replace the strains in Eq.4.27 by

$$\begin{aligned}
\varepsilon_{x0} &= \frac{\partial u_0}{\partial x}, & \varepsilon_{y0} &= \frac{\partial v_0}{\partial y}, & \gamma_{xy0} &= \frac{\partial u_0}{\partial y} + \frac{\partial v_0}{\partial x} \\
\kappa_x &= -\frac{\partial^2 w}{\partial x^2}, & \kappa_y &= -\frac{\partial^2 w}{\partial y^2}, & \kappa_{xy} &= -2\frac{\partial^2 w}{\partial x \partial y}
\end{aligned} \quad (4.28)$$

the strain energy becomes

$$\begin{aligned}
U = & \frac{1}{2} \iint_A \left\{ A_{11} \left(\frac{\partial u}{\partial x} \right)^2 + 2A_{12} \frac{\partial u}{\partial x} \frac{\partial v}{\partial y} + 2A_{16} \frac{\partial u}{\partial x} \left(\frac{\partial u}{\partial y} + \frac{\partial v}{\partial x} \right) + \right. \\
& \left. A_{22} \left(\frac{\partial v}{\partial y} \right)^2 + 2A_{26} \frac{\partial v}{\partial y} \left(\frac{\partial u}{\partial y} + \frac{\partial v}{\partial x} \right) + A_{66} \left(\frac{\partial u}{\partial y} + \frac{\partial v}{\partial x} \right)^2 \right\} dx dy \\
& - \iint_A \left\{ B_{11} \frac{\partial u}{\partial x} \frac{\partial^2 w}{\partial x^2} + B_{12} \left(\frac{\partial v}{\partial y} \frac{\partial^2 w}{\partial x^2} + \frac{\partial u}{\partial x} \frac{\partial^2 w}{\partial y^2} \right) + \right. \\
& \left. B_{16} \left[\left(\frac{\partial u}{\partial y} + \frac{\partial v}{\partial x} \right) \frac{\partial^2 w}{\partial x^2} + 2\frac{\partial u}{\partial x} \frac{\partial^2 w}{\partial x \partial y} \right] + B_{22} \frac{\partial v}{\partial y} \frac{\partial^2 w}{\partial y^2} + \right. \\
& \left. B_{26} \left[\left(\frac{\partial u}{\partial y} + \frac{\partial v}{\partial x} \right) \frac{\partial^2 w}{\partial y^2} + 2\frac{\partial v}{\partial y} \frac{\partial^2 w}{\partial x \partial y} \right] + \right. \\
& \left. 2B_{66} \left(\frac{\partial u}{\partial y} + \frac{\partial v}{\partial x} \right) \frac{\partial^2 w}{\partial x \partial y} \right\} dx dy \\
& + \frac{1}{2} \iint_A \left\{ D_{11} \left(\frac{\partial^2 w}{\partial x^2} \right)^2 + 2D_{12} \frac{\partial^2 w}{\partial x^2} \frac{\partial^2 w}{\partial y^2} + 4D_{16} \frac{\partial^2 w}{\partial x^2} \frac{\partial^2 w}{\partial x \partial y} + \right. \\
& \left. D_{22} \left(\frac{\partial^2 w}{\partial y^2} \right)^2 + 4D_{26} \frac{\partial^2 w}{\partial y^2} \frac{\partial^2 w}{\partial x \partial y} + 4D_{66} \left(\frac{\partial^2 w}{\partial x \partial y} \right)^2 \right\} dx dy
\end{aligned} \quad (4.29)$$

Note that the symbol of mid-plane strains is marked as u and v for simplification.

Assume a symmetrical and balanced stacking laminate with small bending-twisting coupling, the expression is simplified as:

$$\begin{aligned}
U = \frac{1}{2} \iint_A & \left\{ \begin{aligned} & A_{11} \left(\frac{\partial u}{\partial x} \right)^2 + 2A_{12} \frac{\partial u}{\partial x} \frac{\partial v}{\partial y} + \\ & A_{22} \left(\frac{\partial v}{\partial y} \right)^2 + A_{66} \left(\frac{\partial u}{\partial y} + \frac{\partial v}{\partial x} \right)^2 \end{aligned} \right\} dx dy \\
+ \frac{1}{2} \iint_A & \left\{ \begin{aligned} & D_{11} \left(\frac{\partial^2 w}{\partial x^2} \right)^2 + 2D_{12} \frac{\partial^2 w}{\partial x^2} \frac{\partial^2 w}{\partial y^2} + \\ & D_{22} \left(\frac{\partial^2 w}{\partial y^2} \right)^2 + 4D_{66} \left(\frac{\partial^2 w}{\partial x \partial y} \right)^2 \end{aligned} \right\} dx dy
\end{aligned} \tag{4.30}$$

In addition, the small deformation assumption implies that the products of terms $\frac{\partial u}{\partial x}$, $\frac{\partial v}{\partial y}$, $\frac{\partial u}{\partial y}$ and $\frac{\partial v}{\partial x}$, which are the higher order compared with the strains should also be neglected (See section 3.3 of [9]). Thus, the expression of internal potential energy becomes,

$$U = \frac{1}{2} \iint_A \left\{ D_{11} \left(\frac{\partial^2 w}{\partial x^2} \right)^2 + 2D_{12} \frac{\partial^2 w}{\partial x^2} \frac{\partial^2 w}{\partial y^2} + D_{22} \left(\frac{\partial^2 w}{\partial y^2} \right)^2 + 4D_{66} \left(\frac{\partial^2 w}{\partial x \partial y} \right)^2 \right\} dx dy \tag{4.31}$$

Work done by external loads in composite plate

The expression of external work is identical with that illustrated in isotropic plates, which is

$$V = - \iint_A \left[p_z w + \frac{N_x}{2} \left(\frac{\partial w}{\partial x} \right)^2 \right] dx dy \tag{4.32}$$

Minimum potential energy

Combination of Eq.4.31 and Eq.4.32 gives rise to the expression of total potential energy for composite plate under in-plane compression and uniform distributed pressure:

$$\Pi = U + V = \iint_A \left\{ \begin{aligned} & \frac{1}{2} D_{11} \left(\frac{\partial^2 w}{\partial x^2} \right)^2 + D_{12} \frac{\partial^2 w}{\partial x^2} \frac{\partial^2 w}{\partial y^2} + \frac{1}{2} D_{22} \left(\frac{\partial^2 w}{\partial y^2} \right)^2 + 2D_{66} \left(\frac{\partial^2 w}{\partial x \partial y} \right)^2 \\ & - \frac{1}{2} N_x \left(\frac{\partial w}{\partial x} \right)^2 - p_z w \end{aligned} \right\} dx dy \tag{4.33}$$

Combined with the deflection expression Eq.3.3 which satisfies the simply supported boundary condition, the energy becomes

$$\begin{aligned} \Pi = U + V = & \frac{ab}{8} \sum \sum w_{mn}^2 [D_{11} \left(\frac{m\pi}{a}\right)^4 + 2(D_{12} + 2D_{66}) \left(\frac{m\pi}{a}\right)^2 \left(\frac{n\pi}{b}\right)^2 \\ & + D_{22} \left(\frac{n\pi}{b}\right)^4 - N_x \left(\frac{m\pi}{a}\right)^2] - \frac{4abp_z}{\pi^2} \sum \sum w_{mn} \frac{1}{mn} \end{aligned} \quad (4.34)$$

Stationary points is obtained by making the first derivative energy variation into zero

$$\frac{\partial \Pi}{\partial w_{mn}} = 0 \quad (4.35)$$

Thus,

$$w_{mn} = \frac{16p_z}{\pi^4 mn} \frac{a^4}{[m^4 D_{11} + 2(D_{12} + 2D_{66}) \mu^2 m^2 n^2 + n^4 \mu^4 D_{22}] \pi^2 - N_x a^2 m^2} \quad (4.36)$$

Again, the critical load can be solved when the denominator vanishes, which is formed as

$$N_{cr} = \frac{\pi^2 [D_{11} m^4 + 2(D_{12} + 2D_{66}) \mu^2 m^2 n^2 + D_{22} n^4 \mu^4]}{a^2 m^2} \quad (4.37)$$

or

$$N_{cr} = D_{11} \left(\frac{m\pi}{a}\right)^2 + 2(D_{12} + 2D_{66}) \left(\frac{n\pi}{b}\right)^2 + D_{22} \left(\frac{a\pi}{m}\right)^2 \left(\frac{\pi}{b}\right)^4 \quad (4.20)$$

Similar expressions are obtained indicating that critical buckling are not affected by the lateral load under the small-deformation assumption.

4.5 Finite Element Analysis

4.5.1 Model Description

A rectangular plate made from carbon epoxy unidirectional plies IM7/8552 is modeled as conventional shell elements. Mechanical properties of this unidirectional ply (UD) are reported in Table 4.1. To simplification purpose, the composite laminate is modeled identically in geometry with the isotropic plate discussed in Chapter 3, which has a length (denoted by a) of $480mm$, a width (b) of $120mm$ and a thickness (h) of $2mm$. Configuration features and stacking patterns of the laminate are listed in Table 4.2. Layups of the laminate have the plies at 0° , 45° and 90° , stacking in a symmetric pattern, leading to an absence of bending-extension interaction.

E_1 [GPa]	E_2 [MPa]	G_{12} [MPa]	ν_{12}	t_{ply} [mm]
150	9080	5290	0.32	0.125

Table 4.1: Material property of IM7/8552 layers

In Table 4.1, E_1 and E_2 are symbols of Young's modulus of the UD plies in directions of 0° and 90° , respectively. G_{12} represents the in-plane shear modulus while ν_{12} is the Poisson's ratio that corresponds to a contraction in 90° direction when an extension is applied at 0° . t_{ply} is the thickness of single UD layer.

Components	Stacking sequence	Total thickness, mm
Plate	$[45^\circ / -45^\circ / 0^\circ / 90^\circ]_{2s}$	2

Table 4.2: Stacking sequence of the laminate

Boundary condition

All the edges of the plate are simply supported which out-of-plane movements are restricted. Additional boundary conditions such as the in-plane restraints can be referred to that in the isotropic model in Chapter 3(See Fig 3.8 and Table 3.4).

Meshes

Similar to those in Chapter 3, reduced conventional shell elements "S4R" are adopted to define the thin composite plate due to the computationally inexpensive property for dynamic explicit FE simulation. Their mesh sizing for the composite model is 10mm with for the sake of compromising the computational time and prediction accuracy. Refined meshing strategies will be used if higher prediction accuracy is required.

4.5.2 Eigenvalue Analysis

Provided the configuration and stacking information, the buckling load $N_{cr,c}$ for simply supported laminates under uniaxial compression can be obtained via Eq.4.5 in which m is obtained from Eq.4.8. The total corresponding buckling force of composite plates is then calculated by:

$$P_{cr,c} = N_{cr,c} * b = \frac{b\pi^2}{a^4} \left[D_{11}m^2 + 2(D_{12} + 2D_{66})\mu^2 + D_{22}\frac{\mu^4}{m^2} \right] = 15.27kN \quad (4.38)$$

where $P_{cr,c}$ and $N_{cr,c}$ stand for the critical buckling load of plate with the unit of kN and kN/m , respectively. Items in an "ABD" matrix, characterizing the stretching and bending stiffness of the plate, are determined by both material properties and plate stacking patterns.

Prediction process performed in Abaqus for composite plates has the same settings as that in isotropic situation excepted for the material selection. For this reason, duplicated description of the modeling for composite plates will not be repeated unless necessary. Simulation results

of laminates under four loading cases distinguished by the magnitude of lateral pressure are reported in Table 4.3, using linear eigenvalue analysis.

p_z	Values, [MPa]	-	$P_{cr,FEM}$, [kN]	$P_{cr,a}$, [kN]	Diff
p_0	0	0	14.91	15.27	2.35%
p_1	0.013	$0.2P$	14.91	15.27	2.35%
p_2	0.065	P	14.91	15.27	2.35%
p_3	0.13	$2P$	14.91	15.27	2.35%

Table 4.3: Eigenvalue simulation results of laminates

In Table 4.3, $P_{cr,FEM}$ and $P_{cr,a}$ are prediction buckling loads of composite laminates subjected to combined loads by using FEM and analytical equations, respectively. Results are observed to prove that critical buckling loads are unaffected by the presence of normal loading p_z under the linear assumption. Similarly, fairly good consistency is observed between linear eigenvalue predictions and analytical solutions, indicating that linear calculations are insufficient for plates subject to normal pressure. As a result, dynamic explicit FE analysis with nonlinearity taken into account becomes necessary.

4.5.3 Explicit Dynamic Analysis

By employing the same finite element model (except for materials) described in the Section 3.5.3 of Chapter 3, studies on postbuckling behaviours of composite plates under the combined action of edge compression and lateral pressure are conducted in dynamic explicit code Explicit/Abaqus.

A four-second loading process in dynamic explicit analysis is carried out. The applied lateral pressure and edge compression with respect to the loading time are shown in Fig 4.2. Simulation results are graphically exhibited in the form of load-deflection and load-shortening curves associated with deformed configurations at different simulation moment (See Fig 4.4 to Fig 4.9).

With the absence of lateral pressure ($p_z = 0$), deflections and total edge compression are recorded with time as seen in Fig 4.3. An initial imperfection has been introduced by using the first eigenmode with four half-waves, which could be observed at the bifurcation point of the deflection curve. The number of wave changes with the increase of edge shortening and is accompanied by the deflection inverting. Postbuckling responses are exhibited in terms of load-shortening and load-deflection curves as shown in Fig 4.4. The deflection is measured at one-third of the longitudinal symmetric line, which has been explained in Chapter 3. Inflection and strain reversal points in these two plots are pointed out as the first buckling onset of the laminate. Due to the influence of predefined imperfection, adoption of inflection point may only provide approximated predictions.

As for the case when plates are imposing a lateral pressure of $p_1 = 0.013MPa$, a slight deflection is first observed as pressure increases (See Fig 4.5), followed by a plateau as pressure

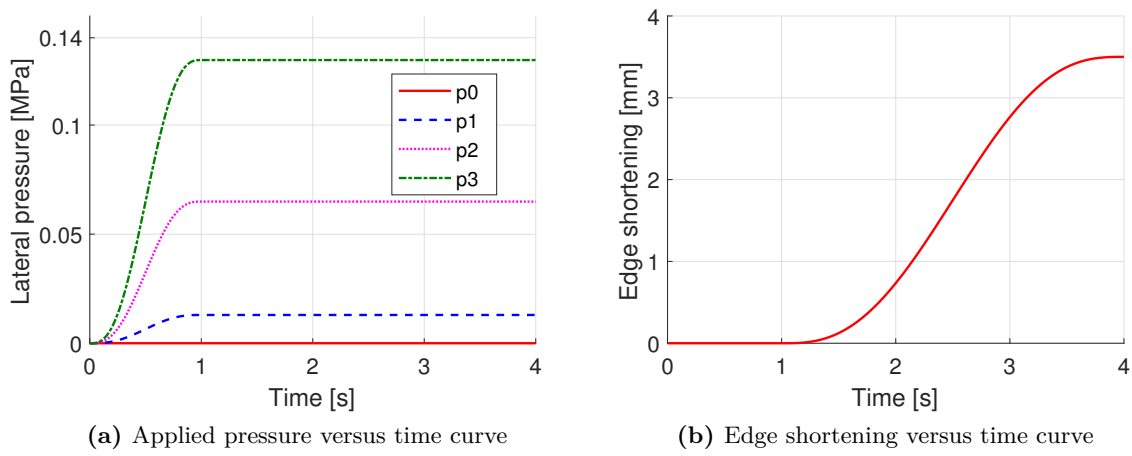


Figure 4.2: Lateral pressure and edge shortening vs time curve

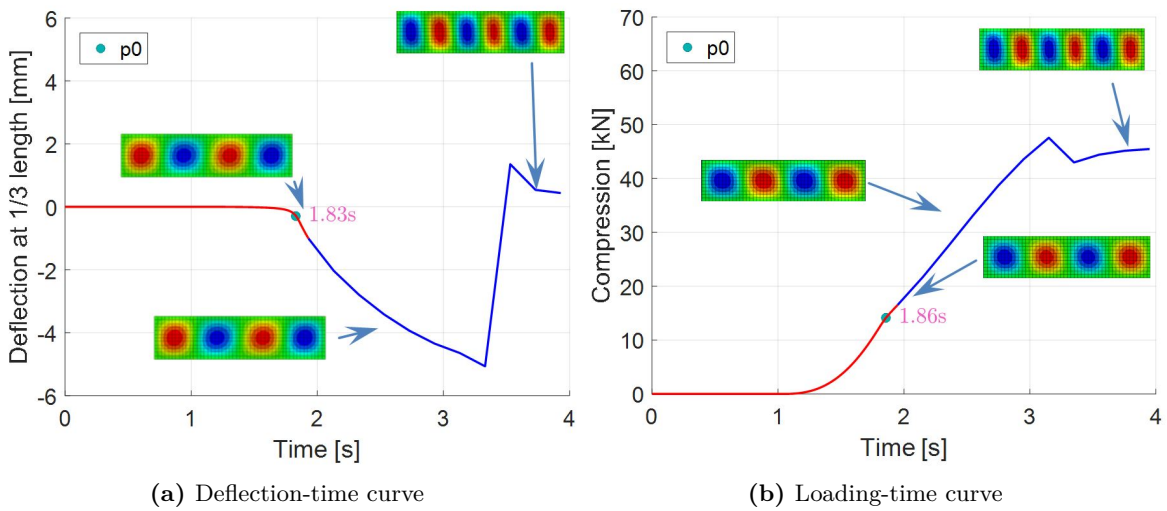


Figure 4.3: Postbuckling behaviour of composite plates and corresponding displacement fields (p_0)

load stay constant. This stable state continues as the edge compression load is added at 1s. A sudden inverting of plate takes place at about 1.9s, implying buckling has been triggered in the laminate. Different from the uniaxial loaded plates, a three-wave buckling configuration has been observed in the plate when lateral pressure is applied. The buckling load, observed from Fig 4.6, witnesses an approximately increase of 20% (from $13.92kN$ to $16.69kN$) compared to that in Fig 4.4.

In Fig 4.7, the plate experiences an even larger out-of-deflection as expected. The occurrence of the buckling has been delayed to 2.55s, and a four-wave deformed configuration is observed as the buckle occurs. The predicted buckling load from Fig 4.8 is found to be tripled as that without lateral pressure.

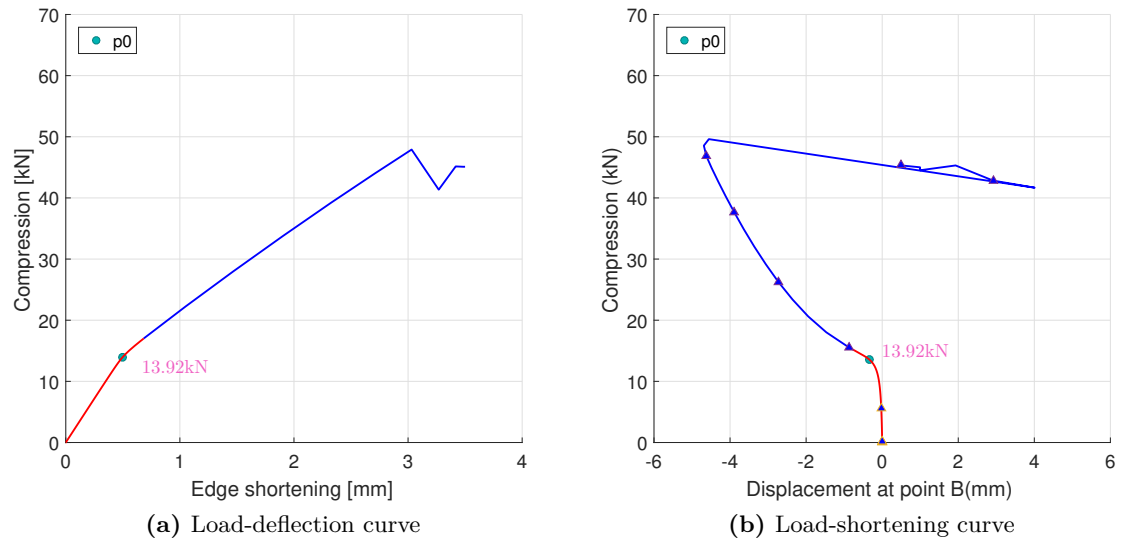


Figure 4.4: Postbuckling behaviour of composite plates (p_0)

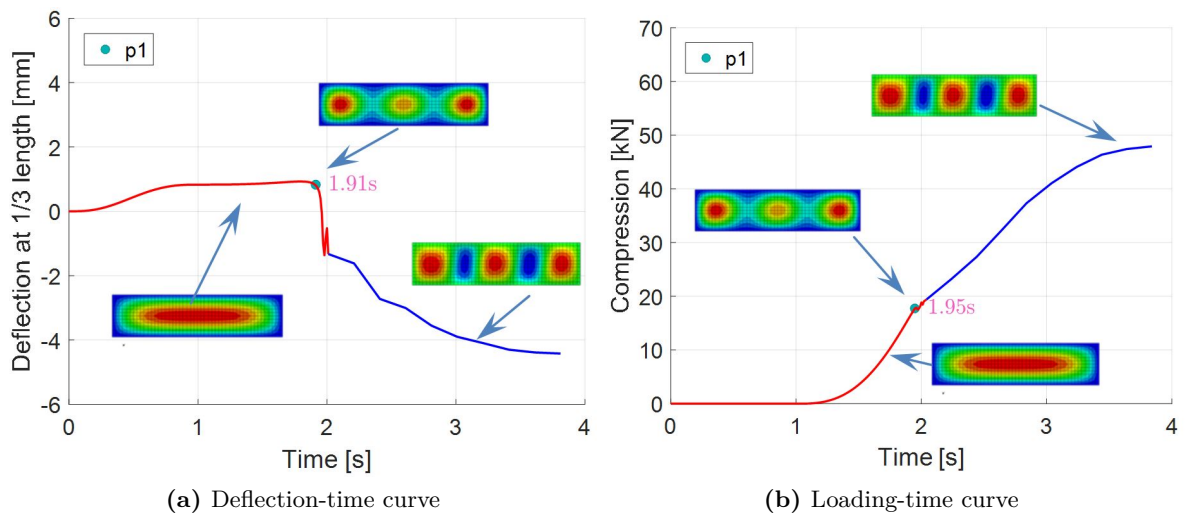


Figure 4.5: Postbuckling behaviour of composite plates and corresponding displacement fields (p_1)

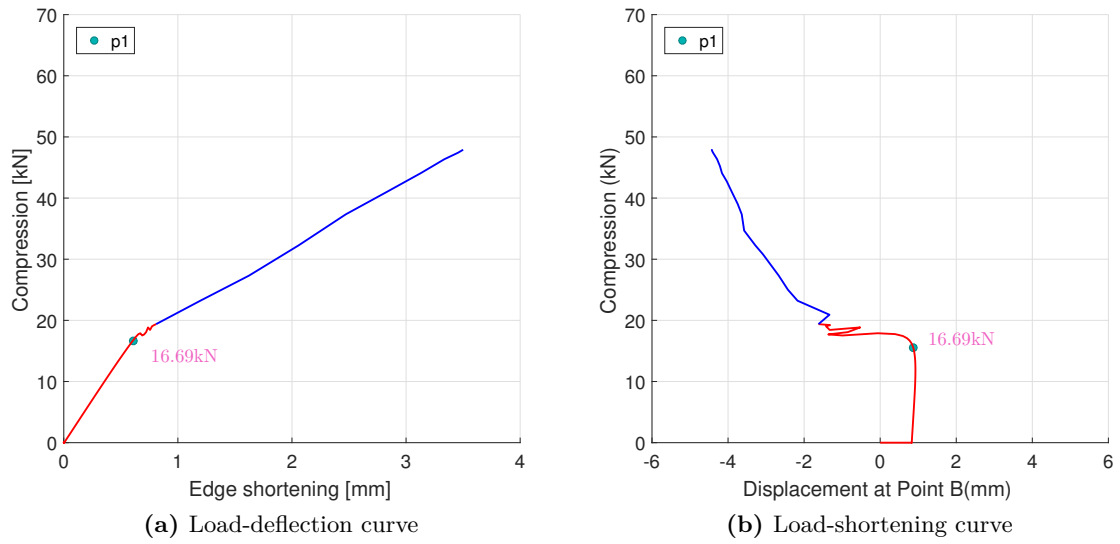


Figure 4.6: Postbuckling behaviour of composite plates (p_1)

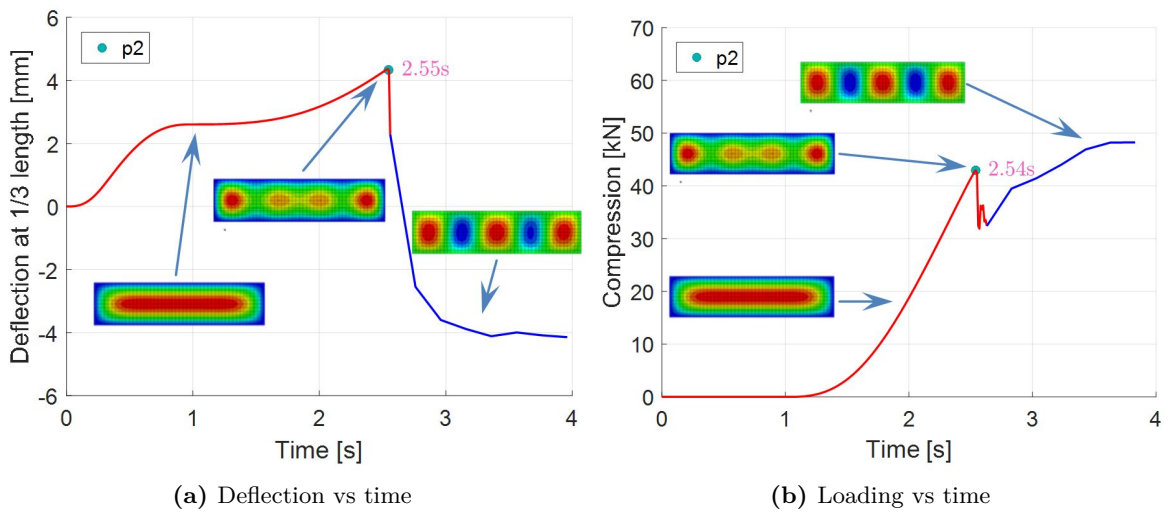


Figure 4.7: Postbuckling behaviour of composite plates and corresponding displacement fields (p_2)

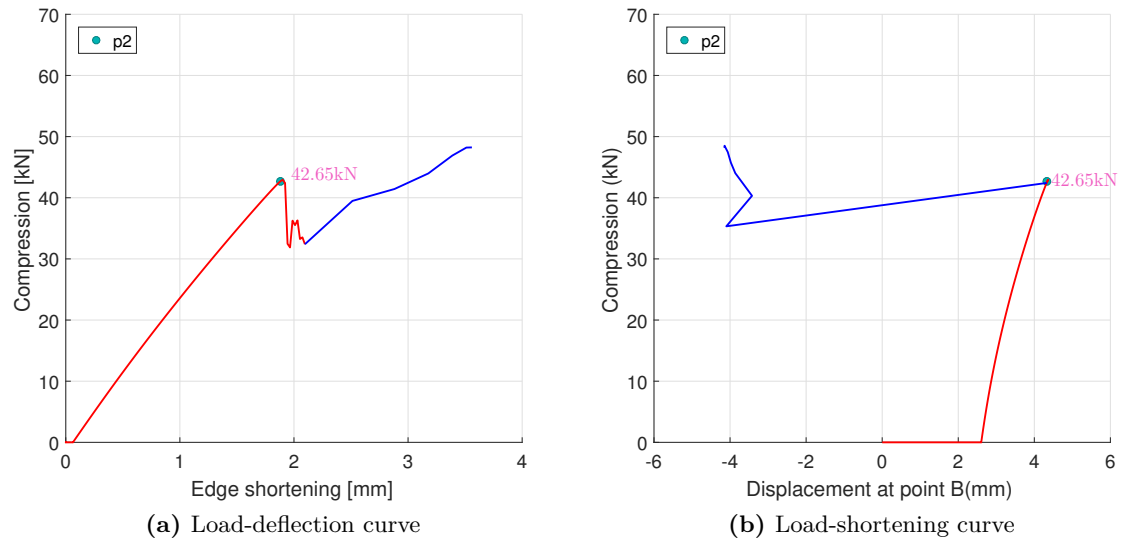


Figure 4.8: Postbuckling behaviour of composite plates (p_2)

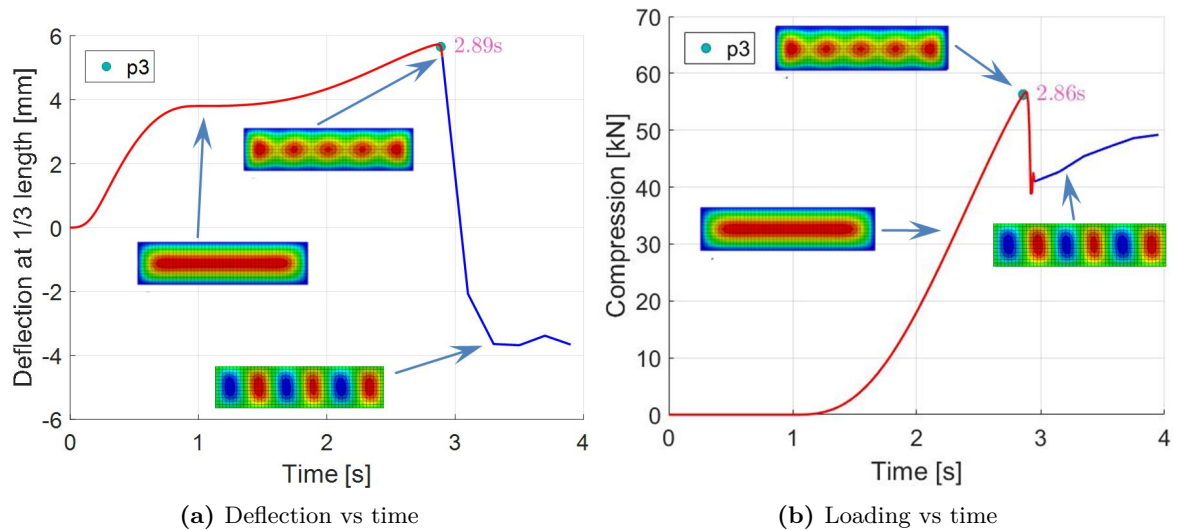


Figure 4.9: Postbuckling behaviour of composite plates and corresponding displacement fields (p_3)

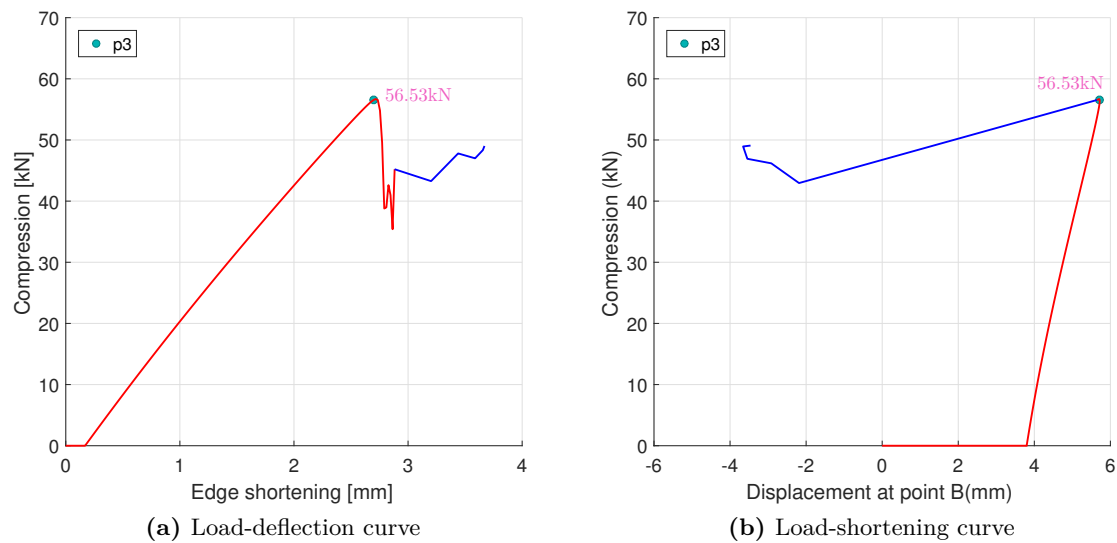


Figure 4.10: Postbuckling behaviour of composite plates (p_3)

It is interesting to see that five-waves configuration appears as the pressure load reaches as large as twice the cabin pressure ($p_3 = 0.13\text{MPa}$) as shown in Fig 4.9. Buckling takes place in an even more abrupt manner, accompanied by the deflection reversal. The buckling load obtained from Fig 4.10 raises to roughly four times as that with single compression load. It should be noted that material failure is not taken into consideration in this simulation, which could yield an early collapse before buckling.

4.6 Conclusions

Buckling and postbuckling behaviours of simply supported rectangular composite laminates under the combined action of edge compression and lateral pressure were investigated by analytical and numerical approaches. For theoretical analysis, classical laminate plate theory was adopted to establish the large deflection von Karman equations whose solutions were solved to characterize the critical buckling load. Those results were observed to be in line with the predictions from eigenvalue buckling analysis of FEM under linear elastic assumptions. However, when the plate experiences large deflection, predicted results of buckling loads using dynamic explicit code Abaqus explicit dynamic suggested that the lateral pressure has significantly enhanced the stability strength of the laminate in a way that behaved analogously to isotropic plates discussed in Chapter 3.

Conceptual Design of the Testing Setups for Buckling Experiments

In previous chapters, theoretical and numerical investigations on single rectangular plates have been developed. Effects of lateral pressure on buckling strength of axially compressed plates are obtained by using finite element methods. The next step is to extend the investigation to stiffened panels. Due to the complicated theoretical process in dealing with buckling and postbuckling behaviours of plates especially for those made of anisotropic materials, it is more convenient for structural engineers to apply FE methods in conjunction with experimental tests. The experimental study can validate prediction results and help stress engineers in gaining a better understanding of buckling and postbuckling phenomena of stiffened panels.

In this chapter, the emphasis is laid on a conceptual design of new testing setups for buckling experiments under combined loads. Difficulties lie in the application of lateral pressure which is exerted accompanied by uniaxial loads. This chapter is divided into three sections. In Section 5.1, existing tests of buckling behaviours of stiffened panels under the action of lateral pressure and axial compression are evaluated concerning the application pattern of pressure loads. In Section 5.2, a conceptual design of small-scale testing setups for an elementary study is described in details. Measures are implemented with the consideration of cost and feasibility based on classical experimental rigs. Shortcomings and recommendations on the design work are given in the last section.

5.1 Evaluation of Existing Experiments

A limited number of studies can be found to develop buckling experiments of flat stiffened panels under compression combined with simultaneous lateral loads. Based on the introductions performed in Chapter 2, limitations and shortcomings inherited in these tests will be

discussed and evaluated regarding, for example, feasibility and cost. The feasibility here can be related to how easy can a buckling experiment under combined loads be compatible with a similar testing setups that was used to test axially loaded panels. Conclusive and comparative observations with respect to the loading pattern of pressure loads in the test are tabulated in Table 5.1.

NO.	Test	Advantages	Disadvantages	Feasibility	Cost
1	COLTS [1]	Accurate	Expensive Complex Less recyclable	★	★
2	Airbag [27]	Less labor force Easy control Inexpensive Recyclable	flatness required Low accuracy Aspect ratio limit	★★ ★★	★★ ★
3	Multiple Airbags [28]	Relatively simple Recyclability	More labor force Preferable horizontally assigned	★★ ★★	★★
4	Pressure Chamber [29]	Accurate Recyclable	Precise required Tightness required	★★	★
5	Points loads [30]	Accurate control Recyclable Low cost	Inaccurate Exatra actuators	★★ ★	★★ ★★

Table 5.1: Advantages and disadvantages of former experiments

The number of black solid stars shown in Table 5.1 stands for the degree of the acceptability of a test with respect to the feasibility and cost. Being adopted to simulate the full-scale pressurized wing box, the COLTS experimental facility, in spite of accurate prediction, need extremely sophisticated manufacturing, which renders its application to the elementary research difficult during preliminary stage, without mentioning the poor compatibility with classical testing setups. The sealed chambers with pressurized air pumped have tightness problems when edge compression is applied to the specimen which is assembled as one of the facets of chamber. The sealing problem can be thoroughly avoided in the case when lateral pressure is considered equivalent to concentrated forces applied by two or three loading jacks as points loads. The adoption of rubber airbags as a compromise methods to solve the problem by way of providing relatively uniform distributed loads without bringing into the sealing problem. What's more, the installation of airbags could be compatible with testing fixtures of classical buckling experiments. In the following sections, a new designed method will be described, focused on the application of uniform distributed lateral pressure.

5.2 Conceptual Design of Test Setups

Due to the similarity in buckling tests of stiffened panels subjected to compressive loads and those with the combination of lateral pressure and axial compression, the new designed experiment system in this section is presented on the basis of a classical buckling experiment.

One of the examples was developed by London College as displayed in Fig 5.1.

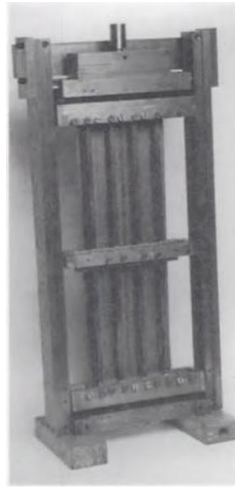


Figure 5.1: Buckling tests by London College [51]

On top of the analysis above, following goals are expected in the new-designed test:

- **Compatibility:** The new designed testing fixtures are capable of being modified from classical buckling experiments.
- **Cost:** The cost, including material, manufacturing, labor forces, should be controlled within a reasonable range.
- **Accuracy:** The actually applied pressure should be precisely controlled and monitored by the internal pressure of the airbag through pressure gauges and sensors.
- **Observability:** Testing rigs should be designed to warrant a sufficient open space for observation during the loading process.

5.2.1 Stiffened Panels

A two-bay stiffened panel with three omega stringers equally spaced is selected as typical structures under test as seen in Fig 5.2. In order to protect the panel ends and ensure a uniform distribution of compression, the specimen is encased in potting tabs at two ends made from resin and aluminum powder. Application of such examples is described in [52]. The end surfaces of the potting tabs are machined to ensure the parallelism between the two loading surface and the verticality between the loading surface and neural plate of the panel. In addition, for the sake of creating a flat contact area for the airbag, a filler pad made of rubber material is adopted with a size fully occupying the panel bay between stringers.

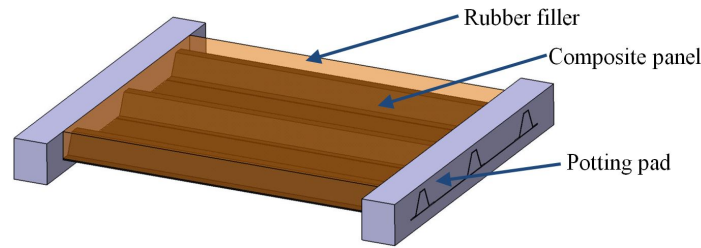


Figure 5.2: Specimen with potting pads at ends

5.2.2 Test Rigs and Supports

Test rigs for buckling experiments under combined in-plane and out-of-plane loads are designed by improving the fixtures of classical buckling tests which have only uniaxial compressed loads. The main supporting components is shown in Fig 5.3(a).

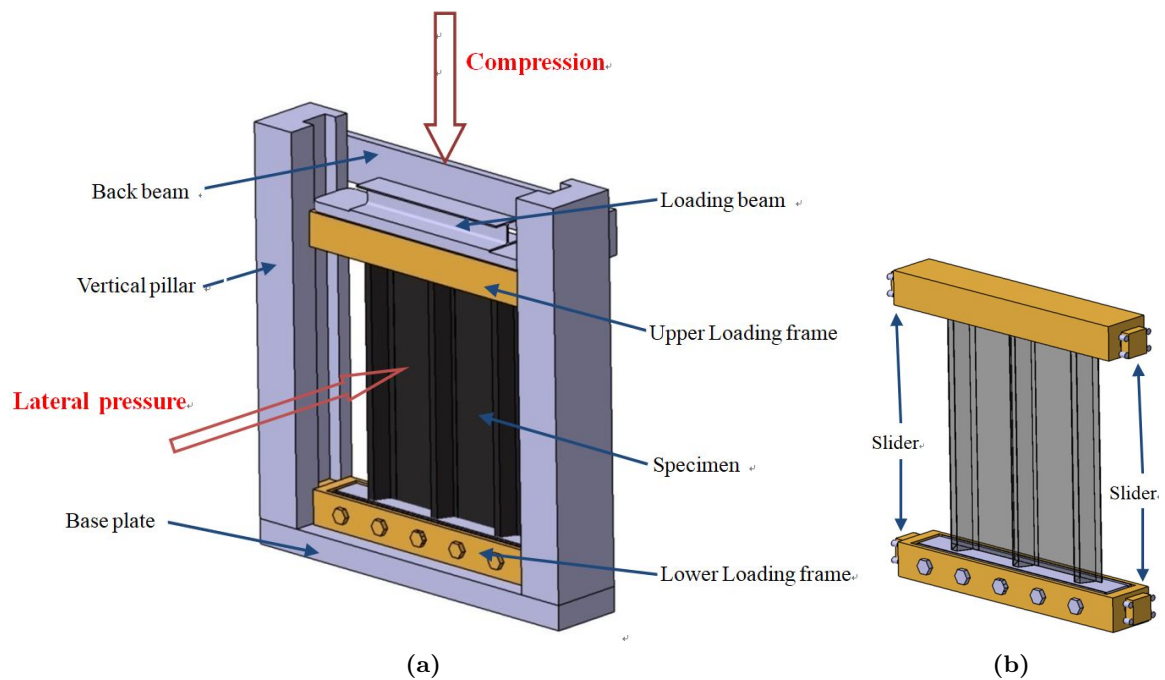


Figure 5.3: Basic supports of the test

A high-capacity rigid frame is built, comprised of two vertical pillars, one base plate, and one back beam, to accommodate the specimen subjected to uniaxial compressive loads and out-of-plane pressure. Vertical pillars are designed with grooves accurately machined to house the sliders which are attached to the loading frame as shown in Fig 5.3(b). Each loading frame has a pair of sliders at its ends and is fitted into the channel of pillars so as to allow the free movement of specimen (constituted of specimen, loading frames and related fixtures) along the guiding channels. The loading frame, providing a rigid support against edge shortening, enables a uniform distributed load of in-plane compression. The loading beam, located on

top of the upper loading frame, is used to transfer the hydraulic compression to the loading frame with the purpose of elimination of eccentricity of jack loads. Lateral pressure is applied horizontally through an inflection airbag which will be discussed in the next section.

5.2.3 Application of Lateral Pressure Loading

As illustrated before, in-plane compression of a stiffened panel is driven by a hydraulic actuator through the upper loading frame while lateral pressure is applied by means of an inflatable airbag located between the stiffened panel and a supporting platform as shown in Fig 5.4. The supporting platform is attached to vertical pillars by clamping screws so that it can support the airbag and sustain out-of-plane reaction forces resulted from the pressurized airbag. Thus, the induced internal loading could be balanced by structural frames without introducing extra hydraulic jacks which were employed Dongqi's experiment [35]. In addition, by doing this, the lateral pressure load can be controlled by monitoring the internal pressure of airbag through a calibrated pressure gauge. Compressed air is pumped into the airbag through an air inlet from the upper side of the airbag as shown in Fig 5.4. To prevent direct contact of the airbags with stiffened panels on the stiffener-side, a filler pad made of rubber material is employed to fill gaps between stiffeners in order to generate a flat contact surface for the airbag and specimen as shown in Fig 5.5. The shape of rubber pads is designed to fit the concave geometry of the panel.

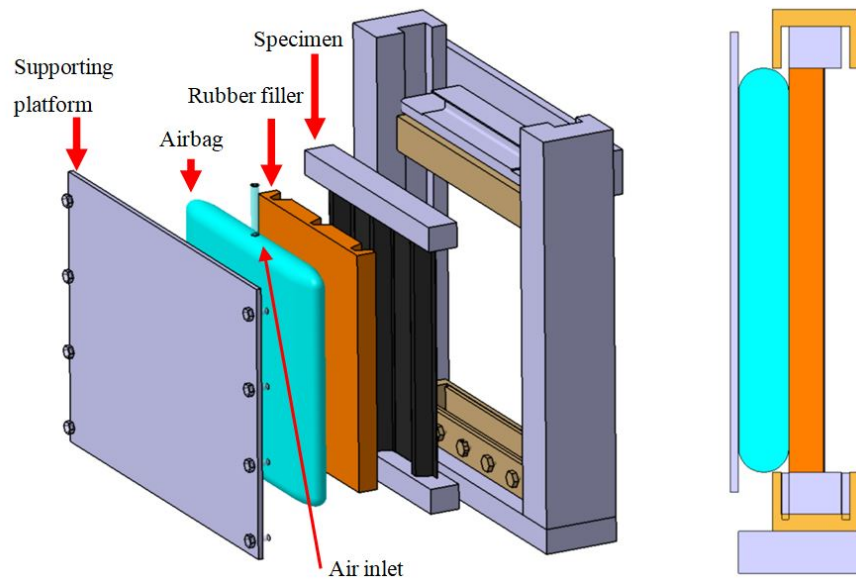


Figure 5.4: The application of lateral pressure by a pressurized airbag

Provided the lateral pressure generated by airbags, reaction forces are inevitable induced and could be balanced by the supporting platform on one side and by four bearings attached to loading frames on the other side as shown in Fig 5.6. In the case of maximum level of lateral pressure ($p_z = 0.13MPa$, see Chapter 3), the resulted lateral loading is completely dependent on the size of testing stiffened panels. The lateral reaction forces in various dimensions of stiffened panels along with the portion assigned to the four bearings are reported in Table

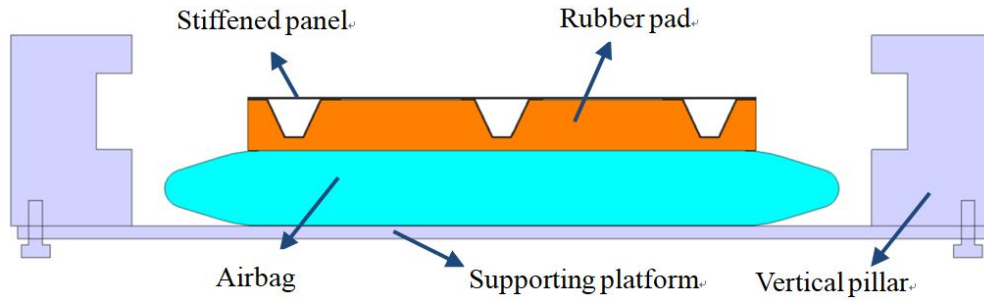


Figure 5.5: Cross-section view of the test setups

5.2.

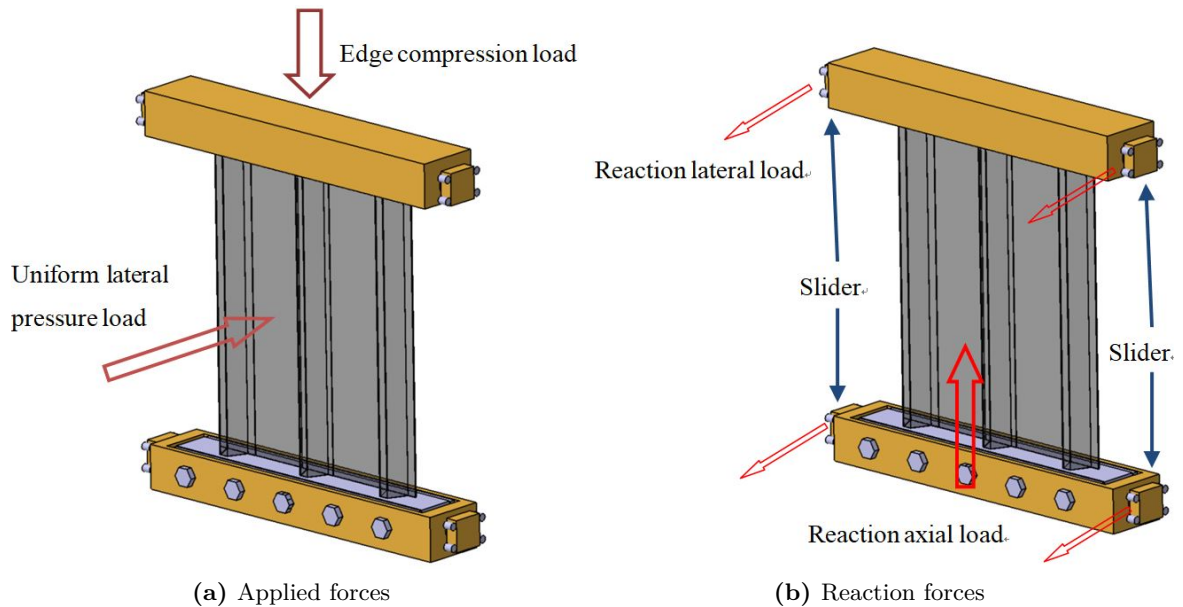


Figure 5.6: Loading cases of specimen fixtures

Dimensions [mm^2]	Bay number	Total reaction forces [kN]	Forces on each bearing [kN]
960 × 600	3	78.88	18.72
960 × 400	2	49.92	9.36
480 × 400	2	24.96	4.68
480 × 200	1	12.48	2.34
240 × 400	2	12.48	2.34
240 × 200	1	6.24	1.17

Table 5.2: Reaction forces resulted from airbags ($p_z = 0.13MPa$)

In Table 5.2, dimensions of stiffened panels are represented by the product of height (unloaded edges) and width (loaded edges). Providing an average width of 200mm for one bay in stiffened panels, a three-bay panel with an area of $960 \times 600mm^2$ is subjected to as high as 18.72 kN

for each cylinder bearing.

Assume that internal pressure of airbags has the same amplitude to the pressure applied to the specimen ($p_z = 0.13MPa$), corresponding skin stresses of different sizes of airbags are reported in Table 5.3. Given an airbag with a thickness of $0.25mm$, membrane stresses under maximum pressure $p_z = 0.13MPa$ vary between $28.4MPa$ and $80.4MPa$.

Dimensions [mm^2]	Airbag thickness [mm]	Airbag skin stress [MPa]
960×600	0.25	80.0
960×400	0.25	73.4
480×400	0.25	56.7
480×200	0.25	36.7
240×400	0.25	39.0
240×200	0.25	28.4

Table 5.3: Skin stresses of various dimensions of airbags ($p_z = 0.13MPa$)

5.2.4 Airbags

In the new-designed buckling experiment with out-of-plane loading involved, the inflation bag plays a key role in applying the pressure load with uniform distribution and controllable amplitude. Since the absence of additional horizontal actuators, lateral loading applied to the specimen in this test is controlled by pressure gauges and assumed to be equal to the internal airbag pressure. In order to eliminate discrepancies between real pressure loading and internal airbag pressure, certain measures should be taken on the airbags regarding the geometry, material and fixture.

Geometry

Airbags can be constructed in multiple shapes. In this test, the geometry of the airbag is dependent on the in-plane dimension of the specimen and the cross-section can be designed as pillow-shape or quasi-rectangular shape by referring to lifting airbags [53] and the air balloon in pressure distribution. In this test, in view of the relatively low pressure loading, maximum $0.13MPa$, it is more convenient to choose airbags with quasi-rectangular cross-sections although further trade-offs regarding fabrication and loading performance are still required.

Lateral pressure loads will not be automatically received by testing panels from inflection airbags unless certain deformations of the airbag occur after contacting the specimen. In order to obtain a uniform distributed pressure loading that equal to the internal pressure of the airbag, measures must be taken to ensure a full platen contact. Potential situations may happen to the airbag during the application of lateral loading as seen in Fig 5.8. In Fig 5.8(a), the specimen is not fully contacted with the airbag, and smaller distance between them is

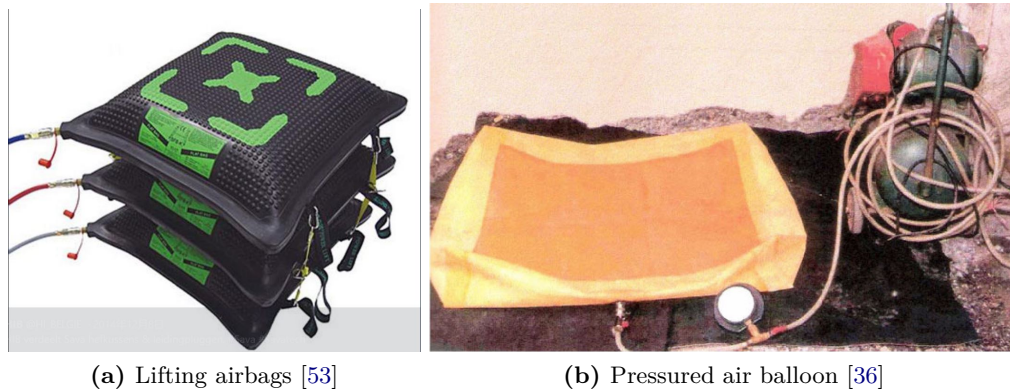


Figure 5.7: High-pressurized lifting airbags and low-pressurized air balloon

necessary. In Fig 5.8(b), the contacting region does not fully cover the stiffened panel surface due to the insufficiently large size of the airbag. In Fig 5.8(c), excessive deformation of the airbag is resulted by the specimen, and improvements are supposed to perform by reducing the bag size or increasing the distance between the supporting platform and the specimen. In Fig 5.8(d), the airbag and specimen fit well each other, and the pressure load is transferred from the internal pressure of the airbag to the specimen with the aid of supporting platform.

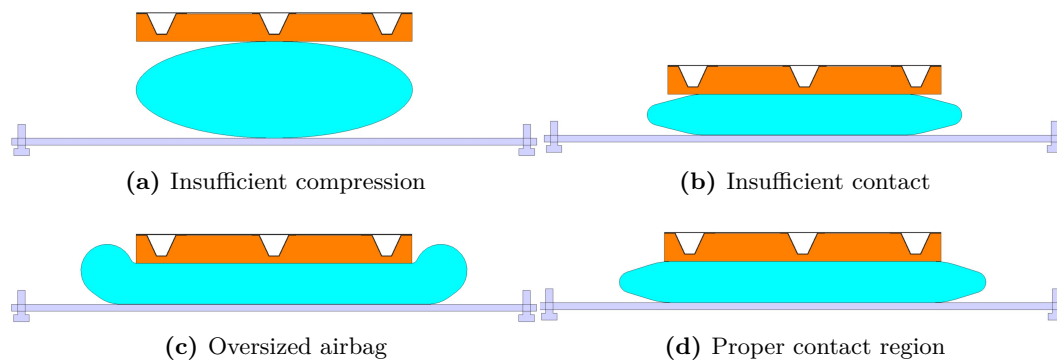


Figure 5.8: Airbag contact situations

In addition, special types of compression sensors which are used to measure the compression loading are fitted to the screw bolts on top of the supporting platform as seen in Fig 5.9. Measurements of every compression sensor are summed up in order to calibrate lateral pressure loads applied to the specimen. The pressure loading applied to the specimen can be approximately calculated by dividing the total forces measured from compression sensors by the project area of the panel.

Material

According to the capacity of pressure loading, airbags can be made of hermetic Neoprene (a family of synthetic rubbers), and reinforced by high-strength wove of steel wire or Kevlar on the base of Neoprene. For the sake of uniform distributed load, it is more convenient to adopt

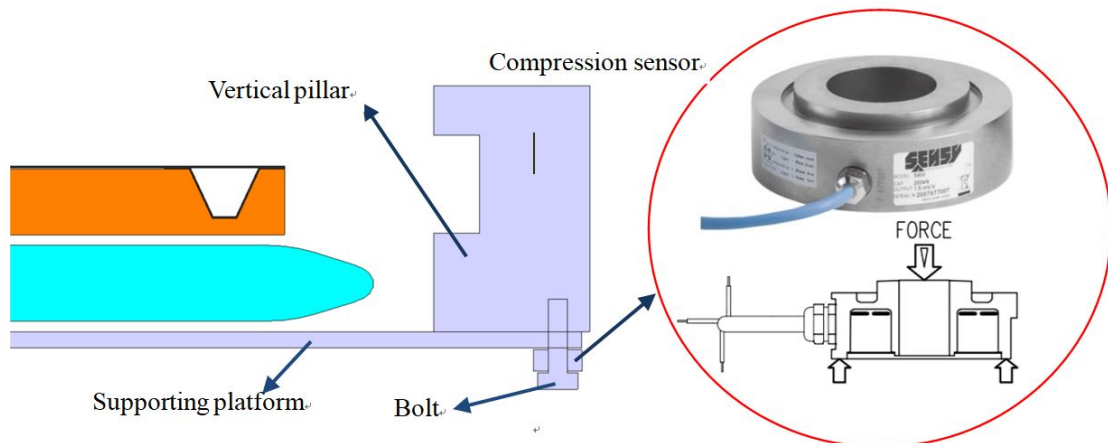


Figure 5.9: Compression sensors for measurement of lateral loads [54]

the Kevlar fabric as reinforcement with its high performance in flexibility and strength.

Fixtures

Airbags are fixed in position through klittenbands which are pasted to the inner face of the supporting platform. The supporting platform is then bolted to the vertical pillar by screw bolts so as to accommodate the airbag as shown in Fig 5.10. The rubber filler pad is located between the specimen and airbag.

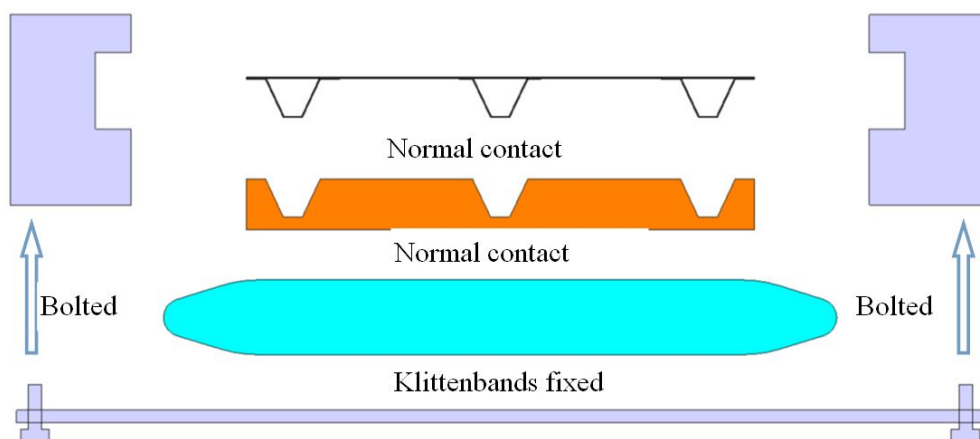


Figure 5.10: The assembly of the testing components

5.2.5 Boundary Fixtures

The specimen in this test is constrained in such ways that loaded edges with potting tabs are clamped by the loading frames while unloaded edges are free from restriction. By using an

adjusting pads that driven by five bolts machined inside the loading frame, two ends of the panel are tightly clipped as illustrated in Fig 5.11. A rubber mat is used to prevent squeeze damages to the specimen. Four square-shaped sliders with cylinder bearings are assembled to the loading frames in order to guarantee the in-plane motion of the specimen, which at the same time provide a rigid support against rotation and out-of-plane motion of the edges. Lubrication treatment is implemented in the channel of the pillar to make sure that the specimen can move frictionlessly inside the pillar groove.

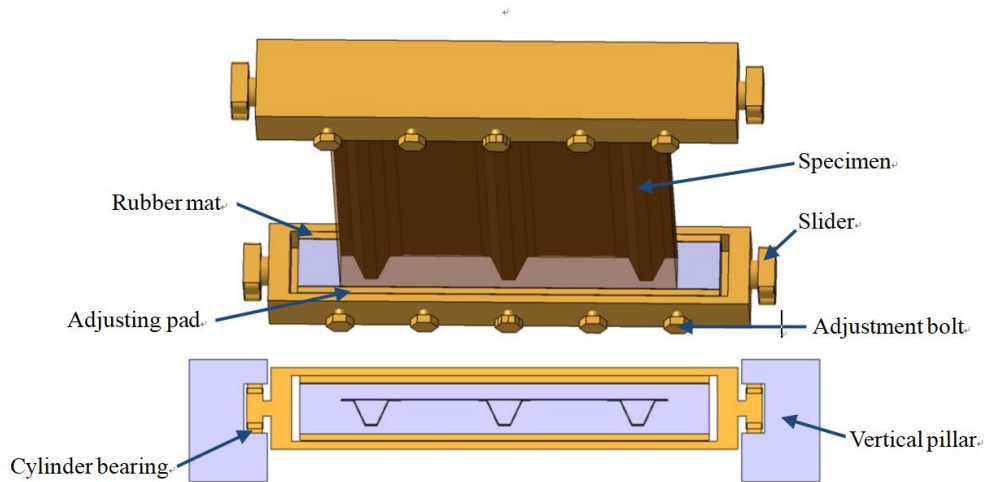


Figure 5.11: Test fixtures

5.3 Conclusions and Recommendations

In this chapter, a conceptual design of an experiment for stiffened panels under the action of combined loading is described. By means of a pressurized airbag, the lateral pressure is expected to be applied without introducing complicated setups. The test rigs are designed with the consideration of compatibility with classical buckling experiments. In the next chapter, the finite element analysis will be conducted in order to obtain an overview of buckling responses in advance.

In the preliminary design work, shortcomings that may potentially affect the accuracy of testing are listed below.

- The displacement field of stiffeners is invisible due to the obstacle of filler materials and airbags on stiffener side of the panel.
- The relation between the internal pressure of airbags and actual lateral pressure acted on the panels is still under investigation.
- The rubber filler pad may be potentially squeezed out at unloaded edges, leading to nonuniform distributed pressure that applied to the panel.

- Frictions between the rubber filler and the panel may result in testing errors and could be eliminated by placing plastic films in between.

Finite Element Modeling of Stiffened Panels in Testing Setups

6.1 Introduction

In Chapter 5, a conceptual design of a buckling experiment of stiffened panels under in-plane compression and lateral pressure has been proposed. Airbags and rubber fillers are used to apply lateral forces. In this chapter, corresponding numerical investigation will be conducted using FE software Abaqus. FE models are established by referring to the specimens in [55] while loading and boundary conditions are based on the experimental setups in order to closely imitate the real testing process. Assessment of the effect of filling materials aforementioned in Chapter 5 on the stability behaviour of the specimen is also studied. For computational simplicity, debonding between stringers and skin is not taken into account.

The analysis in this section is organized as following parts. In Section 6.2, FE models of composite stiffened panels are established in Abaqus. An eigenvalue analysis of the stiffened panel is conducted in Section 6.3. Linear static modules in Abaqus is employed to provide the preloaded base state of panel. Dynamic explicit analyses under different load cases are implemented in Section 6.4. Deformed configurations of both stiffeners and in-between plates are depicted and utilized to determine the buckling initiation. To reveal effects of rubber filler pads on the postbuckling behaviour of stiffened panels, FE models of rubber pads are created and comparisons are carried out between panels with and without rubber filler in terms of load-shortening curves. Conclusions and summaries are given in the last section.

6.2 Model Description

6.2.1 Geometry and Mesh

A typical composite stiffened panel consisting of three hat stringers attached to one side of a rectangular substrate is investigated. Geometries of the in-between plates are selected as same as the unstiffened plate depicted in Chapter 4 in order to reproduce postbuckling responses. Omega-shaped stiffeners are equally spaced across the plate with foot flanges attached to the skin as sketched in Fig 6.1(a).

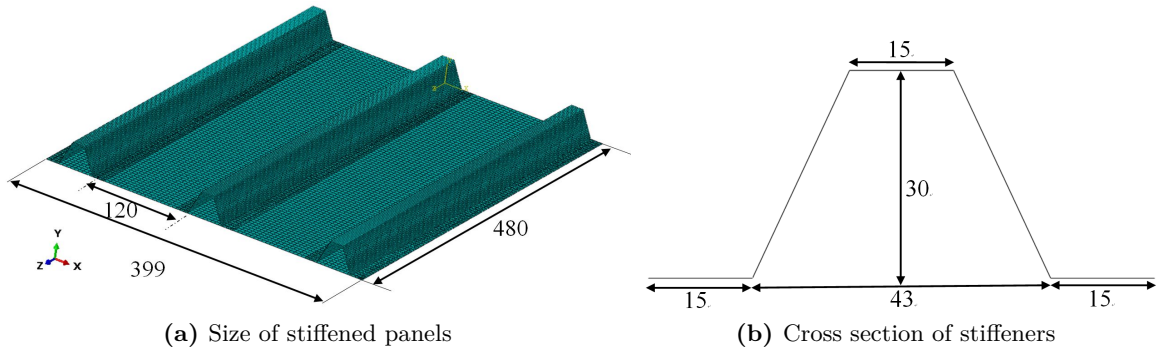


Figure 6.1: The configuration of stiffened panels

FE models are created in the form of assemblies, including one skin and three identical hat stringers. The rectangular skin has a size of 480mm in length and 399mm in width while the stringers have a height of 30mm , a width of 15mm for both crown and foot flanges as shown in Fig 6.1(b). The distance between two foot-flanges is measured as 43mm such that the entire stringer size can be determined due to the symmetry. Stringers are attached to skin by using "tie" couplings. It is noted that the modeling of the cohesive elements between skin and stringers is neglected for simplification perspective.

Both stringers and skin are assigned with IM7/8552 graphite-epoxy material with mechanical properties reported in Table 4.1 (See Chapter 4). A quasi-isotropic laminate is selected for the skin, constituted by 8 unidirectional plies with a stacking sequence of $[45^\circ/90^\circ/-45^\circ/0^\circ]_s$. The stiffener consists of 7 unidirectional plies, stacking symmetrically with respect to the middle ply as a pattern of $[-45^\circ/0^\circ/45^\circ/0^\circ/45^\circ/0^\circ/-45^\circ]$, resulting in a total 0.875 mm thickness. The composite stacking sequences of the model are listed in Table 6.1.

Components	Stacking sequence	Thickness [mm]
Skin	$[45^\circ/90^\circ/-45^\circ/0^\circ]_s$	1
Stringer	$[-45^\circ/0^\circ/45^\circ/0^\circ/45^\circ/0^\circ/-45^\circ]$	0.875

Table 6.1: The stacking sequence and thickness

Reduced conventional shell element *S4R* is employed with a mesh size of 7.5 mm for each component, including 5376 elements in total. A convergence study concerning the mesh

density is conducted in eigenvalue buckling analysis, suggesting that the mesh size of 7.5mm is acceptable with a deviation under 5% compared with refined mesh models.

6.2.2 Boundary Conditions

To imitate the restraints of potting tabs at two ends of the stiffened panel, boundary conditions of the specimen are defined in such a way that nodes at lower edge are completely clamped while those at upper edge are restrained at all six DOFs except for the in-plane motion along z coordinate axis (See Fig 6.2). Nodes of both unloaded edges are free to move and rotate. Multi-point constraints are applied to the nodes in upper edge making it stay straight during loading process. Surface-to-surface tie constraints are used at the connecting regions between stringers and skin.

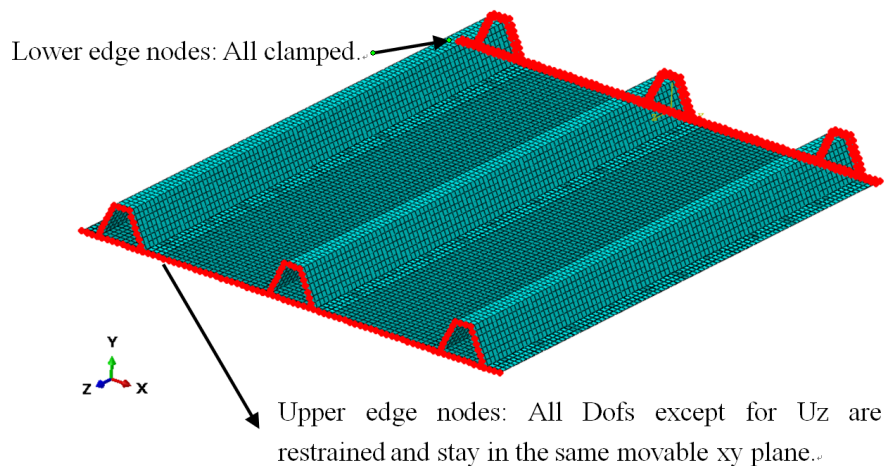


Figure 6.2: Boundary conditions of the panel

6.2.3 Loading Cases

Edge compression of the stiffened panel is applied as an in-plane displacement of nodes in the upper edge, and the amplitude is same as that discussed in Chapter 3. Uniform distributed pressure is applied directly to the surfaces of both stringers and skin as seen in Fig 6.3. Corresponding amplitudes can be referred to the description in Table 3.5 and Fig 3.11 in Chapter 3.

6.3 Eigenvalue Buckling Analysis

An eigenvalue buckling analysis with two loading steps, general static and linear buckling, is conducted. The simulating process is analogous to that of unstiffened plates in Chapter 3 in which lateral pressure and edge compression are added in two sequential steps. Prediction results are reported in Table 6.2.

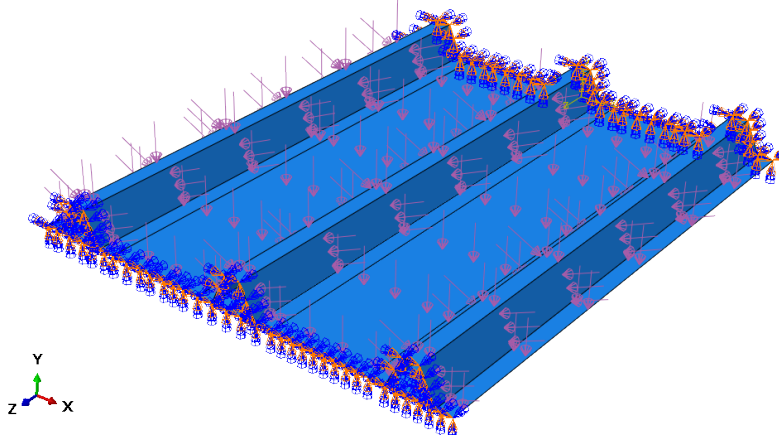


Figure 6.3: Application of pressure load to the stiffened panel

Pressure	p_0		p_1		p_2		p_3	
	e_{cr}	F_{cr}	e_{cr}	F_{cr}	e_{cr}	F_{cr}	e_{cr}	F_{cr}
Buckling displacement, Buckling load	0.163	15.6	0.161	15.5	0.07	4.8	0.005	0.67

Table 6.2: Results of eigenvalue analysis

In Table 6.2, parameters e_{cr} stands for the eigenvalue of the edge shortening while F_{cr} represents corresponding critical buckling loads of stiffeners panels. With the introduction of lateral pressure, predicted buckling loads show a slight deduction (from $15.6kN$ to $15.5kN$) with the pressure being increased from zero to $p_1 = 0.013MPa$. Under the pressure loading $p_2 = 0.065MPa$ and $p_3 = 0.13MPa$, buckling loads become $4.8kN$ and $0.67kN$ respectively, which seems to be unreasonable. Corresponding eigenmode shapes (eigenvectors) of the stiffened panel under various pressure loads are displayed in Fig 6.4.

Due to the anisotropic property of composite panels, buckled waves exhibit a non-symmetric pattern as shown in Fig 6.4. The region near loaded edges of the panel buckles prior to other areas with the increase of lateral pressure. It is observed that only the skin buckling behaviour is captured in the eigenvalue analysis. To further investigate postbuckling behaviours of stiffened panels under combined loads, an explicit dynamic analysis is required.

6.4 Dynamic Explicit Analysis of Stiffened Panels

In this section, composite stiffened panels under different levels of lateral pressure and edge compression are analyzed using the explicit dynamic module in Abaqus to evaluate the results obtained from eigenvalue analyses. Load-shortening curves associated with deformation configurations are derived. According to previous studies, buckling phenomena of structures occur accompanied by the loss of panel stiffness which, to some extent, could be observed from their load-shortening curves.

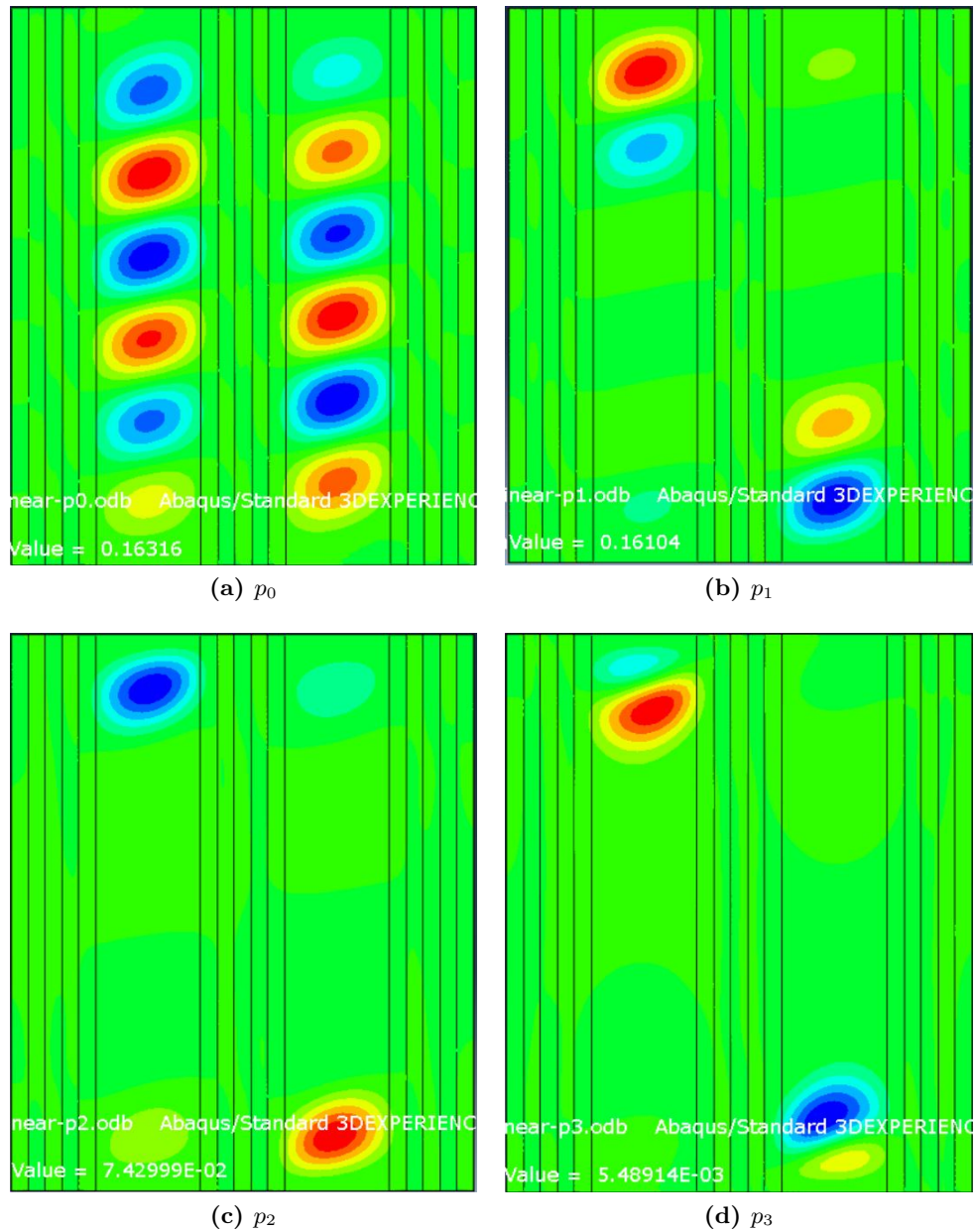


Figure 6.4: Eigenvectors of stiffened panels subjected to combined loading

Potential buckled components of stiffened panels are expected to be the following parts:

- Exposed regions of skin between adjacent stiffeners, abbreviated as "skin";
- Webs of stiffeners, abbreviated as "web";
- Skin covered by stiffeners, abbreviated as "skin under stiffeners";
- Crown top of stiffeners, abbreviated as "crown".

Under the combined action of lateral pressure and uniaxial edge shortening, relations between reaction forces and in-plane displacements are plotted with the buckling initiation of each component pointed out as shown in Fig 6.5 to Fig 6.8. Corresponding deformed configurations are also displayed.

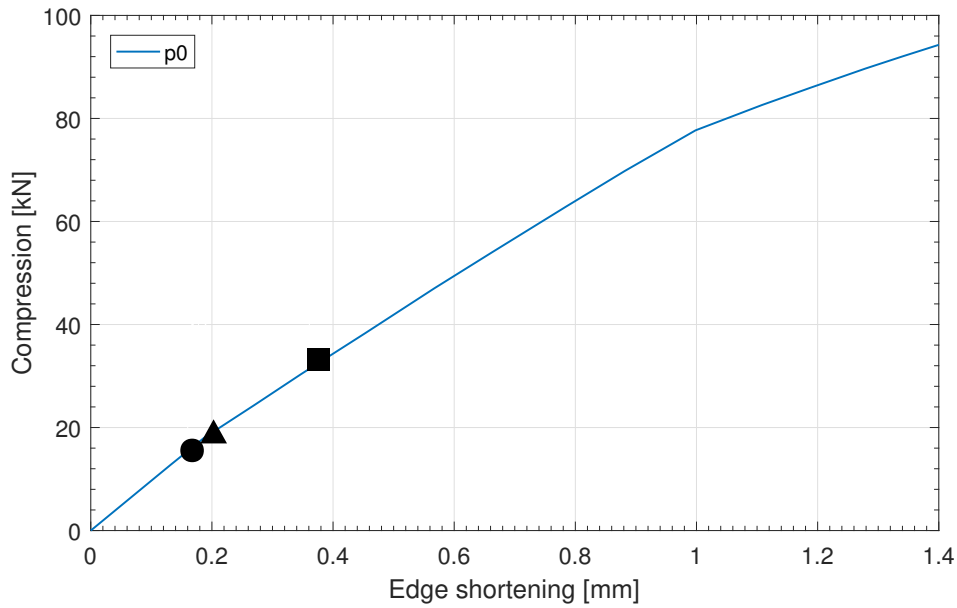
The order of buckling onsets for each component can be observed in Fig 6.5 where skin buckles first followed by stiffeners and skin under them. With the absence of lateral pressure, the skin between stiffeners buckles earlier at about $16kN$ compared to other parts which reach their buckling points at $20kN$ (webs) and $35kN$ (skin under stiffeners), approximately. It is noteworthy that the buckling phenomenon of the crown top is not taken into consideration since buckling waves of crown are difficult to observe from both load-shortening curves and displacement configurations.

In Fig 6.6, as the increasing of lateral pressure, buckling loads of both skin and webs witness an approximate $8kN$ rise while that of skin under stiffeners stays unchanged. As the continuous increasing of lateral pressure to a level of $p_2 = 0.065MPa$, as shown in Fig 6.7, buckling strengths of all assemblies show a considerable increase, which almost double those without lateral pressure. It is also observed that the order of buckling initials stay unchanged and the transition region (inflection area) of the plot become gentle and smooth compared to that with smaller lateral pressure.

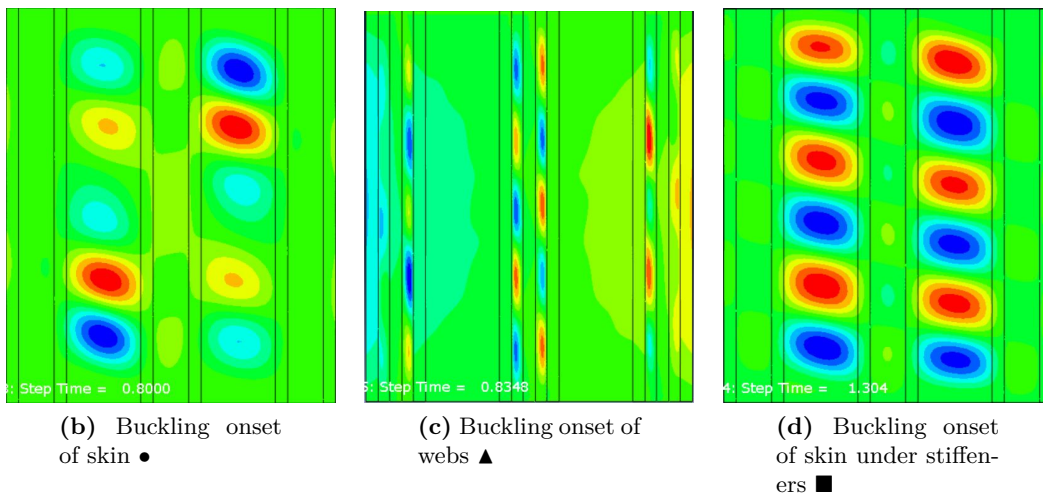
In Fig 6.8, the stiffened panel undergoes a distinct behaviour when suffering from sufficiently large lateral pressure. Stiffeners will buckle first instead of skin. The phenomenon could be explained by the fact that pressure-induced deflection also affects the stiffener by bringing into an in-plane bending moment from the perspective of webs, leading to an early buckling onset of the stiffener. By comparing buckling behaviours between p_2 and p_3 , it can be observed that lateral pressure does not always play a positive role in improving the stability strength of stiffened panels unless it is limited within a specific range. Prediction results of buckling load of each component are summarized in Table 6.3.

In Table 6.3, F_{cr} is the compression load of entire stiffened panel when local buckling of any components takes place. Predicted values using eigenvalue analysis are observed to differ from those in explicit methods, especially at high pressure levels (p_2 and p_3). The reason can be attributed to the large deflection caused by out-of-plane pressure, which invalidates the linear based eigenvalue buckling analysis.

Under a certain lateral pressure load, a local buckling onset always occurs in the skin except for the load case p_3 where stiffeners buckle first. The early buckling of stiffeners at high



(a) Load-shortening curve



(b) Buckling onset of skin ●

(c) Buckling onset of webs ▲

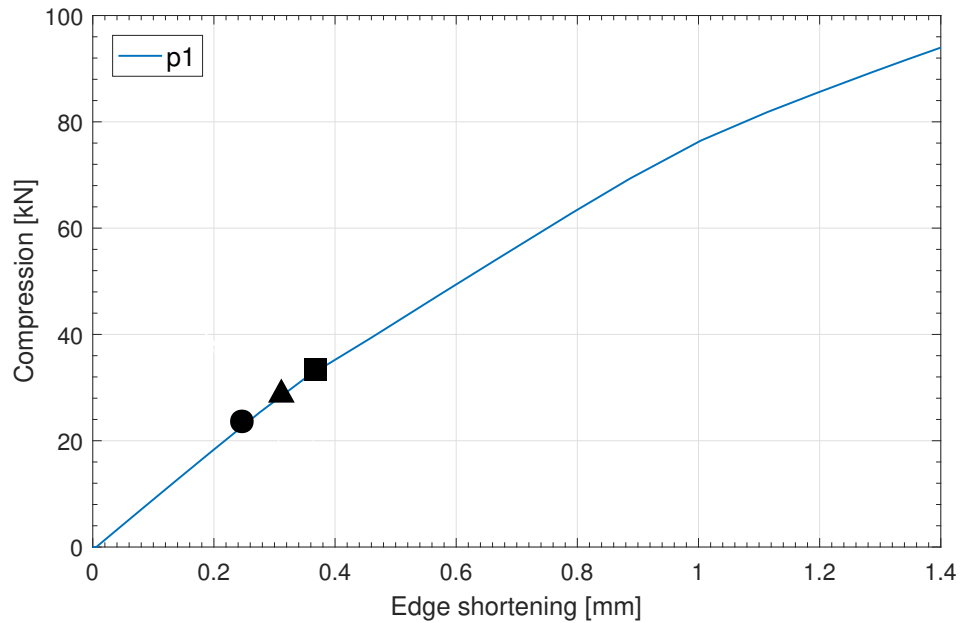
(d) Buckling onset of skin under stiffeners ■

Figure 6.5: Load-shortening curve and out-of-plane displacement of stiffened panel ($p_0 = 0$)

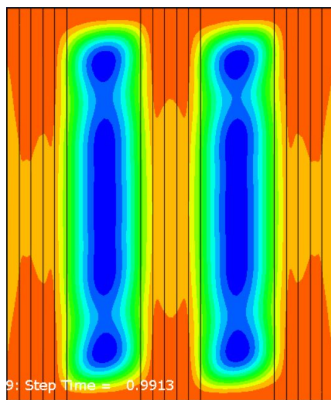
Pressure	p_0		p_1		p_2		p_3	
	Component	F_{cr}	Component	F_{cr}	Component	F_{cr}	Component	F_{cr}
Eigenvalue	●	15.6	●	15.5	●	4.8	●	0.67
Explicit	●	16.7	●	23.7	●	66.5	▲	46.7
	▲	19.0	▲	30.4	▲	69.9	■	70.5
	■	34.9	■	35.9	■	80.9	●	78.5

Notes: ●: Skin; ▲: Webs; ■: Skin under stiffeners.

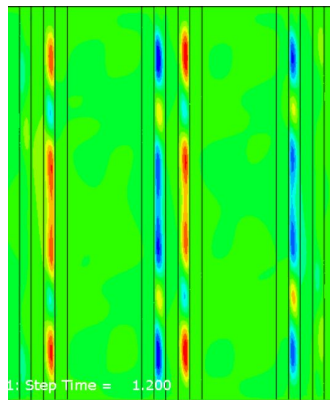
Table 6.3: Buckling loads of components in stiffened panels under combined loads



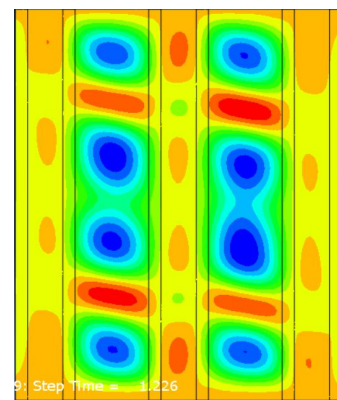
(a) Load-shortening curve



(b) Buckling onset of skin ●

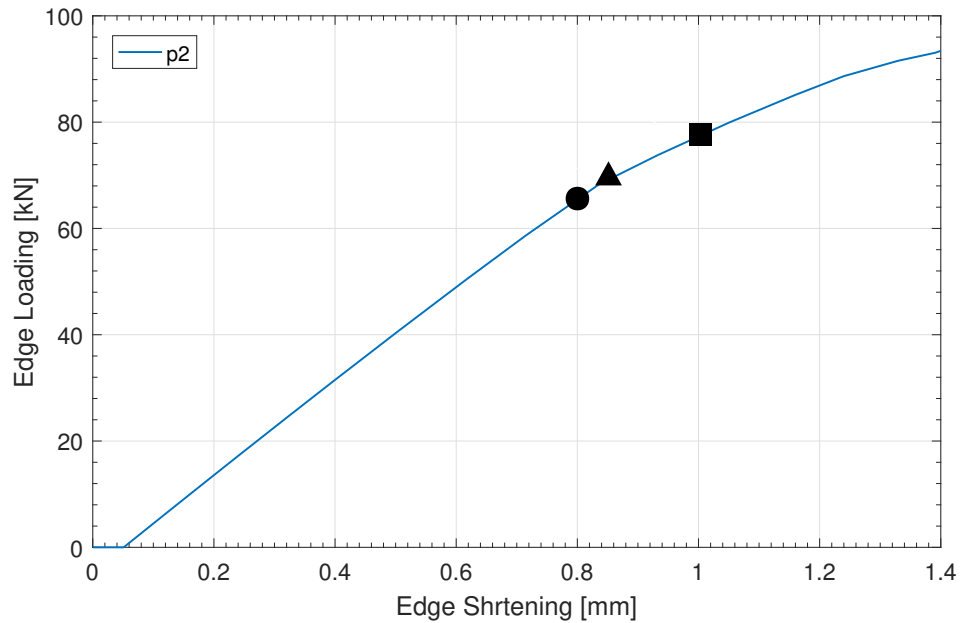


(c) Buckling onset of webs ▲



(d) Buckling onset of skin under stiffeners ■

Figure 6.6: Load-shortening curve and out-of-plane displacement of stiffened panel ($p1 = 0.013MPa$)



(a) Load-shortening curve

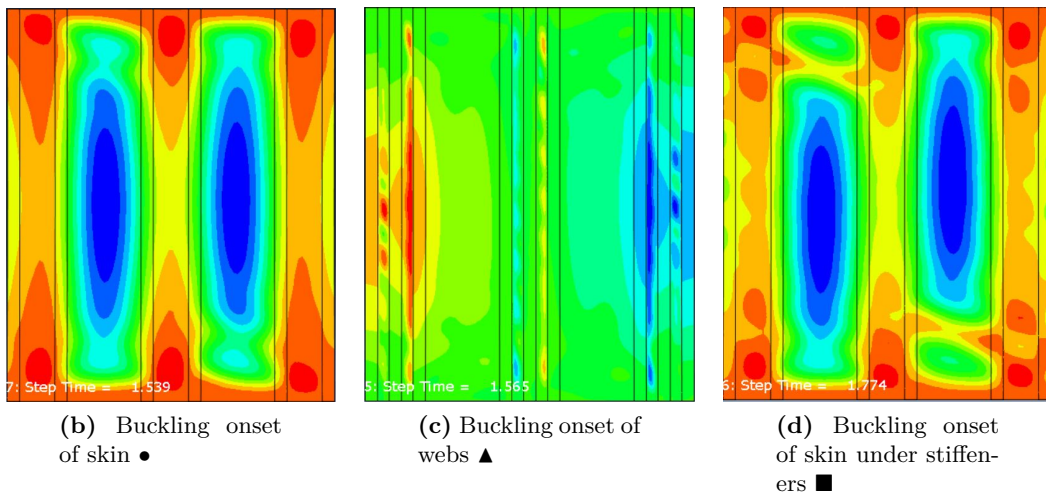
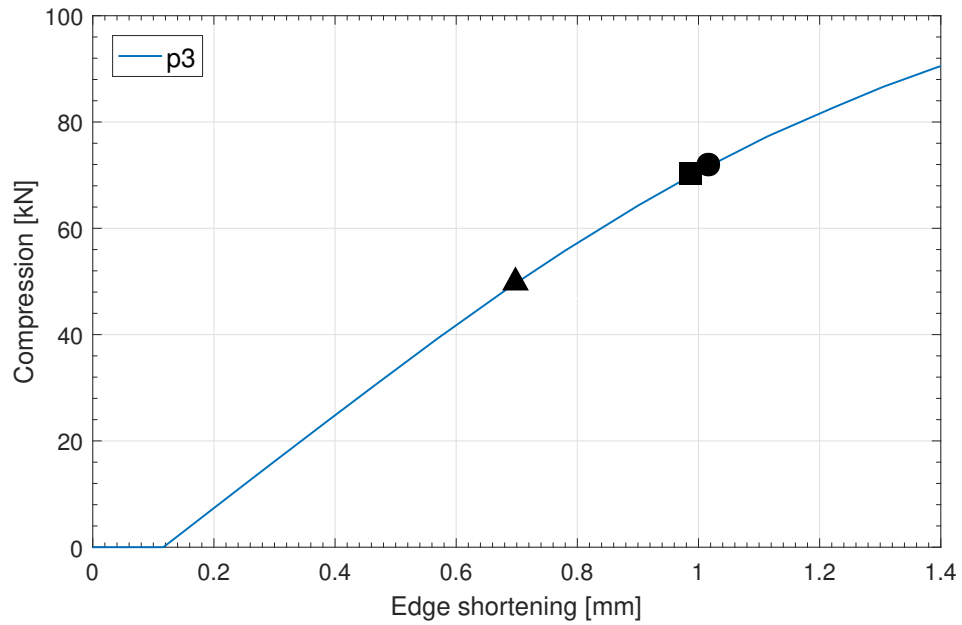
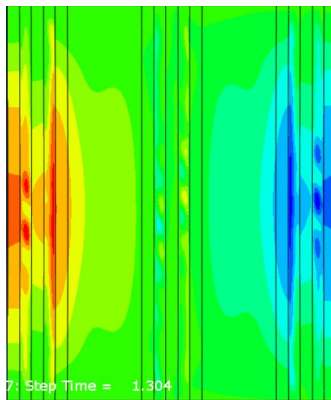


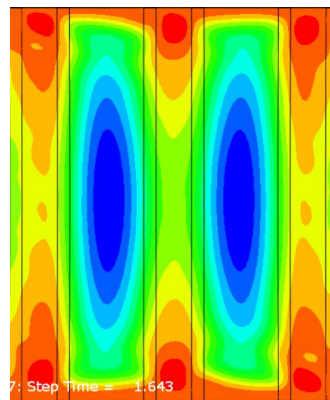
Figure 6.7: Load-shortening curve and out-of-plane displacement of stiffened panel ($p_2 = 0.065 MPa$)



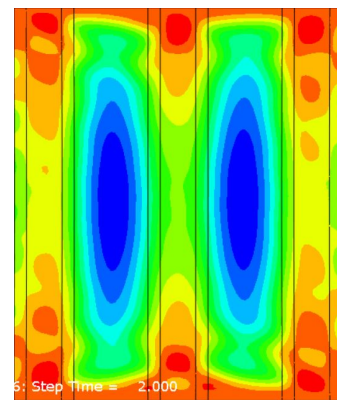
(a) Load-shortening curve



(b) Buckling onset of skin ▲



(c) Buckling onset of webs ■



(d) Buckling onset of skin under stiffeners ●

Figure 6.8: Load-shortening curve and out-of-plane displacement of stiffened panel ($p_3 = 0.13MPa$)

pressure may be result from the induced bending moment by increasingly growing pressure. From simulation results of the explicit analysis, the buckling strength of skin indicates an increased trend with the rise of pressure load while buckling loads of stiffeners and skin under stringers undergo a trend which is initially increasing and then decreasing and peaks at a pressure level of p_2 . It can be concluded that sufficiently large pressure has a more significant effect on the stability capacity of stiffeners and skin under stiffeners compared with that of skin between stringers.

6.5 Dynamic Explicit Analysis of Stiffened Panels with Rubber

As demonstrated in Chapter 5, special rubber filler pads are applied and laid between the panel and airbag in order to generate a flat surface for the application of lateral pressure via airbags. By doing this, potential side effects could be generated and the investigation is consequently required to evaluate the effect of rubber pads on buckling and postbuckling behaviours of panels. Main emphases of this section are located on the comparison of stability responses of panels with and without rubber filler by using dynamic explicit code of Abaqus.

6.5.1 Rubber Material Definition

Generally, rubber-like materials, due to their unique mechanical properties with stress-strain relations significantly different from metallic or composite materials, are considered as hyperelastic in most of the finite element software. In Abaqus, the Mooney-Rivlin constants that characterize hyperelastic materials are adopted as the input data [49]. The compressibility constant D_1 of Mooney-Rivlin stands for the bulk compressibility and is set to zero for fully incompressible rubber while the shear coefficients C_{10} and C_{01} control the mechanical behaviour of the rubber. For the sake of simplification, these constants in Abaqus are made up to be $C_{10}=0.25$, $C_{01}=0.1$ $D_1 = 0.1$ by referring to the literature [56] and [57].

6.5.2 Model Description

In the experiment system discussed in Chapter 5, lateral pressure is applied using pressurized airbags, and a rubber pad is located between the panel and airbag with the purpose of generating uniform distributed pressure loading. In FE analyses, airbag models are neglected for simplification, and the pressure load is assumed uniform distributed and applied directly to the panel. Rubber pads are modeled as three-dimensional "C3D8R" element with length equal to that of the stiffened panel. The rubber pad model is extruded from a cross-section that fully occupies the concave shape surrounded by stiffeners and skin, as shown in Fig 6.9.

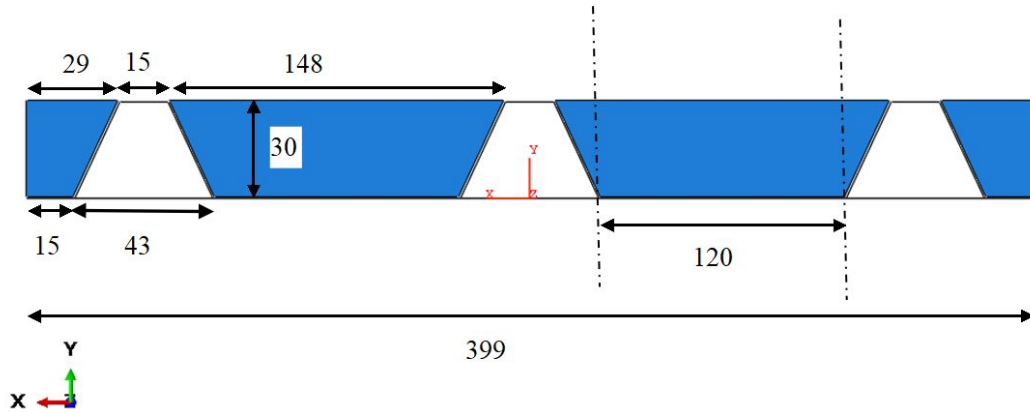
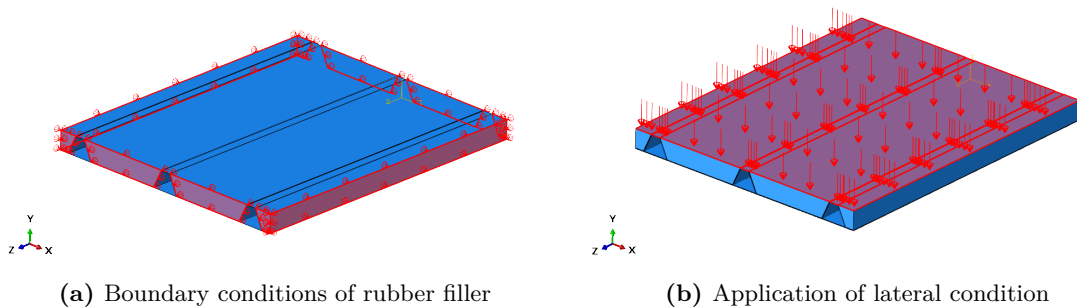


Figure 6.9: Cross section of rubber pads

6.5.3 Boundary and Load Conditions

In addition to the necessary boundary conditions of stiffened panel, rubber filler pad is also constrained in FE models. As seen in Fig 6.10(a), in-plane motion (in the panel plane) of rubber pad edges is limited while the faces contacted with the panel are restrained by contact pairs. A set of surface-to-surface contact pairs between the rubber pad and panel are established with the friction coefficient set to 0.1. Penalty contact method is used to fit the dynamic explicit analysis. The upper faces of rubber pads are free of constraints. Uniform lateral pressure is applied to crowns of stiffeners and the rubber pad as illustrated in Fig 6.10(b).



(a) Boundary conditions of rubber filler

(b) Application of lateral condition

Figure 6.10: Boundary and loading conditions of stiffened panels with rubber filler

6.5.4 Load-Shortening Curves

Comparisons are conducted between stiffened panels with and without rubber filler in terms of load-shortening curves obtained from FE analysis. Both of these models are established using the same settings except for the rubber filler pad. Prediction results are illustrated and compared graphically under four loading cases as shown in Fig 6.11 to Fig 6.14.

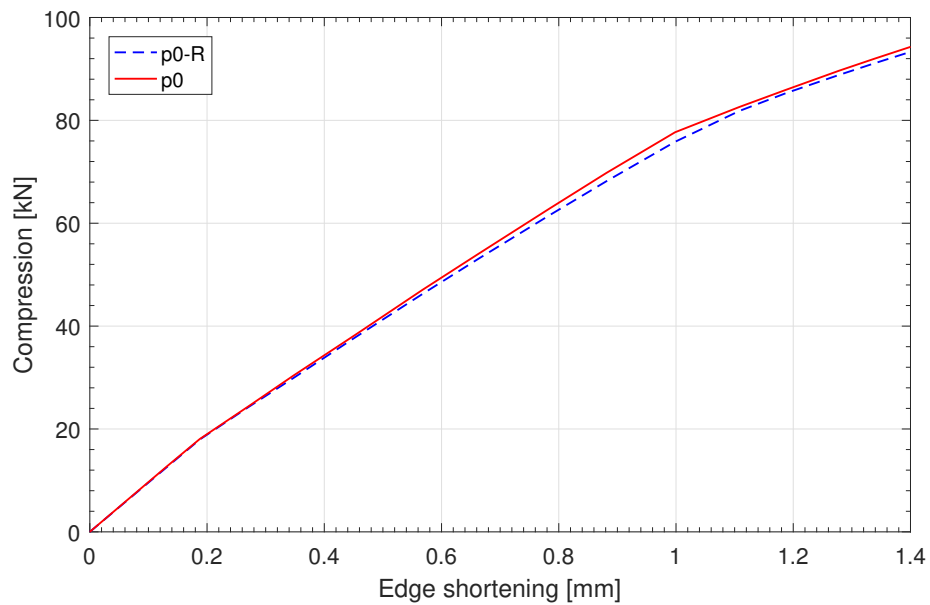


Figure 6.11: Comparison of load-shortening curve of stiffened panels with and without rubber (p_0)

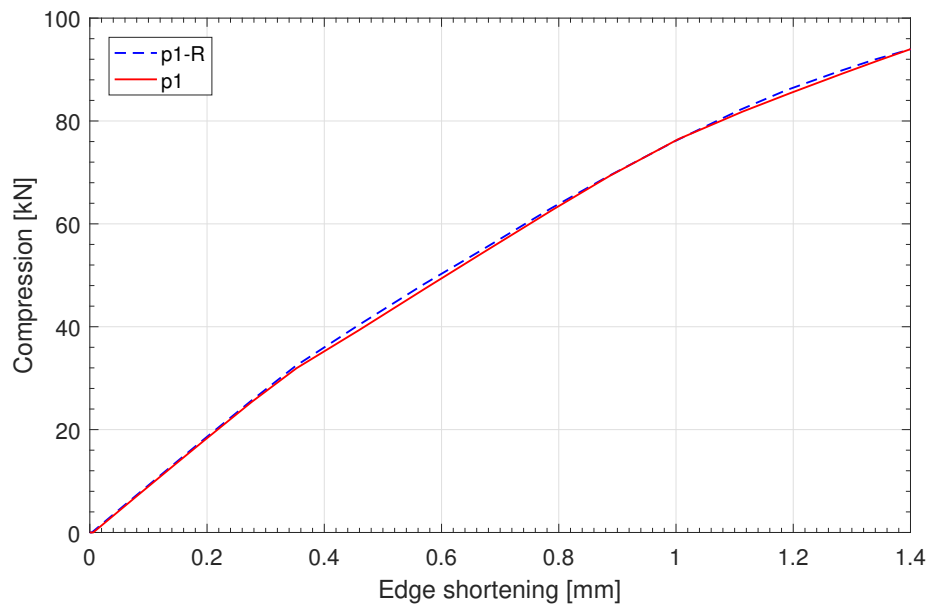


Figure 6.12: Comparison of load-shortening curve of stiffened panels with and without rubber (p_1)

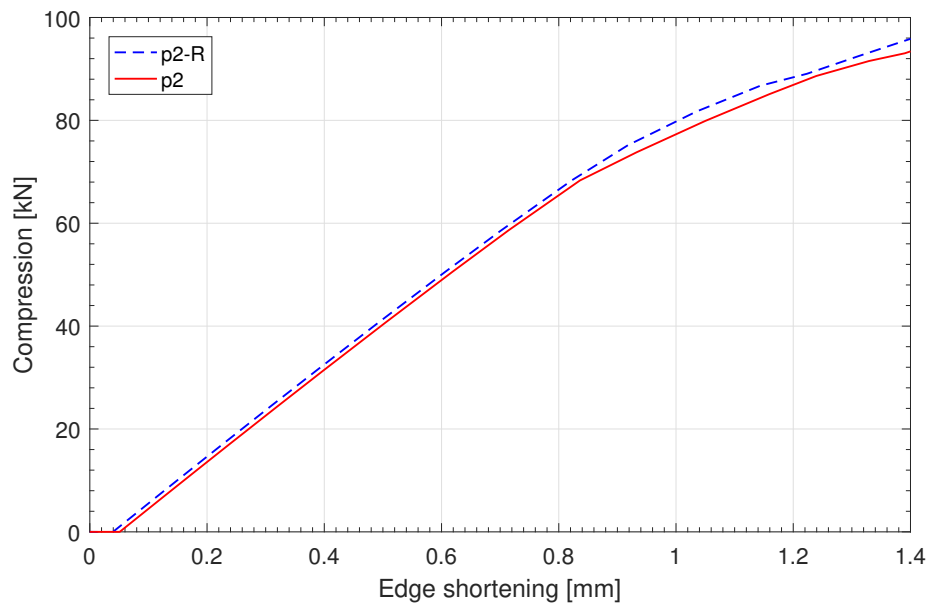


Figure 6.13: Comparison of load-shortening curve of stiffened panels with and without rubber (p_2)

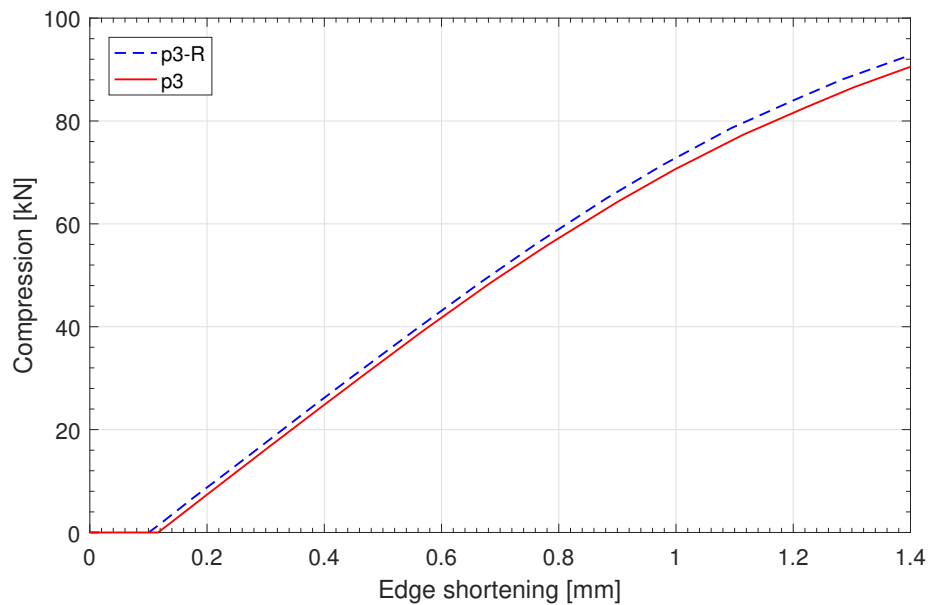


Figure 6.14: Comparison of load-shortening curve of stiffened panels with and without rubber (p_3)

In Fig 6.11 to Fig 6.14, predictions of postbuckling behaviours of stiffened panels under different load cases (distinguished by lateral pressure) are compared. The solid lines stand for the unfilled stiffened panel while dashed lines are those with the rubber filler pads. It is observed that under small pressure (p_0 and p_1), the rubber-affected load-shortening curves become smoother than those without rubber filler pads. The change of stiffness caused by local buckling is eased by the introduction of rubber pads. The rubber pads seem to have minor effects on the amplitude of compression forces. Under relatively larger pressure (p_2 and p_3), Rubber-filled panels are observed to sustain a higher compression load under the same edge shortening displacement, compared with those without rubber filler. The differences are approximately within 10%. It is noteworthy that compression loads of both panels with or without rubber pads under $1.4mm$ edge shortening show an approximate 10% decrease as the lateral pressure increases from $p_2 = 0.065MPa$ to $p_3 = 0.13MPa$. The reason may be due to the fact that significantly large lateral pressure lowers the stiffness of the entire panel, which coincides the conclusions in the previous discussion (See Table 6.3) that stiffened panels have the highest stability capacity at the moderate pressure load of p_2 .

6.6 Conclusion

In this chapter, the FE analysis of composite stiffened panels subjected to compression and lateral pressure is developed using both eigenvalue and explicit dynamic analyses in Abaqus. FE models of stiffened panels are established with shell elements, and eigenvalue analysis is implemented without taken nonlinearity into account. Predictions show that under significantly large pressure, linear eigenvalue analysis cannot give reasonable results. In the following section, an explicit dynamic analysis is conducted to evaluate postbuckling behaviours of stiffened panels. Local buckling onsets of each component are discussed by virtue of load-shortening curves. It is found that the region where buckling waves first appears can be shifted from skin to stiffener as the lateral pressure increases. Finally, effects of rubber pads on the stability behaviours of panels are discussed with results displayed graphically. Numerical predictions show that the effect of rubber filler during the test can be neglected, which suggests that the new-designed setups can be used in buckling experiments under combined loads.

Summaries and Recommendations

7.1 Thesis Overview and Conclusions

The main objective of this thesis is the development of methodologies to solve stability problems of composite stiffened panels under a combined action of in-plane compression and out-of-plane pressure. Due to the large initial deflection caused by lateral pressure, considerable complexities were introduced in terms of load coupling and geometric nonlinearities, which made the analysis both theoretically difficult and computationally intensive. To solve the problem, step by step investigations were performed from unstiffened isotropic plates to stiffened composite panels using both analytical and FE methods.

For the sake of validation and better understanding of buckling phenomena, a new test facility with a high efficiency and good compatibility with classical buckling experiments was developed, by which pressurized airbags were adopted to apply lateral pressure. The main work progressively discussed in previous chapters is concluded as follows.

1. In Chapter 2, literature study was carried out by reviewing studies on buckling and postbuckling behaviours of both stiffened and unstiffened plates under axial compression and lateral pressure. Von Karman governing equations were frequently employed in solving the buckling and postbuckling problems of rectangular plates subjected to combined loads. With the application of a lateral pressure load with a moderate amplitude, stability behaviours of thin-walled structures can be significantly affected. Experimental methodologies were systematically compared concerning the way that lateral pressure was applied to panels. According to the application of lateral forces, those methods can be classified into several groups, namely Combined Loads Test System(COLTS), pressurized airbags, pressure-box and point loads methods. Advantages and disadvantages of each method were examined in terms of cost, feasibility and accuracy. Considering

the limitation of current laboratory conditions, the method using pressurized airbags received the most attraction in trade-off forms. Afterwards, theoretical fundamentals and governing equations of both isotropic and composite panels were presented based on the classical thin plate theory.

2. In Chapter 3, buckling and postbuckling behaviours of rectangular plates made from isotropic material were studied under simply supported boundary conditions and subjected to combined loads. First, plate critical buckling loads were obtained from the analytical method of Gambhir [11], using equilibrium equation and energy method, based on Kirchhoff's hypotheses and small deflection assumptions. Nonlinearities were not taken into account. Solutions derived from these two methods agreed well with prediction results of eigenvalue buckling analysis in Abaqus, indicating that lateral pressure had minor effects on the buckling load of uniaxially compressed plates. Thereafter, large deflection theory was employed to deal with buckling and postbuckling problems of plates under combined loads with nonlinearities taken into account. Critical buckling loads of plates under combine loads obtained from the explicit dynamic analysis were observed to have been affected by lateral pressure in a positive manner. With the application of a magnitude of pressure equal to 0.065MPa , which equals to cabin pressure at a cruise altitude for a modern commercial airplane, plate buckling load became as twice as that in uniaxially compressed plates. By means of Galerkin's technique, implemented formulations for postbuckling responses, describing the maximum plate deflection as a function of pressure loading and average edge compression, were also derived and agreed well with simulation results from the explicit dynamic analysis in Abaqus.
3. In Chapter 4, investigations on buckling and postbuckling analysis have been extended from isotropic plates to composite laminates. First, theoretical methods were employed, including the force equilibrium method based on von Karman equations and energy method based on the principle of total potential energy, to develop buckling responses of composite laminates under a linear elastic assumption. Solutions were validated by finite element eigenvalue analyses with respect to the buckling strength of a simply supported laminates under four different load cases. It was observed that linear-based methods were insufficient in predicting the buckling load of plates under large pressure loads. Explicit dynamic analysis was then applied to capture the buckling onset and foresee postbuckling behaviours with nonlinearities taken into account. Load-shortening and load-deflection curves were depicted in which buckling loads were read from inflection points of derived curves. With the introduction of lateral pressure, stability behaviours of plates made of composite materials exhibited a similar trend with those of isotropic plates.
4. Chapter 5 described a new conceptual design of buckling experiments of stiffened panels under compression and lateral pressure. Based on a comprehensive comparison of the advantages and disadvantages of other experimental schemes, pressurized airbags were employed to apply uniform pressure loading. A test rig was designed with the consideration of compatibility with classical buckling experiments to lower the cost. In-plane compression of the stiffened panel was driven by a hydraulic actuator and lateral pressure loading was applied by means of an inflatable airbag located between the specimen and a supporting platform which was mounted to the testing frame. By doing this, lateral loads can be self balanced so that extra lateral actuators were not required. Rubber

filler pads were used to eliminate the unevenness of stiffened panels on the stringer side and placed between the airbag and specimen.

5. FE analyses for stability properties of composite stiffened panels were conducted in Chapter 6, in order to provide comparable predictions to the experimental results. The stiffened panel was constructed by three hat stringers and one skin which is following the same geometry of the specimen in Chapter 5. Explicit dynamic analysis was developed to evaluate the effect of lateral pressure on buckling and postbuckling behaviours of composite stiffened panels. Local buckling onsets of each component of the stiffened panels, including skin between stringers, stiffeners and skin under stiffeners, were captured through load-shortening curves. Hyperelastic materials using Mooney-Rivlin constants were assigned to FE models of rubber fillers to evaluate potential effects of the filler during simulation. Prediction results were intended to be compared with the data measured by buckling tests through the aforementioned new designed facility.

Conclusions can be made from the proceeding analysis in each chapter.

1. Analytical and finite element methods under small deflection assumption were not able to provide accurate predictions of buckling loads with the inclusion of considerable lateral pressure, which suggested the necessity of postbuckling analyses with geometric nonlinearities considered. Simulated results of explicit dynamic procedures in Abaqus predicted the buckling load fairly well compared with those in literature, revealing that lateral pressure has a positive impact on the stability behaviour of rectangular isotropic plates by postponing the buckling onset.
2. Composite panels behaved similarly as isotropic plates in terms of buckling and post-buckling responses when lateral pressure was introduced. Given the sufficiently large pressure, the critical buckling load of a simply supported plate was able to reach up to four times as that of the uniaxially compressed plate.
3. For composite stiffened panels, locations of the first local buckling onset tended to transfer from in-between plate to stiffener's web with the increase of lateral pressure. As expected, buckling strength of the entire stiffened panels has been enhanced by the increasing amplitude of lateral loading. However, this trend was reversed when the pressure load exceeded certain values at which the stiffener buckling occurs before in-between plates.

7.2 Recommendations

A series of recommendations are presented based on the current analysis. Some of the recommendations are issued for the sake of in-depth studies and others are for the potential improvement of the new-designed experiment.

1. In the present analysis, boundary conditions of the plate were considered as simply supported for simplification. It is more suitable to adopt elastic restraints, which are closer to the real situation in stiffened panels, for further assessments.

2. Initial geometry imperfections of stiffened panels were not taken into account in current FE analysis. In order to obtain more comparable results with testing data, imperfections sensitivity analysis is necessary for future analysis.
3. In this thesis, structure failure is not taken into account in the numerical simulation. In order to have a more meaningful verification, further research with failure criterion input is required.
4. FE analysis of stiffened panels in the new-designed buckling experiment facility is approximated by neglecting the model of pressurized airbags. Detailed modeling is recommended in future work. In addition, the coefficient of static friction between the rubber filler and composite panels is also required to be accurately determined.

References

- [1] A. Przekop, D. C. Jegley, A. E. Lovejoy, M. Rouse, and H.-Y. T. Wu, “Testing and analysis of a composite non-cylindrical aircraft fuselage structure, part I: Ultimate design loads,” *57th AIAA/ASCE/AHS/ASC Structures, Structural Dynamics, and Materials Conference*, 2016.
- [2] A. Przekop, H.-Y. Wu, and P. Shaw, “Nonlinear finite element analysis of a composite non-cylindrical pressurized aircraft fuselage structure,” 2014.
- [3] E. Barkanov, O. Ozolins, E. Eglitis, F. Almeida, M. C. Bowering, and G. Watson, “Optimal design of composite lateral wing upper covers. part I: Linear buckling analysis,” *Aerospace Science and Technology*, vol. 38, pp. 1–8, 2014.
- [4] E. Ventsel and T. Krauthammer, *Thin Plates and Shells: Theory: Analysis, and Applications*. CRC press, 2001.
- [5] S. P. Timoshenko and S. Woinowsky-Krieger, *Theory of Plates and Shells*. McGraw-Hill, 1959.
- [6] Y. Ueda, S. M. H. Rashed, and J. K. Paik, “Buckling and ultimate strength interaction in plates and stiffened panels under combined inplane biaxial and shearing forces,” *Marine Structures*, vol. 8, no. 1, pp. 1–36, 1995.
- [7] M. Shama, *Buckling of Stiffened Panels*, pp. 267–304. Springer Berlin Heidelberg, 2013.
- [8] C. Kassapoglou, *Design and Analysis of Composite Structures: with Applications to Aerospace Structures*. John Wiley & Sons, 2013.
- [9] J. N. Reddy, *Theory and Analysis of Elastic Plates and Shells*. CRC press, 2006.
- [10] T. Yao and M. Fujikubo, “Chapter 5 - buckling/plastic collapse behavior and strength of rectangular plates subjected to combined loads,” in *Buckling and Ultimate Strength of Ship and Ship-Like Floating Structures*, pp. 157 – 206, Butterworth-Heinemann, 2016.

- [11] M. L. Gambhir, *Stability Analysis and Design of Structures*. Springer Science & Business Media, 2013.
- [12] S. Levy, “Bending of rectangular plates with large deflections,” *Report-National Advisory Committee for Aeronautics*, no. 727-751, p. 139, 1942.
- [13] S. Levy, D. Goldenberg, and G. Zibritsky, “Simply supported long rectangular plate under combined axial load and normal pressure,” tech. rep., National Advisory Committee for Aeronautics; Washington, DC, United States, Oct 01, 1944.
- [14] R. M. Woolley, J. N. Corrick, and S. Levy, “Clamped long rectangular plate under combined axial load and normal pressure,” *National Advisory Committee for Aeronautics; Washington, DC, United States*, no. NACA-TN-1047, 1946.
- [15] C. Y. Chia, *Nonlinear Analysis of Plates*. McGraw-Hill International Book Company, 1980.
- [16] M. Yosiki, Y. Yamamoto, and H. Kondo, “Buckling of plates subjected to edge thrusts and lateral pressure,” *Journal of Zosen Kiokai*, vol. 1965, no. 118, pp. 249–258, 1965.
- [17] J. C. Brown and J. M. Harvey, “Large deflections of rectangular plates subjected to uniform lateral pressure and compressive edge loading,” *ARCHIVE: Journal of Mechanical Engineering Science 1959-1982 (vols 1-23)*, vol. 11, no. 3, pp. 305–317, 1969.
- [18] T. Yao, M. Fujikubo, B. Varghese, K. Yamamura, and O. Niho, “Buckling/plastic collapse strength of wide rectangular plate under combined pressure and thrust,” *Journal of the Society of Naval Architects of Japan*, vol. 1997, no. 182, pp. 561–570, 1997.
- [19] E. Steen and S. Valsgard, “Simplified buckling strength criteria for plates subjected to biaxial compression and lateral pressure,” in *Ship Structure Symposium*, 1994.
- [20] E. Byklum and J. Amdahl, “A simplified method for elastic large deflection analysis of plates and stiffened panels due to local buckling,” *Thin-Walled Structures*, vol. 40, no. 11, pp. 925–953, 2002.
- [21] G. L. Giles and M. S. Anderson, “Effects of eccentricities and lateral pressure on the design of stiffened compression panels,” tech. rep., NASA Langley Research Center; Hampton, VA, United States, Jun 01, 1972.
- [22] H. Shen, “Postbuckling of rectangular plates under uniaxial compression combined with lateral pressure,” *Applied Mathematics and Mechanics*, vol. 10, no. 1, pp. 55–63, 1989.
- [23] H. Shen, “Postbuckling of composite laminated plates under biaxial compression combined with lateral pressure and resting on elastic foundations,” *The Journal of Strain Analysis for Engineering Design*, vol. 33, no. 4, pp. 253–261, 1998.
- [24] H. Shen, “Postbuckling of Reissner-Mindlin plates under biaxial compression and lateral pressure and resting on elastic foundations,” *Computer Methods in Applied Mechanics and Engineering*, vol. 173, no. 1-2, pp. 135–146, 1999.
- [25] S.-C. Han, S.-Y. Lee, and G. Rus, “Postbuckling analysis of laminated composite plates subjected to the combination of in-plane shear, compression and lateral loading,” *International Journal of Solids and Structures*, vol. 43, no. 18-19, pp. 5713–5735, 2006.

- [26] M. Khedmati, M. Zareei, and P. Rigo, "Empirical formulations for estimation of ultimate strength of continuous stiffened aluminium plates under combined in-plane compression and lateral pressure," *Thin-Walled Structures*, vol. 48, no. 3, pp. 274–289, 2010.
- [27] N. E. Shanmugam, Z. Dongqi, Y. S. Choo, and M. Arockiaswamy, "Experimental studies on stiffened plates under in-plane load and lateral pressure," *Thin-Walled Structures*, vol. 80, pp. 22–31, 2014.
- [28] J. C. Roberts, G. Bao, and G. J. White, "Experimental, numerical and analytical results for bending and buckling of rectangular orthotropic plates," *Composite Structures*, vol. 43, no. 4, pp. 289–299, 1998.
- [29] J. Reinoso, A. Blázquez, F. París, J. Cañas, and J. Meléndez, "Postbuckling behaviour of a pressurized stiffened composite panel - part I: Experimental study," *Composite Structures*, vol. 94, no. 5, pp. 1533–1543, 2012.
- [30] S. Z. Hu, Q. Chen, N. Pegg, and T. J. E. Zimmerman, "Ultimate collapse tests of stiffened-plate ship structural units," *Marine Structures*, vol. 10, no. 8-10, pp. 587–610, 1997.
- [31] M. Rouse and D. Jegley, *Testing a Multi-bay Box Subjected to Combined Loads*, pp. 173–182. Cham: Springer International Publishing, 2016.
- [32] M. Rouse, *Methodologies for Combined Loads Tests Using a Multi-actuator Test Machine*, pp. 205–214. Cham: Springer International Publishing, 2014.
- [33] D. Ambur, J. Cerro, and J. Dickson, "Analysis of a d-box fixture for testing curved stiffened aircraft fuselage panels in axial compression and internal pressure," *35th Structures, Structural Dynamics, and Materials Conference*, 1994.
- [34] J. Taylor, "An experimental investigation of the behaviour of flat rectangular plates under the action of combined in-plane and lateral pressure," *Experimental Stress Analysis*, vol. Ch 9, pp. 75–85, 1986.
- [35] D. Zhu, "Stiffened plates subjected to in-plane load and lateral pressure," Master's thesis, National University of Singapore, 2004.
- [36] S. M. Kumar, L. C. Kumar, P. Alagusundaramoorthy, and R. Sundaravadivelu, "Ultimate strength of orthogonal stiffened plates subjected to axial and lateral loads," *KSCE Journal of Civil Engineering*, vol. 14, no. 2, pp. 197–206, 2010.
- [37] M. Rouse and D. Anbur, "Fuselage response simulation of stiffened panels using a pressure-box test machine," *36th Structures, Structural Dynamics and Materials Conference*, 1995.
- [38] J. A. August and S. P. Joshi, "Deflection of rectangular orthotropic plates under uniform load," *AIAA Journal*, vol. 34, no. 10, pp. 2205–2206, 2012.
- [39] D. Ambur and M. Rouse, "Design and evaluation of composite fuselage panels subjected to combined loading conditions," *Journal of Aircraft*, vol. 42, no. 4, pp. 1037–1045, 2005.

- [40] D. Ambur, M. Rouse, R. Young, and C. Perez-Ramos, "Evaluation of an aluminum fuselage panel with discrete-source damage and subjected to combined loading conditions," *40th Structures, Structural Dynamics, and Materials Conference and Exhibit*, 1999.
- [41] D. R. Anbur, J. A. Cerro, and J. Dickson, "D-box fixture for testing stiffened panels in compression and pressure," *Journal of Aircraft*, vol. 32, no. 6, pp. 1382–1389, 2012.
- [42] N. E. Shanmugam and M. Arockiasamy, "Local buckling of stiffened plates in offshore structures," *Journal of Constructional Steel Research*, vol. 38, no. 1, pp. 41–59, 1996.
- [43] I. S. San Diego Composites, "San Diego Composites to fabricate stiffened fuselage test panels for sandia national labs' FAA and EASA effort." <http://www.sdcomposites.com/Media/newsarticle4.html>. Accessed: 2017-11-18.
- [44] R. Vescovini and C. Bisagni, "Semi-analytical buckling analysis of omega stiffened panels under multi-axial loads," *Composite Structures*, vol. 120, pp. 285–299, 2015.
- [45] C. L. Dym and I. H. Shames, *Solid Mechanics: A Variational Approach*. Springer, 1973.
- [46] ABAQUS, "Version 6.13 user's manual," *SIMULIA, World Headquarters, Providence, RI, USA*, 2013.
- [47] A. Velicki, "Damage arresting composites for shaped vehicles phase i final report," tech. rep., Boeing Co.; Huntington Beach, CA, United States, 2009.
- [48] J. Quinlan and F. H. Gern, "Conceptual design and structural optimization of NASA Environmentally Responsible Aviation (ERA) Hybrid Wing Body Aircraft," *57th AIAA/ASCE/AHS/ASC Structures, Structural Dynamics, and Materials Conference*, 2016.
- [49] ABAQUS, "Version 6.14 user's manual," *SIMULIA, World Headquarters, Providence, RI, USA*, 2014.
- [50] ABAQUS, "Version 6.10 user's manual," *SIMULIA, World Headquarters, Providence, RI, USA*, 2011.
- [51] J. Singer, J. Arbocz, and T. Weller, *Buckling Experiments: Experimental Methods in Nuckling of Thin-Walled Structures, Volume 2*. John Wiley & Sons, Inc, 2002.
- [52] C. Bisagni and C. G. Dávila, "Experimental investigation of the postbuckling response and collapse of a single-stringer specimen," *Composite Structures*, vol. 108, pp. 493–503, 2014.
- [53] V. GMBH, "Lifting airbags." <https://www.vetter.de>. Accessed: 2017.
- [54] S. C. Limited, "Trough hole (annular) load cells." <http://www.sensy.com/EN/load-limitation/trough-hole-annular-load-cells>. Accessed: 2017.
- [55] C. Bisagni, R. Vescovini, and C. G. Dávila, "Single-stringer compression specimen for the assessment of damage tolerance of postbuckled structures," *Journal of Aircraft*, vol. 48, no. 2, pp. 495–502, 2012.

-
- [56] N. Kumar and V. V. Rao, “Hyperelastic Mooney-Rivlin model: Determination and physical interpretation of material constants,” *Parameters*, vol. 2, no. 10, p. 01, 2016.
- [57] M. Shahzad, A. Kamran, M. Z. Siddiqui, and M. Farhan, “Mechanical characterization and fe modelling of a hyperelastic material,” *Materials Research*, vol. 18, no. 5, pp. 918–924, 2015.

Appendix A

Appendix

A.1 Isotropic Plates under Pure Pressure

The nonlinear expression regarding plate deflections and lateral pressure has been obtained as seen in Eq.3.50,

$$\frac{w_{11}}{h} + \frac{3(1-\nu^2)}{8} \left(\frac{w_{11}}{h}\right)^3 = \frac{4p_z a^4}{\pi^6 D h} \quad (3.50)$$

Similar expressions in literature are:

$$\frac{w_{11}}{h} + \frac{128(1-\nu^2)}{3\pi^4} \left(\frac{w_{11}}{h}\right)^3 = \frac{4p_z a^4}{\pi^6 D h} \quad (\text{Equation 7.91 [4]})$$

$$\frac{\pi^6}{16} \left(\frac{1}{3(1-\nu^2)} \frac{w_{11}}{h} + 0.06429 \left(\frac{w_{11}}{h}\right)^3 \right) = \frac{p_z a^4}{E h^4} \quad (\text{Equation 2-50 [15]})$$

Comparison between Eq.3.50 and those in literature is shown in Fig. A.1.

A.2 Isotropic Plates under Uniaxial Compression and Pressure

The derived expression regarding the plate deflection, external lateral pressure and edge compression is shown in Eq.3.96 (valid for square plates),

$$\frac{w_{11}}{h} \left(1 - \frac{N_x a^2}{4\pi^2 D}\right) + \left(\frac{w_{11}}{h}\right)^3 \frac{3(1-\nu^2)}{8} = \frac{4a^4 p_z}{\pi^6 D h} \quad (3.96)$$

Effects of lateral pressure on postbuckling behavior of square plates are shown in Fig.A.2.

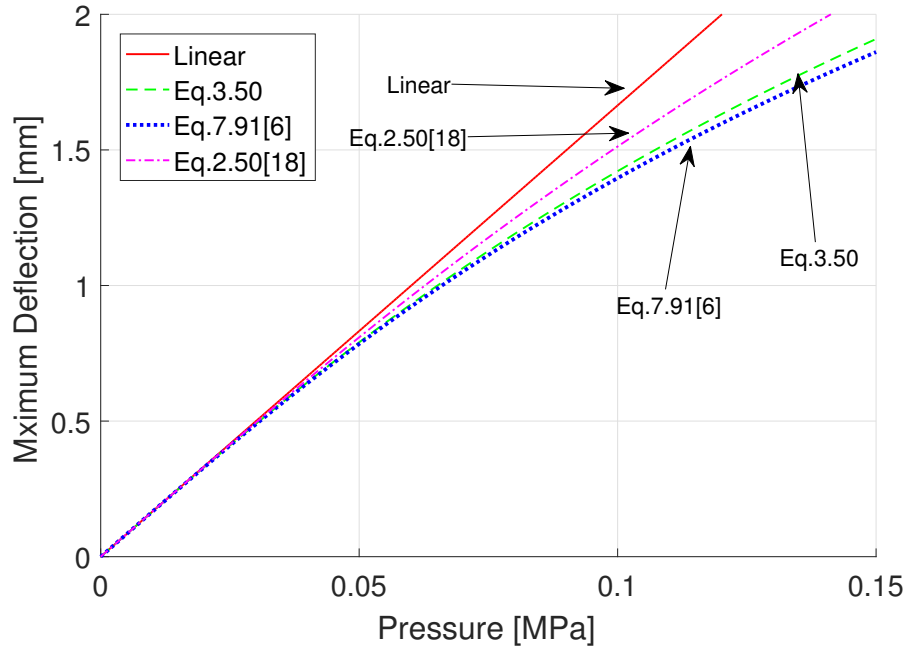


Figure A.1: Central deflection versus uniform lateral pressure for simply supported square plate

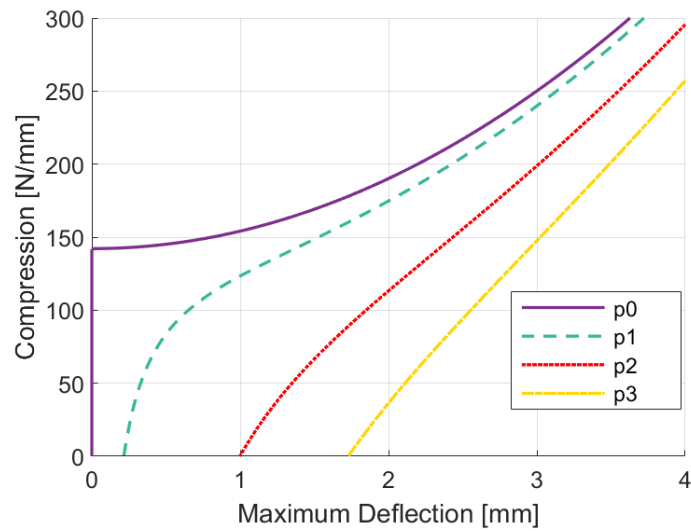


Figure A.2: Effect of lateral pressure on postbuckling behavior of square plates(Eq. 3.96)

A.3 FEM Verification

The FEA is conducted using explicit dynamic code in Abaqus, and simulation results under four load cases (p_0 , p_1 , p_2 and p_3 ,) are graphically compared with analytical solutions to Eq. 3.96 as seen in Fig.A.3.

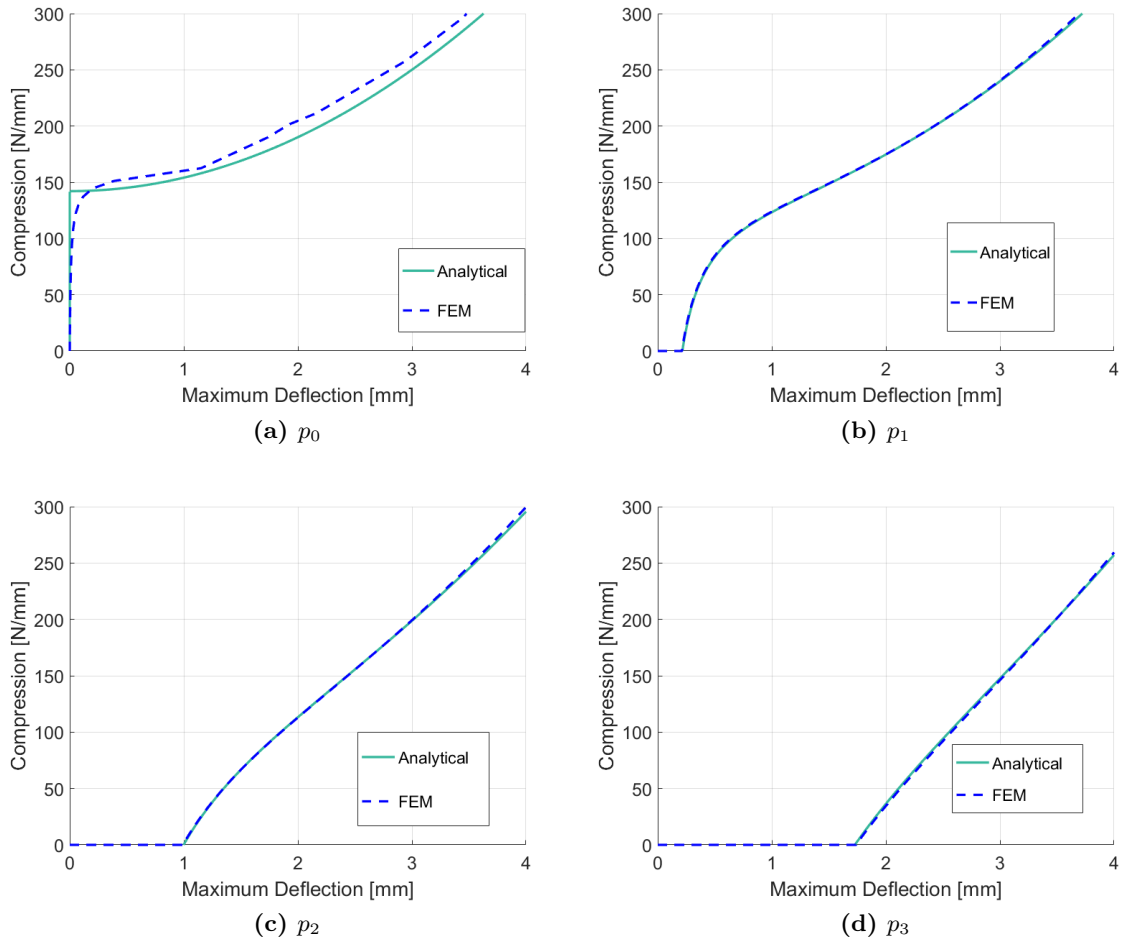


Figure A.3: Verification of postbuckling behaviours of simply supported square plates under various lateral pressure

Good to excellent agreements are observed in the figures, which indicates that the method presented in the thesis are applicable to predict the postbuckling behaviour of isotropic plate although only square plate are available so far.